



UNIVERSITY OF BUCHAREST
Faculty of Physics, ROMANIA
Physics Doctoral School

HASSELT UNIVERSITY
Diepenbeek, BELGIUM

Doctoral Thesis

**MICROFLUORIMETRIC STUDY OF THE MEMBRANE
ORGANIZATION OF MODEL MEMBRANES AND
OLIGODENDROCYTES WHEN SUBJECTED TO
CHOLESTEROL MODULATION FACTORS**

University of Bucharest Promotor: Prof. Dr. Aurel POPESCU

Hasselt University Promotor: Prof. Dr. Marcel AMELOOT

PhD Student
Mihaela BACALUM

Bucharest, 2012

UNIVERSITY OF BUCHAREST
Faculty of Physics, ROMANIA

UNIVERSITY OF HASSELT
Diepenbeek, BELGIUM

Doctoral Thesis

**MICROFLUORIMETRIC STUDY OF THE MEMBRANE
ORGANIZATION OF MODEL MEMBRANES AND
OLIGODENDROCYTES WHEN SUBJECTED TO
CHOLESTEROL MODULATION FACTORS**

Promotor University of Bucharest: Prof. Dr. Aurel POPESCU

Promotor Hasselt University: Prof. Dr. Marcel AMELOOT

PhD Student
Mihaela BACALUM

Bucharest, 2012

Members of the jury

Prof. Dr. Stefan ANTOHE, University of Bucharest, Bucharest, ROMANIA, Chairman

Prof. Dr. Aurel POPESCU, University of Bucharest, Bucharest, ROMANIA, Promotor

Prof. Dr. Marcel AMELOOT, Hasselt University, Diepenbeek, BELGIUM, Promotor

Prof. Dr. Laura TUGULEA, University of Bucharest, Bucharest, ROMANIA, Reporter

Prof. Dr. Jean-Michel RIGO, Hasselt University, Diepenbeek, BELGIUM, Reporter

Assoc. Prof. Dr. Tudor SAVOPOL, „Carol Davila” Medical University, Bucharest, ROMANIA, Reporter

Prof. Dr. Jerom HENDRIK, Hasselt University, Diepenbeek, BELGIUM, Reporter

TABLE OF CONTENTS

TABLE OF CONTENTS	I
LIST OF ABBREVIATIONS	IV
LIST OF SYMBOLS	VI
LIST OF FIGURES	VII
LIST OF TABLES	X
1. GENERAL INTRODUCTION AND AIMS	1
INTRODUCTION	2
1.1. BIOLOGICAL MEMBRANES	3
1.1.1. BIOLOGICAL MEMBRANE COMPOSITION AND ORGANIZATION	3
1.1.2. LIPID BILAYERS	5
1.1.3. PHYSICAL PROPERTIES OF LIPID BILAYER	7
1.1.3.1. LIPID BILAYER FLUIDITY	7
1.1.3.2. PHASE SEGREGATION OF LIPID SYSTEMS	8
1.1.4. SUPRAMOLECULAR ORGANIZATION OF BIOLOGICAL MEMBRANES	10
1.2. OLIGODENDROCYTES	11
1.2.1. OLIGODENDROCYTES MEMBRANE COMPOSITION	14
1.2.2. MULTIPLE SCLEROSIS	16
1.3. CHOLESTEROL METABOLISM IN CNS	17
1.3.1. CHOLESTEROL SYNTHESIS	18
1.3.2. STATINS – HMG-COA INHIBITORS	19
1.3.3. LIVER X RECEPTOR AND T09	21
1.4. TGF-B	22
1.5. AIM OF THE STUDY	24
2. PRINCIPLES OF FLUORESCENCE	25
2.1. FLUORESCENCE PRINCIPLES	26
2.2. FLUOROPHORES	30
2.2.1. SOLVATOCHROMIC DYES	31
2.2.2. LAURDAN	31
2.2.3. BODIPY	33
2.3. FLUORESCENCE SPECTROSCOPY	34
2.3.1. STEADY – STATE FLUORESCENCE	34
2.3.2. TIME RESOLVED FLUORESCENCE	36

2.4. FLUORESCENCE MICROSCOPY	37
2.4.1. CONFOCAL FLUORESCENCE MICROSCOPY	38
2.4.2. MULTIPLE-PHOTON EXCITATION FLUORESCENCE MICROSCOPY	39
2.4.3. FLUORESCENCE LIFETIME IMAGING. TWO-PHOTON FLUORESCENCE LIFETIME IMAGING	40
3. MATERIAL AND METHODS	41
3.1. CELL CULTURE	42
3.1.1. OLN-93 CELLS	42
3.1.2. HEK293T CELLS	42
3.1.3. CELL TREATMENT	42
3.1.4. CELL STAINING	43
3.1.5. DETERMINATION OF CELL VIABILITY	43
3.1.6. DETERMINATION OF APOPTOSIS	44
3.2. LIPID VESICLES	44
3.2.2. LUVS PREPARATION	45
3.2.3. GUVS PREPARATION	45
3.3. SPECTROSCOPY MEASUREMENTS	46
3.4. FLUORESCENCE MICROSCOPY MEASUREMENTS	47
3.4.1. FLIM	47
3.4.2. FRAP	47
3.5. DATA PROCESSING	48
4. A NEW METHOD OF ANALYZING LAURDAN SPECTRA WHEN INSERTED IN LIPID MEMBRANES	51
INTRODUCTION	52
4.1. SOLVENT MEASUREMENTS AND SHAPE PARAMETERS RELATIONSHIPS	53
4.2. DECOMPOSITION OF EMISSION SPECTRA OF LAURDAN INSERTED IN LUVS	55
PARTIAL CONCLUSIONS	60
5. EXPLORING THE CORRELATION BETWEEN GENERALIZED POLARIZATION AND TIME-RESOLVED FLUORESCENCE OF LAURDAN IN LIPID MEMBRANES	61
INTRODUCTION	62
5.1. MEASUREMENTS ON LUVS	63
5.2. MEASUREMENTS ON GUVS	68
5.3. MEASUREMENTS ON HEK293T CELLS	77
5.4. DISCUSSION	83
5.4.1. LIFETIMES ARE MORE SENSITIVE TO LIPID COMPOSITION THAN <i>GP</i>	84
5.4.2. CORRELATIONS BETWEEN <i>GP</i> AND LIFETIMES DIFFERENTIATE COEXISTING LIPID PHASES IN GUVs	86
5.4.3. <i>GP</i> -LIFETIME TOPOGRAPHICAL MAPS REVEAL COMPLEX ORGANIZATION OF THE PLASMA MEMBRANE OF THE LIVING CELL	90

PARTIAL CONCLUSIONS	94
<u>6. MEMBRANE ORGANIZATION OF OLIGODENDROCYTES WHEN SUBJECTED TO CHOLESTEROL MODULATION FACTORS</u>	<u>95</u>
INTRODUCTION	96
6.1. SIMVASTATIN EFFECTS ON OLN-93 CELLS MEMBRANE	97
6.2. T09 EFFECTS ON OLN-93 MEMBRANE	106
DISCUSSION	112
PARTIAL CONCLUSIONS	114
<u>7. A BLUE EMITTING BODIPY BASED LIPID PHASE SENSITIVE PROBE</u>	<u>115</u>
INTRODUCTION	116
7.1. FLUORESCENCE PROPERTIES OF BNP IN ORGANIC SOLVENTS	117
7.2. FLUORESCENCE PROPERTIES OF BNP IN SMALL UNILAMELLAR VESICLES	121
7.3. DISCRIMINATION OF LIPID PHASES IN GIANT UNILAMELLAR VESICLES BY BNP	125
7.4. MEASUREMENTS OF BNP IN BIOLOGICAL CELLS	130
7.5. DISCUSSION	132
PARTIAL CONCLUSIONS	135
<u>8. TGF-B EFFECT ON OLN-93 CELLS</u>	<u>137</u>
INTRODUCTION	138
8.1. PRELIMINARY STUDIES OF TGF-B EFFECTS ON OLN-93 CELLS	139
8.2. DISCUSSION	145
PARTIAL CONCLUSIONS AND PERSPECTIVES	146
<u>GENERAL CONCLUSIONS</u>	<u>147</u>
<u>BIBLIOGRAPHY</u>	<u>149</u>

LIST OF ABBREVIATIONS

AC	Alternating current
BNP	BODIPY-new probe
BP	Bandpass
BODIPY	4,4-difluoro-4-bora-3a,4a-diaza-s-indacene
Chol	Cholesterol
CL	Cardiolipin
CLSM	Confocal laser scanning microscope
CNS	Central nervous system
DC	Dichroic mirror
DiI-C18(5)	1,1'-dioctadecyl-3,3',3'-tetramethylindodicarbocyanine perchlorate
DMEM	Dulbecco's modified Eagle medium
DMPC	1,2-dimyristoyl -sn-glycero-3-phosphocholine
DPH	1,6-Diphenyl-1,3,5-hexatriene
DPPC	1,2-dipalmitoyl-sn-glycero-3-phosphocholine
DOPC	1,2-dioleoyl-sn-glycero-3-phosphatidylcholine
DRM	Detergent-resistant membranes
EAE	Experimental autoimmune encephalomyelitis
ER	Endoplasmic reticulum
FBS	Fetal bovine serum
FLIM	Fluorescence lifetime imaging microscopy
FRAP	Fluorescence recovery after photobleaching
FWHM	Full width at half maximum
<i>GP</i>	Generalized polarization
GPI	Glycosylphosphatidylinositol
GUV	Giant unilamellar vesicle
HBSS	Hank's balanced salt solution
HEK293T	Human embryonic kidney 293T
HMG CoA	3-hydroxy-3-methylglutaryl CoA
IRF	Instrument response function
ITO	Indium tin oxide
LN	Log-normal function
LUV	Large unilamellar vesicle
LXRs	Liver X receptors
MAG	Myelin-associated glycoprotein
MAL	Myelin and lymphocyte protein
M β CD	Methyl- β -cyclodextrin
MBP	Myelin basic protein
MOG	Myelin oligodendrocyte glycoprotein
MS	Multiple sclerosis
OL(s)	Oligodendrocyte(s)
OPE	One photon excitation
PA	Phosphatidic acid
PBS	Phosphate-buffered saline
PC	Phosphatidylcholine,
PE	Phosphatidylethanolamine
PG	Phosphatidylglycerol
PI	Phosphatidylinositol
PLL	Poly-L-lysine
PLP	Proteolipid protein
PS	Phosphatidylserine
RR-MS	Relapsing-remitting multiple sclerosis

SM	Sphingomyelin
SUV	Small unilamellar vesicle
SV	Simvastatin
T_m	Transition temperature
T09	T0901317 - N-(2,2,2-trifluoroethyl)-N-[4-[2,2,2-trifluoro-1-hydroxy-1-(trifluoromethyl) ethyl]phenyl]-benzenesulfonamide
TCSPC	Time-correlated single photon counting
TGF- β	Transforming growth factor- β
TPE	Two photon excitation

LIST OF SYMBOLS

c	Speed of light
D_{τ}	Diffusion coefficient
h	Planck constant
L_{α}	Fluid (liquid-crystalline) phase
L_d	Liquid-disordered phase
L_o	Liquid-ordered phase
λ_{ex}	Excitation wavelength
λ_{em}	Emission wavelength
Φ	Quantum yield
n	Refractive index
τ	Fluorescence lifetime
τ_D	Diffusion lifetime
S_o	Gel phase

LIST OF FIGURES

Figure 1.1. Lipid molecular shape and a schematic representation of the supramolecular organization they adopt.....	6
Figure 1.2. Microdomains (rafts) structure in biological membranes.....	11
Figure 1.3. A schematic representation of OLs morphological differentiation stages.....	13
Figure 1.4. Schematic representation of myelin sheath segregation.	16
Figure 1.5. Mevalonate pathway	18
Figure 1.6. Statin mechanism of action (left). HMG-CoA and Simvastatin structure.	20
Figure 2.1. Jablonski diagram in which are described the electron transitions of a molecule between ground state and different excited states after absorption of light.	28
Figure 2.2. Schematic representation of solvent relaxation process	31
Figure 2.3. Laurdan molecule (left) and Laurdan emission spectra in the gel and fluid phase of the lipid bilayer	32
Figure 2.4. Structure of the BODIPY core and of the 8-amino BODIPY.....	33
Figure 2.5. Schematic of an epi-fluorescence microscope.....	37
Figure 2.6. Schematic of a confocal microscope	38
Figure 2.7. A schematic representation of Jablonski diagrams for OPE and TPE (Up). Schematics of the fluorescence emission in the microscope focus for OPE and TPE (down).....	39
Figure 4.1. Normalized absorption and emission spectra of Laurdan in homogeneous solutions.	55
Figure 4.2. Decomposition of Laurdan spectra by LN function.	56
Figure 4.3. The relative areas resulted from the fitting with LN function.	57
Figure 4.4. ΔAr -difference between relative areas of elementary calculated for Laurdan inserted in LUVs prepared from DMPC or DPPC(A). The ratio of the LN peak areas (S_G/S_B) for LUVs prepared from DMPC and DPPC(B).	59
Figure 5.1. Fluorescence emission spectra of Laurdan inserted into the membrane of LUVs.	63
Figure 5.2. Variation of GP values with temperature.	64
Figure 5.3. Fluorescence lifetimes of Laurdan.	65
Figure 5.4. Fluorescence lifetimes in the blue and green channel recorded for Laurdan in LUVs (Figure 5.3) versus GP values (Figure 5.2) at corresponding temperatures.....	67
Figure 5.5. Laurdan measurements on GUVs prepared from DPPC.	68
Figure 5.6. Laurdan measurements on GUVs prepared from DOPC.	69
Figure 5.7. Angular dependence of GP and fluorescence lifetimes of Laurdan	70
Figure 5.8. Laurdan in GUVs with L_o/L_d phase separation observed with horizontally, linearly polarized excitation light.....	71
Figure 5.9. Laurdan in GUVs with L_o/L_d phase separation observed with circularly polarized excitation light.	72
Figure 5.10. Distribution of the pixelwise correlation between lifetimes and GP for Laurdan in GUVs.	73
Figure 5.11. Correlation map between GP and fluorescence lifetimes for homogenous GUVs.	74
Figure 5.12. Laurdan in GUVs observed with linearly polarized excitation light at room temperature.	75
Figure 5.13. Laurdan in GUVs observed with circularly polarized excitation at room temperature. ...	76
Figure 5.14. GP and fluorescence lifetime images obtained for Laurdan in HEK293T cells at 21 °C. 77	

Figure 5.15. Laurdan in the plasma membrane of HEK293T cells.....	78
Figure 5.16. Topographic maps of Laurdan in the plasma membrane of HEK293T cells.	79
Figure 5.17. Histogram of <i>GP</i> and fluorescence lifetime values for Laurdan in the plasma membrane of HEK293T cells.	80
Figure 5.18. Average values of <i>GP</i> and fluorescence lifetime for Laurdan in the plasma membrane of HEK293T cells.....	81
Figure 6.1. Morphological changes of OLN-93 cells.	97
Figure 6.2. OLN-93 cell recorded at 21 °C.	98
Figure 6.3. FLIM measurements on OLN-93 cell recorded at 21 °C.....	98
Figure 6.4. Laurdan in the plasma membrane of OLN-93 cells recorded at 21 °C.....	99
Figure 6.5. Laurdan in the plasma membrane of OLN-93 cells recorded at 37 °C.....	100
Figure 6.6. Average <i>GP</i> values for each experimental condition.	101
Figure 6.7. Average values of fluorescence lifetime recorded in the blue channel.	102
Figure 6.8. Average values of fluorescence lifetime recorded in the green channel.	103
Figure 6.9. Topographic maps of Laurdan in the plasma membrane of OLN-93 cells.....	104
Figure 6.10. Topographic maps of Laurdan in the plasma membrane of SV treated OLN-93 cells...	105
Figure 6.11. Laurdan in the plasma membrane of OLN-93 cells recorded at 21 °C.....	106
Figure 6.12. Laurdan in the plasma membrane of OLN-93 cells recorded at 37 °C.....	107
Figure 6.13. Average <i>GP</i> values recorded for each experimental condition.	108
Figure 6.14. Average values of fluorescence lifetime recorded in the blue channel.	109
Figure 6.15. Average values of fluorescence lifetime recorded in the green channel.	110
Figure 6.16. Topographic maps of Laurdan in the plasma membrane of T09 treated OLN-93 cells.	111
Figure 7.1. Chemical structure of the BNP.....	117
Figure 7.2. Spectral characteristics of BNP in different solvents	118
Figure 7.3. Plot of Stokes' shift versus different solvent polarity parameters.	119
Figure 7.4. Plot of the absorption and emission maxima of BNP as a function of $f(n^2) = (n^2-1)/(2n^2+1)$ for all the studied solvents.	119
Figure 7.5. Fluorescence spectra of BNP in SUVs.....	122
Figure 7.6. Excitation and emission spectra of BNP in DPPC SUVs (left) and DSPC SUVs (right)	123
Figure 7.7. Anisotropy curves of BNP in LUVs.....	124
Figure 7.8. Fluorescence intensity image showing the uniform distribution of BNP for a GUV prepared from DOPC.	126
Figure 7.9. Fluorescence intensity images showing BNP and DiI-C18 partitioning in lipid phases of different types of GUVs.....	127
Figure 7.10. The intensity image of GUVs obtained by superimposing the images from a z-stack...	128
Figure 7.11. Distribution of the lifetime values obtained for different lipid phases.	129
Figure 7.12. OLN-93 cells stained with BNP: cross-section (left) and bottom membrane (right).	130
Figure 7.13. BNP fluorescence recorded on OLN-93 cells.	131
Figure 8.1. Effect of different concentration of SV or T09 on the OLN-93 viability.....	139
Figure 8.2. Effect of different concentration of TGF- β on the OLN-93 viability.....	140
Figure 8.3. Effect of different concentration of SV and TGF- β on the OLN-93 viability.....	141
Figure 8.4. Effect of different concentration of T09 and TGF- β on the OLN-93 viability.....	142
Figure 8.5. Apoptotic effects of different concentration of SV and TGF- β on the OLN-93.	143
Figure 8.6. Apoptotic effects of different concentration of SV and TGF- β on the OLN-93.	143
Figure 8.7. Apoptotic effects of different concentration of T09 and TGF- β on the OLN-93.	144

LIST OF TABLES

Table 1.1. Major lipid components of different biological membranes.....	4
Table 1.2 Lipid phases observed in membranes	9
Table 1.3. Composition of CNS myelin in human and rat brain.....	15
Table 4.1. Spectral characteristics of Laurdan emission solvents of varying polarities	54
Table 4.2. T_m of lipids obtained from the fitting with LN function	58
Table 5.1. Transition temperatures (in °C) obtained by analyzing the temperature dependence of GP and lifetimes.....	66
Table 5.2. Fluorescence lifetimes of Laurdan in solvents (room temperature).....	66
Table 7.1. Spectroscopic properties of the probe dissolved in different solvents.....	120
Table 7.2. Lifetimes obtained after 1-photon (342 nm) and 2-photon excitation (840 nm).	121
Table 7.3. Spectroscopic properties of BNP inserted in SUVs with different composition at room temperature	123
Table 7.4. Fluorescence lifetime of BNP in DPPC and DSPC SUVs.....	125
Table 7.5. Average fluorescence lifetimes (in ns) of BNP obtained for the different lipid phases in the various types of GUVs.....	129

CHAPTER 1

GENERAL INTRODUCTION AND AIMS

INTRODUCTION

Although it is known now that biological membranes are complex and dynamic structures, their image evolved over time from a simple model where the lipids were seen solely as a matrix for the embedded proteins to a new image in which lateral heterogeneity prevails. Recently it was shown that local lipid unmixing gives rise to liquid-ordered microdomains, so-called *lipid rafts*, which are characterized by a specific lipid composition and spatial arrangements (Pike 2003). These microdomains are rich in cholesterol and sphingolipids, and characterized by a lower lateral mobility of its components. They received a considerable attention after it was found that raft components can modulate many cellular processes such as signal transduction, endocytosis, etc.

Despite of the intense study, the characterization of biological membrane is burdened by its complexity. For this reason, some of the techniques used to study membrane organization, which are also presented in this Thesis, are applied on model membranes or on cells treated with cholesterol depleting agents.

In this chapter is presented an overview of the biological membrane and some properties of lipid bilayers in general. A description of *oligodendrocytes* (OLs), i.e. the myelin-producing cells of the central nervous system (CNS), and particularly their membrane is also presented. Myelination processes is briefly presented with comparison to neurodegenerative diseases (particularly multiple sclerosis - MS). Because *statins* were suggested in some studies as treatment for MS, cholesterol synthesis and properties of some cholesterol modulation factors (Simvastatin and T0901317) are emphasized.

1.1. Biological membranes

Biological membranes form the protective layer around the cells and cell organelles (mitochondria, endoplasmic reticulum, chloroplasts, lysosomes). Membranes are one of the essential features of the cells as they are responsible for a number of functions indispensable to life, such as transport processes, signal transduction, adhesion, and cell to cell communication. These properties are determined by the chemical composition and especially by the structural features of biomembranes, particularly the proteins, which varies not only among different species, but also among different cell types or different organelles (Berg *et al.* 2002; Hardin *et al.* 2011).

1.1.1. Biological membrane composition and organization

Composed mostly of lipids and proteins, and a small amount of carbohydrates linked covalently to the lipids or proteins, biomembranes are characterized by an impressive molecular diversity. The lipid molecules form the lipid bilayer, the structural frame for all biological membranes in which proteins are embedded.

The lipids found in biomembranes can be divided in three major classes: *phospholipids* (glycophospholipids), *glycolipids* (sphingolipids) and *sterols* (Berg *et al.* 2002). Both phospholipids and glycolipids have an *amphiphilic* structure consisting of a *polar headgroup* covalently linked to two *hydrophobic acyl chains*. Sterols are especially found in eukaryotes. In mammalian cells they are represented by *cholesterol* (Chol) while in plant cells Chol is replaced by other sterols. Although it still has an amphiphilic character, Chol has a completely different structure: a four-ring steroid structure with a short hydrocarbon chain and a hydroxyl group. Because of its structure, Chol is a rigid molecule which cannot form membranes on its own, but plays an important role in maintaining and modulating membrane characteristics. It is found in different quantities depending on the cells, the highest concentration (around 28 %) being found in structures that have a role in protection, like the myelin sheets. Almost all intracellular membranes have a low content of Chol (Berg *et al.* 2002). Conversely, no Chol is found in the membrane of bacteria. As

showed in Table 1.1 not only Chol but also the other lipids have a distinct distribution depending on the type of membrane (Vance and Vance 2002). Because it is essential to the function of certain proteins, the *cardiolipin* (CL), a diphosphatidylglycerol, is mostly found in the inner layer of the mitochondrial membrane and bacterial membranes, similar with phosphatidylglycerol (PG).

An important characteristic of biological membrane is that lipid bilayers are asymmetric, with the different lipid types distributed unequally over the inner and outer layers. While the outer one is enriched in phosphatidylcholine (PC), as well as sphingolipids and sphingomyelin (SM), the inner one is enriched in phosphatidylinositol (PI), phosphatidylserine (PS) and phosphatidylethanolamine (PE) (Vance and Vance 2002). Chol is present in both layers, but in a higher concentration in the outer layer compared with the inner one. Besides the differences between the two layers, it was observed that also, within the membrane plane, lipids have a heterogeneous organization, forming microdomains (rafts).

Table 1.1. Major lipid components of different biological membranes.

Membrane	PC	PE	PS	PI	PG	CL	SM	Glycolipid	Chol	Others
Erythrocyte (human)	20 ^a	18	7	3	–	–	18	3	20	11
Plasma (rat liver)	18	12	7	3	–	–	12	8	19	21
Neurons	48	21	5	7	–	–	4	3	11	1
Myelin	11	17	9	1	–	–	8	20	28	6
Mitochondria	38	29	–	3	–	14	–	trace	3	13
Nuclear membrane	44	17	4	6	–	1	3	trace	10	15
Lysosome	23	13	–	6	–	~5	23	–	14	16
ER	48	19	4	8	–	–	5	trace	6	10
Golgi	25	9	3	5	–	–	7	–	8	43
Inner and outer membrane (<i>E. Coli</i>)	–	70	–	–	20	10	–	–	–	–

^a The values represent the weight percentage of total lipids
Adapted from (Vance and Vance 2002)

Biological membranes contain also many types of proteins and their composition reflects some specialized membrane functions such as ion channels, pumps, receptors, enzymes, etc. Similar to lipids, proteins have both *hydrophobic* and *hydrophilic regions*. The hydrophobic regions are shielded from water and can interact with the hydrophobic regions of the bilayer, while the hydrophilic regions are exposed to the water molecules. Membrane proteins can be classified as *peripheral* (extrinsic) or *integral* (transmembrane) proteins.

Integral proteins can have only a small region inserted into lipid bilayer or can pierce all the way through the lipid bilayer stretching the membrane. Within the membrane, strong interactions are exerted between the hydrophobic regions of the protein and the hydrocarbon chains of the lipids, thus these proteins can be extracted only using detergents. On the contrary, most peripheral membrane proteins are globular proteins that interact with the membrane components by electrostatic forces and hydrogen-bonds. Special types of proteins are the ones anchored to the lipid bilayer through a covalently attached hydrophobic chain (i.e. glycosylphosphatidylinositol (GPI)-anchored proteins). Proteins activity is modulated by the lipid anchors that can either attach or detach from these proteins. The mass ratio of proteins to lipids varies from 0.25, in myelin, to ~ 3, in bacterial membranes, and 3.5 in the inner membrane of mitochondria (Hardin *et al.* 2011).

Far less numerous than lipids and proteins, *carbohydrates* are also essential to cells and cell organelles. They are linked either to lipids (glycolipids) or proteins (glycoproteins) and play a role mostly in binding adjacent cells and communication between cells or cells and their environment. The presence on the external layers of the glycolipids and peripheral proteins contribute even more to the structural asymmetry of biological membranes.

1.1.2. Lipid bilayers

As a consequence of their amphiphilic structure, lipids in aqueous media spontaneously self-assemble into structures that keep their non-polar tails together protected from water, while only the polar heads are facing the water.

Depending on the shape of the lipids (the number of tails and the saturation degree) some lipids form bilayer (cylindrical shaped lipids) and non-bilayer structures (cone shaped and inverted cone shaped lipids) (Figure 1.1). Cardiolipin is the only lipid able to form both bilayer and non-bilayer structures. The non-bilayer structures are represented by the micellar phase and the hexagonal phase. Lipid bilayers are formed from two layers of lipids. Their hydrophobic core acts as a permeability barrier and is formed by the lipid tails while the lipid head groups are facing the aqueous medium forming polar surfaces. The non-bilayer forming lipids (salts of fatty acids, with only one chain, or lipids such as PE, PA, CL) can change the properties of the bilayers if they are mixed with the bilayer forming lipids (PC, PS, PI and SM) (Figure 1.1) (Lasic 1998; Vance and Vance 2002)

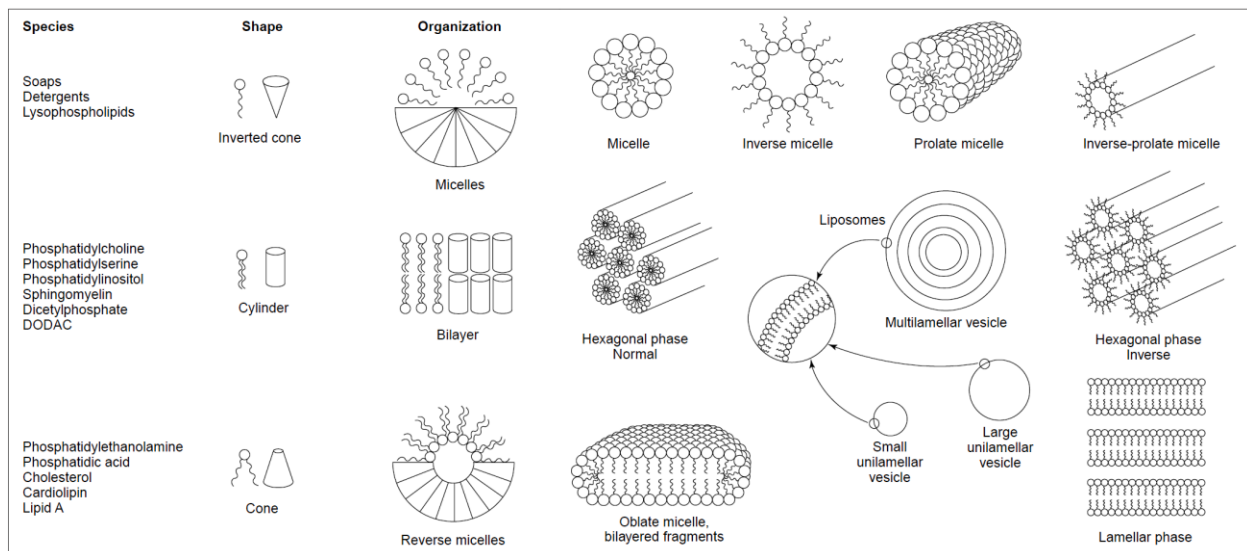


Figure 1.1. Lipid molecular shape and a schematic representation of the supramolecular organization they adopt.

Depending on the shape of the lipids (cylinders, cones or inverted cones) and the ratio between lipids and water, lipid molecules can generate different structures, such as bilayer structure or the non-bilayer ones. Adapted from Lasic (Lasic 1998)

The driving force of lipid bilayers formation is given by the interactions that appear between lipids and other molecules such as lipids or water. As the bilayer forms and the tails interact by hydrophobic forces, the water molecules are excluded from the non-polar core. The close packing of the tails is governed by van der Waals attractive forces, while the interactions between the polar head groups and water molecules are electrostatic and hydrogen-bonding forces. All these forces, but mostly the hydrophobic interactions, held the lipids together in stable structures. Another consequence of these interactions is observed when the bilayer systems that tend to become too extended. In order to protect the lipid chains, found at the edges, to get exposed to water, these systems tend to close on themselves, forming vesicles.

These lipid vesicles (liposomes) are small aqueous compartment surrounded by a lipid bilayer (Figure 1.1). The ability of lipids to form these vesicles has been exploited and now they represent an important tool in both research and medical fields.

1.1.3. Physical properties of lipid bilayer

The lipid bilayers are considered the structural basis of natural membranes. Lipid bilayers properties depend on the type of lipids composing the membrane (saturated, unsaturated or sterols), but also on the temperature of the medium. Thus, their most obvious features are: fluidity, essential for biological systems, and the lateral organization dictated by the interactions between the numerous components.

1.1.3.1. Lipid bilayer fluidity

Biological membranes are dynamic structures where both lipids and proteins are able to diffuse. If the proteins can only diffuse laterally or rotationally around an axis (perpendicular to the bilayer), lipid molecules are capable to three types of movements: rotation around its long axis, lateral diffusion, and jump (“flip-flop”) between the monolayers. All these movements are also encountered in the model membranes. Depending on the membrane composition, the lipid molecules can diffuse laterally very rapidly (0.1-10 $\mu\text{m}^2/\text{s}$). Conversely, the rate of transversal diffusion is slower (once a week) for the model membranes compared with the natural membranes (once in a few hours). The difference is determined by the presence of some enzymes (*flippases*) that facilitate these transitions (Hardin *et al.* 2011).

An important feature of the lipid bilayer is its capacity of transition between two states (phases) characterized by different properties: from a *solid (gel)* phase to a *liquid-crystalline (fluid)* phase upon a sufficient temperature increase. The transition between these two states is observed at a temperature at the *transition temperature (T_m)* which is considered the melting point of the membrane. The movement of membrane molecules, which increases with temperature, is characterizing the *membrane fluidity*. Maintaining the same fluidity of the membrane is essential for the correct operation of membrane processes such as *signal transduction* or *membrane transport*. Membrane fluidity is regulated by phospholipids composition (the length of lipid chains and the degree of saturation), but also by the presence of Chol (Hardin *et al.* 2011).

At low temperature, lipids provided with saturated tails show a tight packing favoured by the interactions between the straight hydrocarbon chains, which leads to a reduced

fluidity. The degree of lipid packing is determined by the length and the degree of unsaturation of the lipid chains. The presence of a double bond causes a kink in the lipid chain disrupting the tight packing, which results in a lower lowering thus the T_m . As there are less interaction between the shorter chains the fluidity is increased with the decrease of lipid chain length (Berg *et al.* 2002). Thus each phospholipids display a characteristic T_m (Silvius 1982).

A special effect on the membrane properties is produced by Chol. Chol inserts into bilayer with its axis along the lipid chains and because of its shape, it disrupts the interactions formed between the phospholipids chains. One consequence of this leads to changes in membrane fluidity: at temperatures above T_m , Chol makes the membrane less fluid, but more fluid at temperatures below T_m (Berg *et al.* 2002). Chol also associates preferentially with some of the lipids (i.e., SM) and proteins, thereby forming specific regions inside the membranes.

Although the facts presented above were mostly obtained on model membranes, they are also relevant for biological membranes. Because the biological membranes contain a wide variety of lipids and also proteins, the phase transition is not so well defined. However, it is known that they still have a T_m bellow the body temperature.

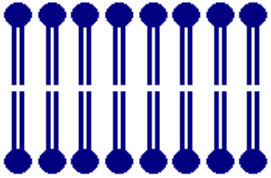
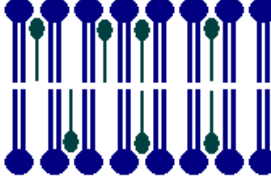


1.1.3.2. Phase segregation of lipid systems

Both biological membranes and model membranes made of lipid mixtures display lateral organization. Many lipid domains with different physical properties can coexist in the membrane (Simons and Vaz 2004). These domains can be directly observed in lipid vesicles.

Usually, one can describe 3 lipid phases: the *solid (gel) ordered* (S_o) phase, the *liquid ordered* (L_o) phase and the *liquid disordered* (L_d)/*liquid-crystalline* (L_α) phase which describe the same phase.

For most of the phospholipids, the S_o phase is observed at lower temperatures. This phase is characterized by a close packing of the hydrocarbon tails which leads to a high molecular order, a reduced fluidity, and low diffusion coefficients. The degree of lipid packing is determined by the length and the degree of unsaturation of the lipid chains. The L_α phase is observed at temperatures above the T_m when the lipid chains “melt” to a more liquid state. This phase is characterized by a low molecular order and high diffusion coefficients (Table 1.2).

Table 1.2. Lipid phases observed in artificial membranes

Lipid phase	Characteristics	Schematic representation
S₀ (pure component)	A rigid lamellar phase (slow translational diffusion) with ordered lipid chains $D_{\tau} = \text{Slow } (10^{-3} \mu\text{m}^2\text{s}^{-1})^1$	
L_o (Binary or ternary mixtures)	A fluid lamellar phase (rapid translational diffusion) with ordered lipid chains $D_{\tau} = \text{Fast } (\sim 1 \mu\text{m}^2\text{s}^{-1})$	
L_d* (Binary or ternary mixtures)	A fluid lamellar phase (rapid translational diffusion) with disordered lipid chains	
L_a* (pure component)	$D_{\tau} = \text{Fast } (\sim 1 \mu\text{m}^2\text{s}^{-1})$	

¹ D_{τ} – diffusion coefficient of the lipid

* For the lipid bilayer with L_o/L_d phase coexistence Chol can be present in both phases, although the concentration in the L_d is much lower than the one in the L_o . Because of this we make a separation between the fluid phase (L_a) attained in one component system and the fluid phase (L_d) attained in binary or ternary lipid systems. The presence of Chol modifies membrane fluidity.

It is important to note that the characterization of these phases is done in a pure lipid system. Upon addition of more lipids, such as Chol, the phase diagram of the bilayer changes. The transitions between phases are not so well defined, an apparent T_m is observed, and different intermediate lipid phases can be found.

Mixing two types of phospholipids with different T_m leads to S_o/L_d phase co-existence (McMullen *et al.* 2004). When mixed with phospholipids, Chol and sphingolipids can cluster together forming two phases (McMullen *et al.* 2004): the L_d formed mostly from phospholipids and a phase enriched in SM and Chol, the liquid ordered phase (L_o). This phase can be considered an intermediate phase between S_o and L_d as it preserves properties

from both of them: a high lipid order, similar to S_o phase but a high lipid mobility, similar to L_d phase.

1.1.4. Supramolecular organization of biological membranes

Although the presence of different lipid domains is easily demonstrated in model systems, the situation is far more complicated for the cellular plasma membrane due to the small size, the finite persistence time of lipid domains and to huge diversity in membrane components (Munro 2003; Simons and Vaz 2004).

In the last decades, a new image of the membrane emerged in which lateral heterogeneity prevails. The local lipid unmixing gives rise to specific microdomains, so-called lipid rafts, which are characterized by different lipid compositions and spatial arrangements (Pike 2003). Thus, the properties of the observed phases in model membranes are thought to be indicative of the microdomains in the plasma membrane (Munro 2003). The L_o/L_d phase separation is used as a simplified model to describe the lipid rafts as L_o microdomains surrounded by a L_d phase. Biological membranes exist mostly in the L_d phase, but the organism can modulate it depending on its needs.

Chol and sphingolipids cluster together with specific proteins found in plasma membrane or in intracellular membranes. The lipid rafts are described as a liquid ordered assemble and are characterized by a reduced lateral diffusion (Brown and London 1998; Edidin 2003; London 2002; Simons and Ikonen 1997). While membrane phospholipids have at least one fatty acid that is kinked, due to one or more double bonds, sphingolipid hydrocarbon chains lack the double bonds. This can be an explanation of why Chol and sphingolipids associate forming microdomains (Simons and Vaz 2004). They are small size regions, on a range of a few tens or hundreds of nanometers, and are considered to be dynamic structures which can associate and dissociate on a nanosecond timescale (Lingwood and Simons 2010) to form stable platforms that are important in signal transduction, viral infection, membrane trafficking and endocytosis (Brown and London 1998; Simons and Ikonen 1997). Lipid rafts are enriched in glycosylphosphatidylinositol- (GPI-) anchored proteins found on their outer side. Also, on the cytoplasmic side proteins are anchored by saturated lipid chains.

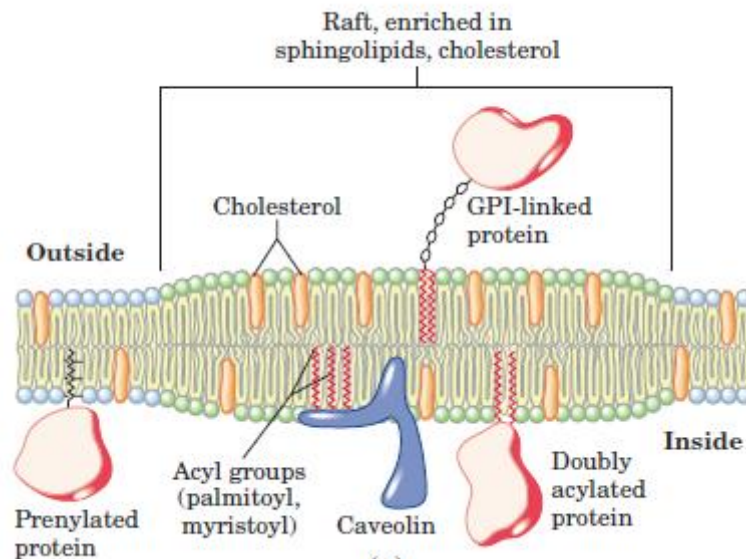


Figure 1.2. Microdomains (rafts) structure in biological membranes, adapted from (Nelson and Cox 2005).

Still under debate, one of the methods used to isolate and characterized lipid rafts is detergent solubilization. The rafts were first suggested when *detergent-resistant membranes* (DRM) were extracted from membranes by means of detergents. These DRM are aggregates of proteins and lipids considered to be tightly packed and thus unable to solubilize in detergents. Although it is accepted that these DRMs are formed during the treatment and are not the real *in vivo* microdomains, they are the starting point for rafts (Brown 2006). The raft hypothesis is still heavily debated as their size is considered too small (< 200 nm) to be detected using the current techniques (Munro 2003).

1.2. Oligodendrocytes

Nervous system cells can be divided into two major categories: *neurons* (cells specialized in electrical signaling) and *neuroglia* (assuring a supporting structure for neurons) (Jessen 2004). Despite glial cells exceeding the number of neurons, half of brain volume are glial cells (Jessen 2004), they were first described by Virchow in 1846 as a connective tissue that glues neurons together (Baumann and Pham-Dinh 2001). Although the glial cell types were characterized by microscopy more than ten years ago (Baumann and Pham-Dinh 2001), their

role in brain development and functioning of the adult organisms were described only recently using molecular biology techniques. In the CNS there are described three types of glial cells: *astrocytes*, *oligodendrocytes* (OLs) and *microglia* cells. In the peripheral nervous system (PNS) two types of cells are found: myelinating and non-myelinating Schwann cells (Jessen 2004).

OLs originate first as motor neuron precursors from the subventricular zone, which start to develop after neuronal and astrocytic signaling (Baumann and Pham-Dinh 2001; Bradl and Lassmann 2010; Jackman *et al.* 2009). Even though a neuronal regulator has not been identified, it is assumed that OLs differentiation is initiated by signaling from neurons that need to be myelinated.

From OL progenitors to myelin-producing cells, OLs go through several differentiation stages, characterized by both distinct morphologies and expression of specific markers (both lipids and proteins) (Figure 1.3). Although immature, OLs can express more markers at the same differentiation stage (Liu *et al.* 2002), some studies showing that immature OLs can also be found in adult brain (Baumann and Pham-Dinh 2001; Polito and Reynolds 2005).

Specific markers for both OL progenitors and pre-OLs are A2B5, GD3 and NG2, which disappear in the latter stages. Compared with OL progenitors which are bipolar, pre-OLs elaborate slightly more processes. In addition glycolipids and sulfatides can be recognized by a new marker, O4 (Jackman *et al.* 2009).

In the Pre-GalC stage, the proliferation stops and represents a transition stage to the terminal differentiation. After this stage, the first OLs surface marker, GalC (galactocerebroside) is present in immature OLs. Beside O4 and GalC, immature OLs also express CNP (2',3'-Cyclic nucleotide-3'-phosphohydrolase), the first specific myelin protein (Baumann and Pham-Dinh 2001; Jackman *et al.* 2009). Non-myelinating OL (observed also *in vitro*) express myelin proteins such as myelin basic protein (MBP), proteolipid protein (PLP), myelin-associated glycoprotein (MAG). Myelin oligodendrocyte glycoprotein (MOG) is expressed only for myelinating mature OL.

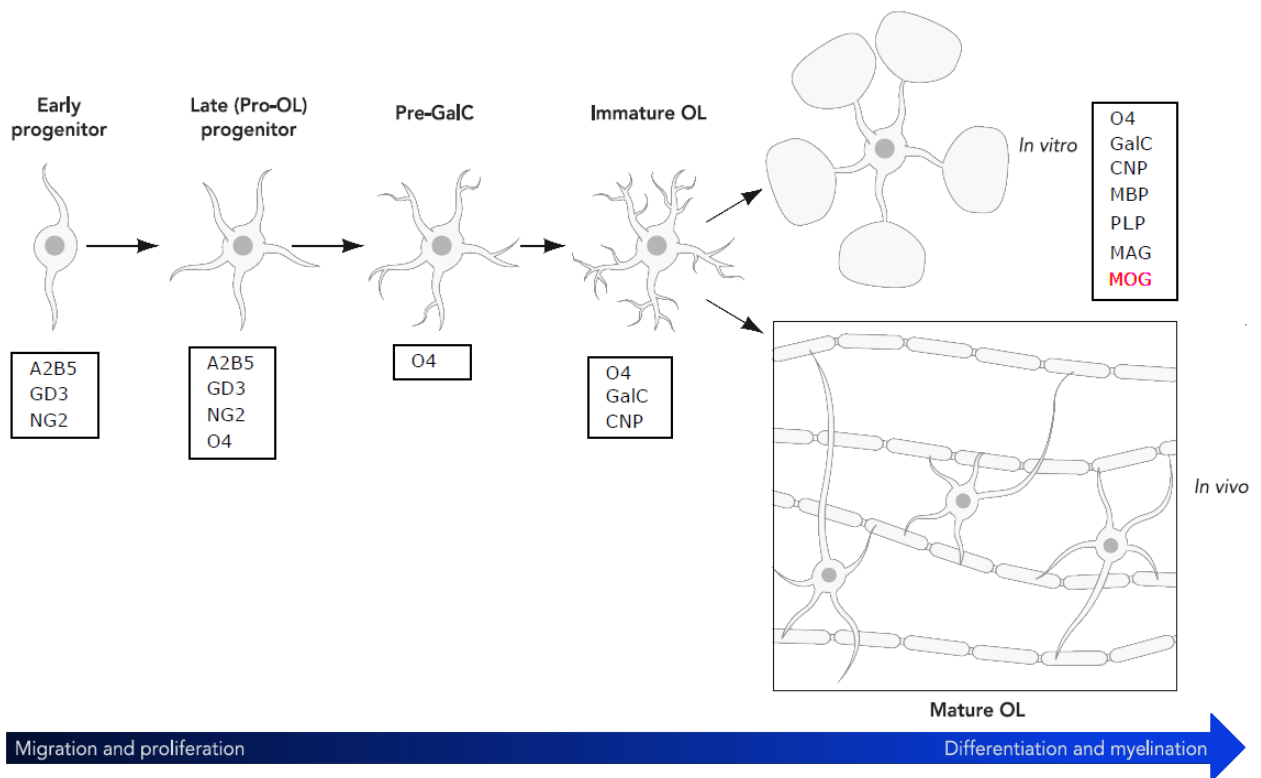


Figure 1.3. A schematic representation of OLs morphological differentiation stages

The stage-specific markers, expressed for each stage, starting from migratory and mitogenic progenitor cells to myelin-producing cells are presented in boxes. Adapted from (Baumann and Pham-Dinh 2001; Jackman *et al.* 2009).

Formation of myelin sheaths around the neuronal axons (myelination) is carried out by the OLs in the CNS and myelinating Schwann cells in the PNS (Jessen 2004). Contrary to Schwann cell, which can form only one myelin sheath around a single axon, single OL can extend many processes which wraps around more than 40 different axons forming the myelin sheaths (Quarles *et al.* 2006). Also, on the same axon, the segments of myelin can belong to different OLs

During myelination both marker expression and OLs morphology is changing and three steps can be observed: (1) extension of OLs processes and formation of a highly branched OL, (2) contact with the axon and initial wrapping and finally (3) formation of the compact myelin sheath (Bauer *et al.* 2009).

The flattened cellular processes are circling around the axon so that the membrane bilayers stacking leads to the formation of the multilayered myelin sheath, which promotes the saltatory conduction. Myelin segments, around 12 nm thick and around 150 μm long,

which provide an electrical insulation around the axon, are separated by *Ranvier nodes* (Aggarwal *et al.* 2011).

The changes that OLs undergo during myelin formation are mediated by cytoskeleton and is thought that microtubules and microfilaments ensures the stability of the extended processes (Bauer *et al.* 2009).

Once assembled, the myelin is a highly stable structure, close to the thermodynamic equilibrium state. This is caused by the high number of hydrophobic molecules (both lipids and proteins) which exercise a repulsive force towards the aqueous regions, but also due to the attractive forces exerted between lipids (Aggarwal *et al.* 2011).

1.2.1. Oligodendrocytes membrane composition

Considering the described processes, the myelin sheaths assembly and stability are ensured by its composition. Thus, myelin proved to be an exception, having a unique composition and architecture. In contrast to most cell membranes, where the percentage of lipids is between 30 % and 50 %, myelin contains more lipids (70-85) % and only (15-30) % represents the proteins, which mostly are myelin specific proteins (Aggarwal *et al.* 2011; Jackman *et al.* 2009; O'Brien and Sampson 1965; Quarles *et al.* 2006). Also, *in situ* myelin has about 40 % water in its composition (Quarles *et al.* 2006). Although myelin composition remains the same, during the different development stages of the brain, there is a variation of the fractions of its components (O'Brien and Sampson 1965; Quarles *et al.* 2006).

Although the galactolipids (galactosylceramide and sulfatide) are not 'myelin-specific' lipids, their concentration is proportional to the quantity of myelin. Aside cerebroside, Chol, found in a higher concentration than in usual membranes (around 25 %), and phospholipids, there are the other two major lipids of myelin. Chol is mostly found on the extracellular face of the myelin membrane.

Even though all mammalian species have the same brain myelin composition, however, some differences are observed: i.e. a lower quantity of sphingomyelin is found in rat myelin compared with the human one (Table 1.3) (Quarles *et al.* 2006).

Table 1.3. Composition of CNS myelin in human and rat brain

Components^{1,2}	Human	Rat
Protein	30	29.5
Total Lipid	70.0	70.5
Cholesterol	27.7	27.3
Cerebroside	22.7	23.7
Sulfatide	3.8	7.1
Lecithin	11.2	11.3
Sphingomyelin	7.9	3.2
Phosphatidylserine	4.8	7
Phosphatidylinositol	0.6	1.2
Plasmalogen³	12.3	14.1
Ethanolamine phosphatides	15.6	16.7

¹Adapted from(Quarles *et al.* 2006)

²Protein and lipid values are given for percentage of dry weight.

³Plasmalogens are primarily ether phospholipid

The highest percentage of myelin proteins is made up of specific proteins, like PLP its isoform DM20 and MBP. Aside from these, in an important amount, which varies with species and age there are: CNP, MAG, MOG. The last two are transmembrane proteins and all can be used as biological markers in identifying the differentiations stages of the cells (Quarles *et al.* 2006).

In the mature myelin sheath, it can be described two clear regions (a compact and a non-compact region), characterized by distinct domains with a different lipid and protein content. The compact region is enriched with galactolipids and the major myelin proteins (MOBP, MBP, PLP, MAL), which have the role to stabilize the membranes. Cytoplasm is excluded from this region. In the non-compact region cytoplasm can still be found. This region includes the abaxonal loops, periaxonal loops, cytoplasmic incisures, and paranodal loops and is enriched with CNP, MAG, MOG, Cx32 (Figure 1.4) (Aggarwal *et al.* 2011; Baumann and Pham-Dinh 2001; Kramer *et al.* 2001).

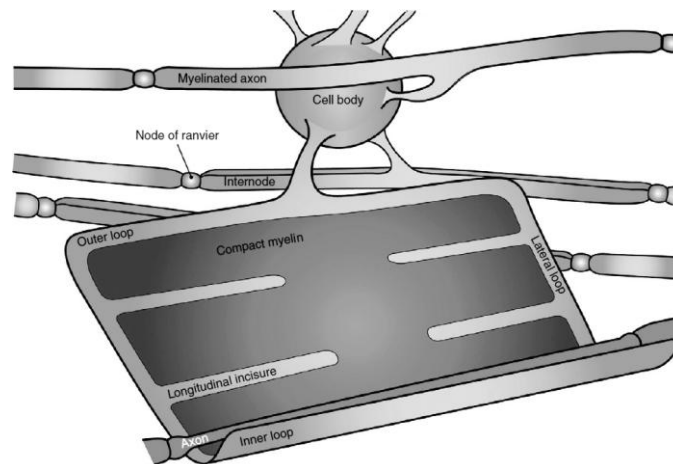


Figure 1.4. Schematic representation of myelin sheath segregation.

Adapted from (Aggarwal et al. 2011; Baumann and Pham-Dinh 2001; Kramer et al. 2001).

The unique architecture of myelin membrane consists of a number of functional microdomains, such as lipid rafts, *caveolae*, different *cellular junctions*, and *tetraspanin-enriched microdomains* (Debruin and Harauz 2007).

Among many others, a possible mechanism by which OLs preserve the myelin membrane composition and structure can be by lipid rafts (DeBruin *et al.* 2005; Gielen *et al.* 2006), .

Different types of proteins have been localized in lipid rafts from Schwann cells, OLs, while CNP and MOG were isolated in DRMs. It was assumed that these microdomains are involved in the signaling mechanisms which initiate myelination, but also in the transport mechanisms of the proteins to the membrane. Aside from these proteins, MBP can also partition into membrane microdomains (DeBruin *et al.* 2005).

Myelin sheaths are essential for the normal activity of the CNS and any change can lead to deficiencies which are observed in some neurological diseases such as *multiple sclerosis* (MS) (Baumann and Pham-Dinh 2001).

1.2.2. Multiple sclerosis

Multiple sclerosis has become one of the most recognized degenerative diseases which affect the glial cells from the CNS. MS is a progressive *autoimmune disease* characterized by myelin breakdown and OLs death *via* apoptotic or necrotic pathways. The myelin is affected by inflammatory mediators produced by activated T cells and afterwards,

the damaged myelin is phagocytosed by macrophages, which may lead to cell death (Bruck and Stadelmann 2003; Merrill and Scolding 1999).

Even if initially it is considered that demyelination leads only to axonal signal transduction loss, with no effects to axons, recently it was shown that axons are directly damaged as well. Axonal degeneration can take place either in the same stage of demyelination, or afterwards, caused by inflammatory mediators (Bruck and Stadelmann 2003). The pathological trademark of MS is the demyelinated plaque followed by the formation of astrocytic scars.

MS appears in early adulthood (between 20 and 40 years), and it is believed to occur in genetically susceptible people (Noseworthy *et al.* 2000; O'Connor 2002), although the factors that initiate the disease are still unknown. A number of symptoms such as fatigue, paralysis, vertigo, visual and sensory loss, cognitive impairment and others were described (Miller and Leary 2007; Noseworthy *et al.* 2000; O'Connor 2002). A high number of patients become walking impaired and for the majority of patients (80-85) % it was observed a relapsing-remitting MS (RRMS), with a higher incidence towards females (2 to 1) (O'Connor 2002). The RRMS episodes are followed by partial or full recovery (Miller and Leary 2007; Noseworthy *et al.* 2000). Because of the neurological losses caused by the disease, approximately half of the patients dies (O'Connor 2002).

Because the causes of MS are not fully understood, studies are still performed both to elucidate the mechanisms and to improve the treatment.

1.3. Cholesterol metabolism in CNS

Chol is one of the most important sterols found only in eukaryotes, mostly in animals and only in smaller amounts in plants and fungi, but which is totally absent in prokaryotes. Although was first observed at the end of XVIII century, its structure was determined only at the beginning of XX century. Chol presence within the membrane leads to an increased lipid order. Found in high quantities in caveolae and involved in the formation of membrane lipid-rafts, it is believed that Chol plays an important role in *endocytosis* and cellular signaling processes (Figure 1.5). Chol is also the essential precursor for the synthesis of steroid hormones (progesterone, testosterone, estradiol, and cortisol), bile acids and vitamin D. Because Chol is essential for the normal functioning of the cell, the modulation of Chol concentration inside the membrane is realized by different internal mechanisms.

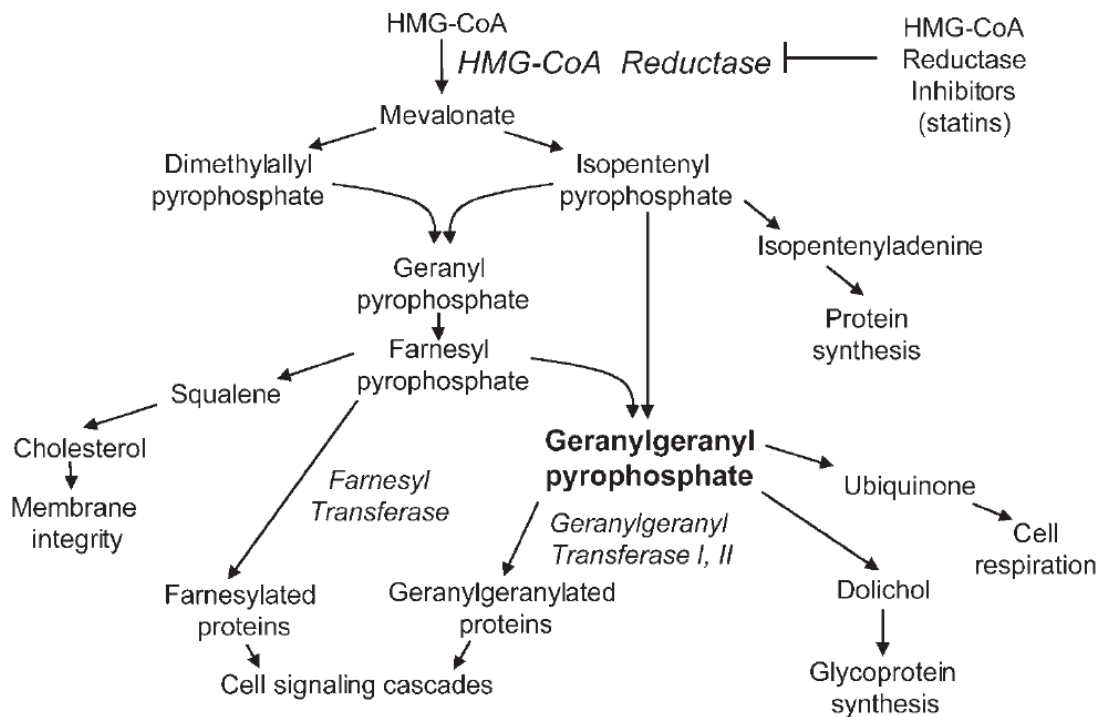


Figure 1.5. Mevalonate pathway (Wong *et al.* 2002)

In the CNS almost all Chol is unesterified and comes from two “pools”: one is represented by myelin (up to 70% of the brain Chol) and the second one by the plasma membrane of neurons and astrocytes (Orth and Bellosta 2012).

Cholesterol is essential for normal brain development and alteration of Chol biosynthesis and transport, cellular uptake of lipids or functioning of the signaling molecules can lead to CNS disease (Orth and Bellosta 2012).

1.3.1. Cholesterol synthesis

The cholesterol used by the body comes both from the *de novo* biosynthesis and dietary cholesterol and has to be closely regulated for a good functioning of the body and to prevent wrong accumulation and deposition within the body, which can lead in the end to different diseases. The biosynthesis of Chol can take place in the liver (~10%) or intestines

(~15%), in the cytoplasm and endoplasmic reticulum (ER) of the cells in a 5 major stage process:

- Starts in cytoplasm with the formation of 3-hydroxy-3-methylglutaryl CoA (HMG CoA) from acetyl-CoA and acetoacetyl-CoA;
- HMG CoA is converted into mevalonate by the enzyme HMG-CoA reductase. This step is important in the control of biosynthesis (see Statins);
- Mevalonate is converted in three steps into 3-isopentenyl pyrophosphate (IPP)-the building block of cholesterol;
- IPP is converted in squalene;
- Squalene is converted into Chol after a chain of reactions (Figure 1.5).

Because Chol synthesis is a process which can consume a large amount of energy, in the adult brain the Chol is synthesized by other cells, like astrocytes, and transported to neurons(Orth and Bellosta 2012).

In CNS there are a number of components involved in Chol metabolism like these:

- apolipoproteins (E, I and J) – that play a role in the distribution of Chol throughout the body (Meir and Leitersdorf 2004),
- ATP binding cassette (ABCA1, ABCG1 and ABCG4) – are Chol transporters and can reorganize the membrane by expanding the non-raft domains (Dean *et al.* 2001),
- Liver X receptors – that are responsible for the maintenance of Chol homeostasis (Laurencikiene and Ryden 2012).

Aside from the internal mechanisms that regulate Chol content, external compounds can be involved when the normal level of Chol is disturbed.

1.3.2. Statins – HMG-CoA inhibitors

Found in high concentrations, Chol represents a major risk factor for human health. Thus, drugs which could keep under control its concentration are permanently under development. The drugs used until 1970 (i.e. niacin, cholestylamin, etc.) had a reduce efficiency and were also unsafe. In 1970, Endo observed that inhibition of HMG-CoA reductase (3-hydroxy-3-methylglutaryl coenzyme A) reduces the Chol concentration (Endo 2008).

The first compound from statin family was mevastatin (Endo 2008). The high efficiency of this class of drugs was due to their competition with HMG-CoA for HMG-CoA reductase, stopping the conversion of HMG-CoA to mevalonate (A. Gaw *et al.* 2003) (Figure 1.6). All statins have a structure similar with HMG-CoA (Figure 1.6) and because of it can bind to the HMG-CoA reductase with a higher affinity than HMG-CoA.

Based on their origin, statins can be divided in natural ones (derived from fungi, like simvastatin, lovastatin, mevastatin, and pravastatin) or synthetic ones (atorva- fluva-, ceriva-, pitava- and rosuvastatin). Also, statins can be divided according to their hydrophilic character into: hydrophilic (pravastatin), hydrophobic (lovastatin, simvastatin, atorvastatin and cerivastatin) and with intermediat characteristics (fluvastatin) (Stancu and Sima 2001).

Statins are responsible for inhibiting HMG-CoA reductase activity and so reducing the synthesis of mevalonate, a precursor not only for Chol but also for a group of proteins involved in the pathways related to the cell proliferation (Chapman-Shimshoni *et al.* 2003; Gullu *et al.* 2005). Inhibiting HMG-CoA reductase the mevalonate pathway is disrupted leading to reduce Chol synthesis and thus modifying the organization of the membranes, reducing the density of Chol found in rafts and so restricting the activity of receptors found in these membrane rafts. Besides its cholesterol-lowering effect, recent experiments have been showed that simvastatin (SV) and other statins have also anti-inflammatory and immunosuppressive effects, facilitating organ transplantation by reducing the incidence of rejecting the new organ (Bjorkhem and Meaney 2004; Yakupoglu *et al.* 2005).

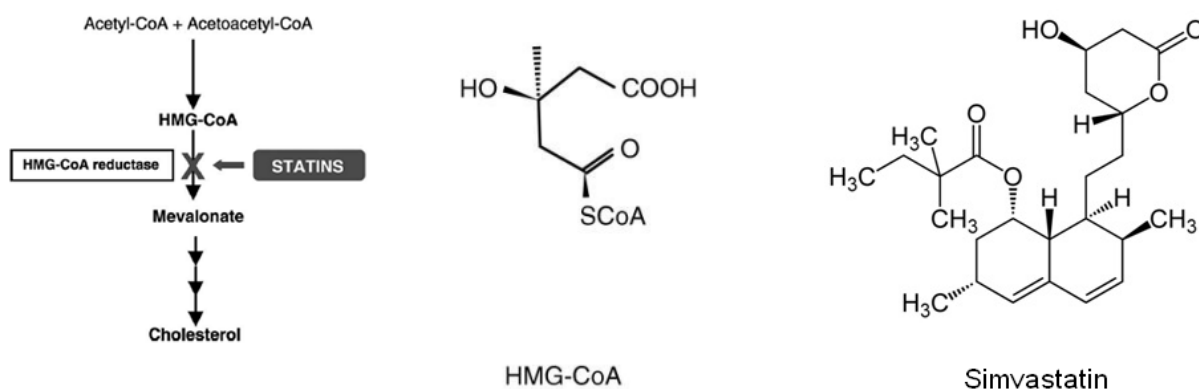


Figure 1.6. Statin mechanism of action (left). HMG-CoA and SV structure.

Adapted from (Vance and Vance 2002)

In the recent years, due to the importance of Chol in the development of neurodegenerative diseases, more reports showed the use of statins in treatment of CNS autoimmune diseases (Bjorkhem and Meaney 2004).

In vivo studies on mice/rat with EAE (Experimental autoimmune encephalomyelitis) were used to understand the benefits of statins in the prevention or the delay of the disease, these findings being further used to clinical trials on patients with RR-MS. Although some studies reported the reduction of the number lesion and relapses (Lanzillo *et al.* 2010; Sena *et al.* 2003), there are also a number of studies that report no significant changes (Paul *et al.* 2008; Rudick *et al.* 2009; Vollmer *et al.* 2004) or even an increase in the disease development (Salvatore *et al.* 2009).

1.3.3. Liver X receptor and T09

Liver X receptors (LXRs) are part of the nuclear receptor superfamily of ligand-activated transcription factors and have two isoforms LXR α (NR1H3) and LXR β (NR1H2) (Baranowski 2008; Zhao and Dahlman-Wright 2010). LXR α is mostly expressed in liver, kidney, adrenal tissue, intestine, adipose tissue, and macrophages, while LXR β can be found in all tissues (Calkin and Tontonoz 2010; Mitro *et al.* 2007). LXRs act as receptor for oxidized Chol and can regulate a variety of physiological processes, like cholesterol, bile acid, triglyceride and glucose homeostasis, but also inflammation and intestinal lipid absorption (Houck *et al.* 2004; Laurencikiene and Ryden 2012). LXR target genes such as ABCA1 and ABCG1 promote the efflux of cellular Chol and help maintain sterol homeostasis. It was suggested that ABCA1 and ABCG1 do not affect membrane Chol content but induce a redistribution of Chol and SM from rafts to non-rafts (Landry *et al.* 2006; Orłowski *et al.* 2007; Vaughan and Oram 2003; Vaughan *et al.* 2009).

T0901317 (T09), one of the most studied agonists for LXR α/β , is used to explore the physiological processes regulated by LXR (Baranowski 2008; Zhao and Dahlman-Wright 2010). *In vivo* it is used for therapeutic effects in different diseases, like atherosclerosis, diabetes, or inflammatory diseases (Baranowski 2008; Mitro *et al.* 2007). Because T09 activates also the bile acid receptor FXR (NR1H4), a receptor with an important role in

glucose metabolism, can induce an increase of hepatic lipogenesis which results in serum hypertriglyceridemia (Houck *et al.* 2004; Mitro *et al.* 2007).

T09 treatment can also lead to a similar change in morphology of OLGs as obtained by simvastatin (Nelissen *et al.* 2010) and it was showed that LXR are responsible for regulating Chol homeostasis in OLs (Nelissen *et al.* 2012).

1.4. TGF- β

Transforming growth factor- β (TGF- β) is a *regulatory cytokine* that mediates physiological processes such as growth inhibition or stimulation, cell differentiation, extracellular matrix synthesis and immune response. It has been shown that TGF- β also has an anti-inflammatory activity (Chen *et al.* 2007). The main function of TGF- β in the immune system is to maintain tolerance *via* the regulation of lymphocyte proliferation, differentiation, and survival. Understanding the function and regulation of TGF- β offers therapeutic promise for the control of autoimmune diseases such as multiple sclerosis (Mirshafiey and Mohsenzadegan 2009). Transforming growth factor- β receptors (TGF- β -R) are also expressed in different cell lines, e.g. oligodendroglial cells (OLI-neu and OLN-93 (Strelau and Unsicker 1999)). Some studies relate the TGF- β -R function to lipid rafts (Chen *et al.* 2007).

TGF- β cytokines binds to two different receptors (type I and type II) that contain serine/threonine kinase domains. Because type I and II receptors have a high affinity for each other form oligomeric complexes with different composition depending on the environment: the oligomeric complexes found in lipid rafts have a larger number of type I receptor leading to a lower binding ratio of TGF- β , whereas the oligomeric complexes localized in non-lipid rafts have more type II receptor and so have a greater binding ratio of TGF- β (Chen *et al.* 2008).

Recent studies shown that lipid-rafts have a role in the regulation of the TGF signaling in different cells: muscular, endothelial, neuronal and Jurkat T-lymphocytic cells (Huang and Huang 2005; Stehr *et al.* 2004). The mechanism that regulates the signal transduction implies capturing the activators of the signaling, preventing the binding of the inhibitors and a rapid assembling of protein-complexes (Stehr *et al.* 2004). Due to this the responsiveness of TGF- β may be potentiated or suppressed changing the cell-surface

environment or plasma membranes components. By Chol depletion using different Chol binding agents, would lead to lipid rafts destabilization and the migration of the proteins to non-lipid rafts domains thus modifying the activities of the proteins. Ma *et al.* studies also show that in the presence of nystatin, the lipid-rafts are destabilized and the interaction between type I and II receptors are affected, leading to a lower binding of the TGF- β thus affecting the signal transduction (Ma *et al.* 2007).

1.5. Aim of the study

Apart of biochemical studies it is important to have also information about the structural organization of OLs both in normal conditions and subjected to Chol depletion treatments. For the studies performed *in vitro* were used OLN-93 cells

The main aim of this Thesis is to observe the changes induced by Chol modulating factors (SV and T09) on membrane organization of OLN-93 cells (RichterLandsberg and Heinrich 1996) derived from spontaneously transformed cells in primary rat brain glial cultures by applying macroscopic and microfluorimetric methods.

This was investigated by microfluorimetric studies of Laurdan and both *generalized polarization (GP)* and *fluorescence lifetimes* were used.

Laurdan, an environment sensitive fluorescent dye was selected because of its unique characteristics: (i) a phase-dependent shift of almost 50 nm of the emission spectra maximum from ~440 nm in ordered lipid phases to ~490 nm in fluid phases, (ii) an equal distribution into the ordered and disordered lipid phases, and (iii) a negligible fluorescence when soluble in water. The behaviour of Laurdan was characterized by *generalized polarization (GP)* based on the spectral changes, and by fluorescence *lifetimes* determined in the *blue channel* for the ordered phase and the *green channel* for the fluid phase.

In a first step, before the studies performed on cells, both spectroscopic and microscopic studies were performed on model membranes (both large and giant unilamellar vesicles) to calibrate and check the rightness of our assumptions.

Based on the model proposed for the model membranes, the studies were extended to the plasma membrane of OLN-93 cells to investigate the changes induced by Chol modulating factors.

One of Laurdan drawback comes from its dipole moment orientation when inserted into the membrane, which causes a photoselection effect. Thus a third step was to use a new fluorescent dye, with the dipole moment orientated parallel to the normal of the membrane. The new probe was first characterized and FRAP measurements were performed in order to obtain information regarding the fluidity of the plasma membranes.

Finally, because the rafts component are considered to modulate cellular processes like TGF signaling, the indirect effects induced by applying Chol modulating agents were observed on OLN-93 cells.

CHAPTER 2

PRINCIPLES OF FLUORESCENCE

Fluorescence techniques (spectroscopic and microscopic) have become some of the most useful biophysical techniques used to study the functions and structures of biological molecules and systems, like the lipid membrane and its components.

This chapter is an overview of fluorescence principles and highlights some particular techniques used in this Thesis.

2.1. Fluorescence principles

The phenomenon in which a molecule or an atom returns from an excited state to its ground state by emission of light (ultraviolet, visible or infrared photons) is called *luminescence*. Based on the nature of excitation method, different types of luminescence can be described: photoluminescence, radioluminescence, chemiluminescence, etc (Valeur and Berberan-Santos 2012). In the particular case of *photoluminescence*, the molecule gets to an electronically excited state by absorption of a photon with the appropriate energy (Lakowicz 2006; Valeur and Berberan-Santos 2012).

After the absorption of a photon, the molecule resides only for a short time in the excited state from where it returns to the ground state through either a *radiative process* (emission of photons) or a non radiative one (heat dissipation). If the excited state, from which the emission takes, is considered, the photoluminescence can be divided in two categories: *fluorescence* (takes place from the excited singlet state) and *phosphorescence* (takes place from the triplet state).

The absorption of a photon by a molecule, promotes an electron from a ground state orbital (HOMO - Highest Occupied Molecular Orbitals) to an unoccupied anti-bonding orbital (LUMO – Lowest Unoccupied Molecular Orbitals) and an excited state is created.

If an electron found on a higher energy orbital has an opposite spin orientation relative to electron in the lower orbital, the multiplicity (the quantity of unpaired electron spin) is 1 (singlet) In this case the molecule is in a *singlet excited state*. When the two electron spins are unpaired (the two electrons have parallel spins), the multiplicity is 3 (triplet) and the molecule is in a *triplet excited state*. Usually, the triplet states will have a lower energy than the corresponding singlet states.

Transitions between states are governed by *Franck-Condon principle* and only those between states with similar multiplicities are allowed: i.e. singlet-singlet and triplet-triplet. Exceptions from the rule can appear because of spin-orbit coupling and are named *intersystem crossing*.

The molecular orbitals that can be occupied in the ground state by electrons are σ , π and n (non-bonding electrons from heteroatoms). When it is excited, the electrons can jump to an anti-bonding orbitals (σ^* and π^*) depending on the energy absorbed. Although a variety of transitions are possible, UV-VIS photons carry energies for which the only possible electronic transitions are from π and n orbitals to π^* orbital. For a transition from σ to an anti-bonding orbital to take place a higher energy is needed.

The amount of energy, E , needed for an electron to jump from an orbital to an anti-bonding one is transported by light in the form of photon:

$$E = hc/\lambda \quad (2.1)$$

where h is Planck's constant ($h = 6.63 \times 10^{-34}$ J s), c is the speed of light in a vacuum ($\sim 3 \times 10^8$ m/s), and λ is the wavelength. As it is observed from the equation (2.1) the energy depends only on the light wavelength: for shorter wavelengths (UV) the photon has a high energy, while for longer ones a smaller amount of energy is transported. Thus, each molecule absorbs only a specific amount of energy which determines an electron to jump to a higher energy state.

The processes that take place from the moment a molecule absorbs the light, till its return to the ground state, are easily explained by Perrin-Jablonski diagram (Figure 2.1). In this diagram the singlet electronic states, depicted by S_0 (ground state) and S_1 , S_2 , etc., for excited states and the triplet states by T_1 are presented. Also, for each electronic state the spin orientation of electrons is sketched. Each of these electronic states are divided in vibrational levels (0, 1, 2, etc.) which can be occupied by the electrons with different energies.

Usually, at room temperature, a molecule is found in the lowest vibrational energy level of S_0 . Absorption of a photon induces the transition of an electron to a higher vibrational level of singlet excited states. This transition is shown in the diagram by upward vertical arrows.

The excited states formed after photon absorption is energetically unstable, thus de-excitation processes, both radiative and non-radiative, will occur quickly.

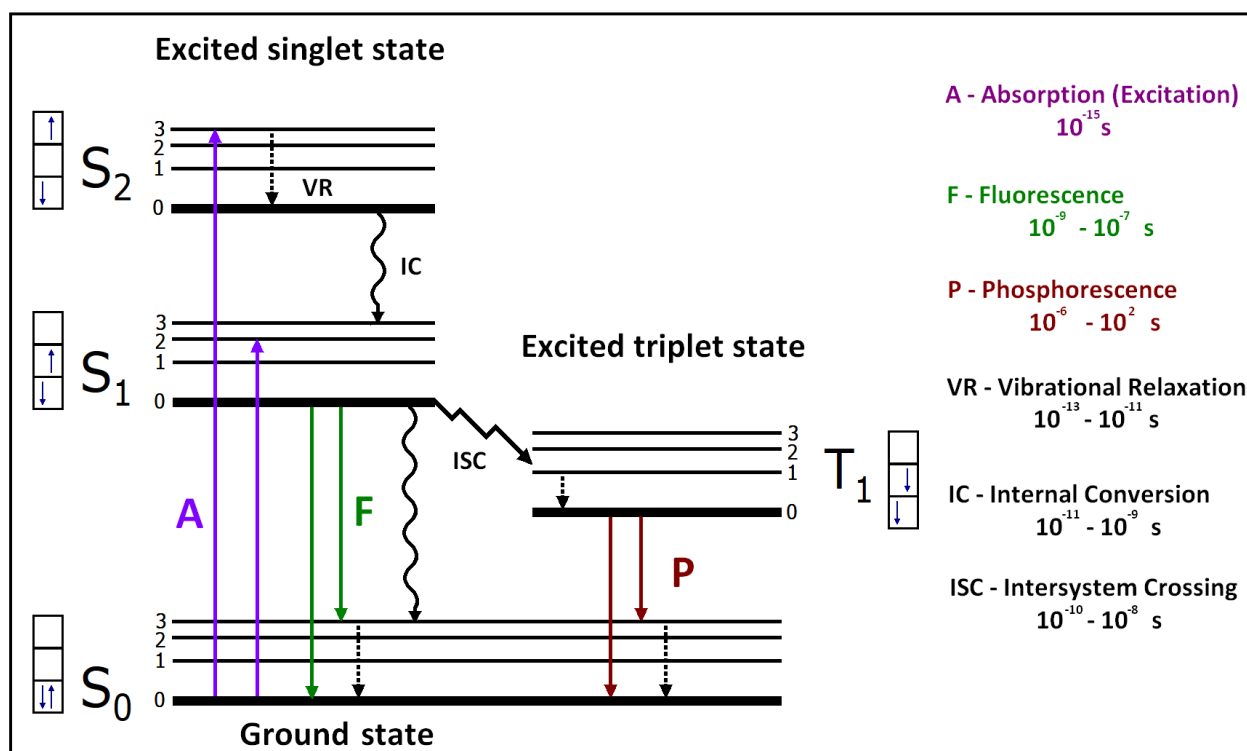


Figure 2.1. Jablonski diagram in which are described the electron transitions of a molecule between ground state and different excited states after absorption of light.

Vibrational relaxations takes place when an electron found on a higher vibrational level of S_1 , rapidly (10^{-13} - 10^{-11}) s relaxes to the lowest vibrational level of S_1 . Internal conversion: IC (10^{-11} - 10^{-9}) s followed by vibrational relaxations to S_1 is observed for molecules excited to a singlet excited state higher than S_1 . Both processes are non-radiative.

De-excitation $S_1 \rightarrow S_0$ (downward arrows) is accompanied by the emission of a photon (fluorescence) with a lower energy (emission is shifted towards longer wavelengths). Usually the electron returns to a higher vibrational level of the ground state, which is observed in fluorescence spectra as vibrational structures. As observed from Perrin-Jablonski diagram, the emitted light will have a longer wavelength (lower energy) than the absorbed light due to energy lost through non-radiative processes like vibrational relaxation.

The difference between the maximum of fluorescence emission peak and absorption is called *Stokes shift*. Based on the explanation presented above we can say that Stokes shift is caused by non-radiative decay. Also the shift can be influenced by solvent effect or different reactions that take place in the excited state.

An electron found in the S_1 state can undergo a de-excitation (non-radiative) process to T_1 , and is called *intersystem crossing*. Singlet-triplet transitions are usually forbidden, but can appear because of spin-orbit coupling, leading to a spin conversion. De-excitation from

T_1 can be either non-radiative (solutions at room temperature) or radiative (at low temperatures). Emission from T_1 is called *phosphorescence* and is red shifted compared with fluorescence. Because transitions from T_1 are forbidden the time of the triplet state can last longer, up to microseconds.

Fluorescence lifetimes and quantum yields of a fluorophore

The most important intrinsic properties of a fluorophore are: *excitation* and *emission wavelengths*, *quantum yield* (Φ) and *fluorescence lifetime* (τ). The last two are dependent on the photophysical characteristics of the fluorophore, such as the radiative and non-radiative de-excitation processes.

The quantum yield represents a quantitative expression of fluorescence efficiency. Φ can be described as the *ratio* of the number of emitted photons over the number of absorbed photons, representing the population of molecules which return to the ground state through a radiative decay, being described by the expression:

$$\Phi = \frac{k_r}{k_r + k_{nr}} \quad (2.2)$$

where k_r and k_{nr} are the radiative and non-radiative decay rates of a molecule, respectively. The non-radiative rate includes all types of non-radiative de-excitation processes.

By definition the values of Φ range between 0 and 1. The value of Φ of a fluorophore depends on the molecular structure and on the environment (i.e. pH, temperature, solvent, polarity, hydrogen bonding, presence of quenchers, etc). Thus, under given conditions, each fluorophore has a specific Φ . The higher the value of Φ the brighter the emission is and easier it is to observe the fluorophore. Small values are a result of a higher fraction of non-radiative decay.

Φ of fluorophores is determined by comparing the integrated emission intensity of the desired molecule with a standard (Williams *et al.* 1983).

The fluorescence lifetime, another important parameter, describes the average time spent by a molecule in the excited singlet state before returning to the ground state, having the following expression:

$$\tau = \frac{1}{k_r + k_{nr}} \quad (2.3)$$

Fluorescence lifetimes range from a few picoseconds (ps) to hundred of nanoseconds (ns). Similar with Φ , fluorescence lifetime of a molecule is influenced by the interactions of the molecule with the environment during its excited state. As τ is characteristic for each

fluorophore and independent of the probe concentration, lifetimes can give additional information that cannot be obtained from fluorescence intensity alone. For example, it may be used to distinguish two fluorophores with almost identical fluorescence emission spectra.

Increasing temperature cause a decrease of both Φ and τ because of the amplification of non-radiative processes dependent on thermal agitation.

Also, k_{nr} is influenced by interactions of the molecule with the local environment (quenching, H-bonding, vibrational relaxation). Thus, changes of k_{nr} determine changes of fluorescence lifetime values, making it a useful tool in investigating the events involving a fluorophore. As τ is characteristic for each fluorophore and independent of the probe concentration, lifetimes can give additional information that cannot be obtained from fluorescence intensity alone.

2.2. Fluorophores

The fluorescent probes (fluorophores) are mostly aromatic molecules which present π bounds. They can be divided into *intrinsic* (found in the system studied) and *extrinsic* (attached to the system to make it fluorescent).

There are only a few intrinsic fluorophores, like aromatic amino acids (tryptophan, tyrosine and phenylalanine), NADH, flavin and chlorophyll, with a poor distribution *in vivo* (like proteins and cells). The presence of these molecules, especially of the amino acids, causes the cells to be fluorescent and this fluorescence is called also cell *autofluorescence*.

Considering that the majority of the systems studied do not exhibit an endogenous fluorescence, the need to “view” these ones, leads to generation of specialized fluorescent probes. The numbers of extrinsic fluorophores are growing in time as new dyes are synthesized to meet the expectations of researchers. Some examples are: fluorescein, rhodamine, prodan, *Laurdan*, BODIPY’s family, DiI’s. Membrane probes can be obtained either by labeling lipid molecules with fluorescent dye or by syntheses of new probes with specific properties: fluorophores sensitive to polarity (i.e. Prodan, *Laurdan*), or to electric potential (ANEPPS).

2.2.1. Solvatochromic dyes

After excitation a molecule is characterized by a new electron arrangement on the higher orbitals, usually resulting in the *increase* of the *dipole moment* compared with the ground state. Because in this situation the solvent molecules surrounding the dye aren't be in the lowest energy arrangement, they suffer a rapid (10^{-11} s) relaxation which leads to a new arrangement characterized by a lower energy (Figure 2.2). For all the dyes sensitive to solvent polarity the loss of energy is observed by a shift to longer emission wavelengths. After emission occurs, the molecule returns to the ground state with the previous arrangement of solvent molecules where a new solvent relaxation process takes place. Because the spectral shift is dependent on the solvent polarity, solvatochromic dyes are considered solvent polarity indicators. Prodan and its derivatives like Laurdan are an example of solvatochromic dyes.

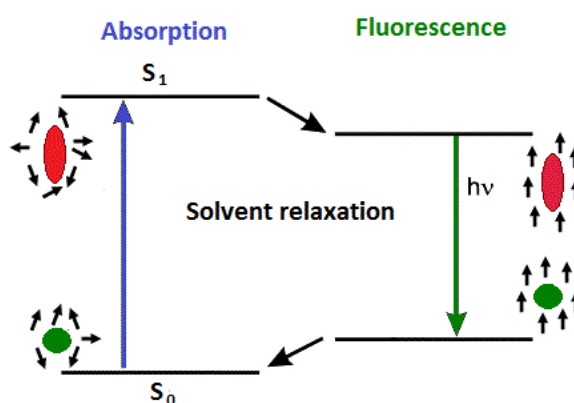


Figure 2.2. Schematic representation of solvent relaxation process

2.2.2. Laurdan

The solvatochromic dye Laurdan (6-dodecanoyl-2-dimethylamino naphthalene) has been shown to be useful in the exploration of membrane properties (Bagatolli *et al.* 1999; Parasassi *et al.* 1991). In homogeneous solutions an increase of the solvent polarity (from dodecane to methanol) induces a shift of the emission maximum from ~ 390 nm to ~ 500 nm (Parasassi *et al.* 1991). Laurdan has a 12 carbon aliphatic tail, facilitating the insertion into lipid membranes (Figure 2.3). It is generally assumed that the dipole moment of the naphthalene moiety is oriented along the normal to the membrane (Bagatolli 2006; Bagatolli *et al.* 1999; Sanchez *et al.* 2007). Upon excitation the dipole moment increases (Tomin *et al.*

2003). The red spectral shift due to the relaxation of water molecules near the naphthalene moiety depends on the state of the lipid phase (Figure 2.3) (Parasassi *et al.* 1998; Sanchez *et al.* 2007).

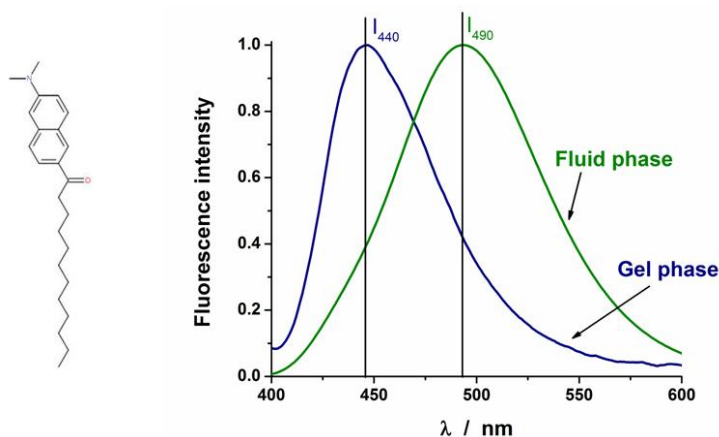


Figure 2.3. Laurdan molecule (left) and Laurdan emission spectra in the gel and fluid phase of the lipid bilayer

Because of the orientation of the naphthalene moiety in the membrane, the fluorescence intensities depend on the orientation of the membrane with respect to the polarization of the incident light. The resulting photoselection depends on the lipid packing order. For giant unilamellar vesicles (GUVs) composed of a single type of lipid which are in gel phase (i.e., S_0) the fluorescence intensity depends strongly on the orientation of the membrane. A much reduced dependency is observed for the liquid-crystalline phase (i.e., L_α) because of the rather loose packing of the lipids (Bagatolli and Gratton 1999; Parasassi *et al.* 1997).

Using the fluorescence intensities of Laurdan at 440 nm (I_{blue}) and 490 nm (I_{green}), the so-called generalized polarization (GP) is defined as the ratio $(I_{blue} - I_{green}) / (I_{blue} + I_{green})$. Theoretically, GP values can range from +1 (no solvent effects) to -1 (strong solvent effects) (Parasassi *et al.* 1991). The GP has been proven to be an adequate tool for characterizing lipid phases in small and large unilamellar vesicles (Parasassi *et al.* 1990; Parasassi *et al.* 1991; Parasassi *et al.* 1994; Parasassi *et al.* 1998), GUVs and cell membranes (Bagatolli and Gratton 2000; Kubiak *et al.* 2011; Owen *et al.* 2012; Sanchez *et al.* 2011; Yu *et al.* 1996). Both lifetime spectroscopy measurements (Mukherjee and Chattopadhyay 2005; Parasassi *et al.* 1995) and fluorescence lifetime imaging microscopy (FLIM) (Schneckenburger *et al.* 2004; Yu *et al.* 1996) showed that the fluorescence lifetime of

Laurdan depends on the lipid packing order. The lifetime measurements reported in the literature are considering the whole emission band and are analyzed in terms of a single relaxation constant. Also lifetime gating has been suggested to enhance the *GP* contrast (Owen and Gaus 2010).

2.2.3. BODIPY

Throughout the family of fluorescent dyes, derivatives of 4,4-difluoro-4-bora-3a,4a-diaza-s-indacene (BODIPY) have a high potential due to their spectroscopic properties (Krasnowska *et al.* 1998).

BODIPY based dyes have strong absorption and fluorescence bands in the visible spectral range and have, depending on their specific structure and the environment, a high fluorescence quantum yield. Their potential was first noticed after they were used as laser dyes. They are characterized by high laser efficiencies, high photostability and efficiency, low non-radiative deactivation rate constants, low triplet-triplet absorption, and low sensitivity to medium effects (Baumgart *et al.* 2007; Niu *et al.* 2009).

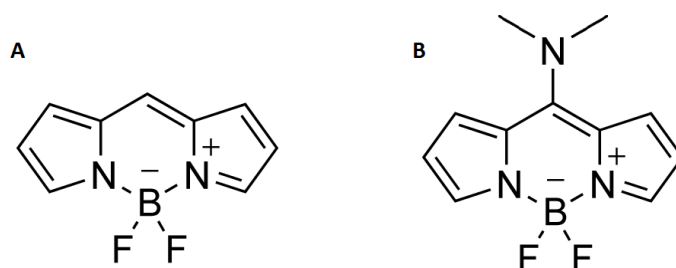


Figure 2.4. Structure of the BODIPY core and of the 8-amino BODIPY.

Attaching an amino group in the mezzo position (B) makes the emission spectra blue shifted compared with the unsubstituted form (A).

There is growing interest in using BODIPY based probes in life-science research (Baumgart *et al.* 2007). These newly developed BODIPYs can be used as fluorescent sensors (Boens *et al.* 2011) as well as biological labels obtained by linking biomolecules to one of their pyrrole rings (Boldyrev *et al.* 2007). New probes synthesized by covalently linking fatty acids, phospholipids, glycolipids or sterols to the BODIPY hydrophobic core, proved to be

useful for membrane research (Boldyrev *et al.* 2007; Jorge Bañuelos *et al.* 2012; Juhasz *et al.* 2012; van Meer *et al.* 2008).

While most BODIPY dyes have an emission in the red region of the spectrum, blue light emitting BODIPY probes are far less considered (Bañuelos *et al.* 2011). An example of a blue emitting BODIPY based probe is shown in Figure 2.4.

2.3. Fluorescence spectroscopy

Fluorescence signals contain information related to the microenvironment of the dye. The necessity to properly measure these signals determined the construction of the instruments able to record fluorescence intensity, fluorescence spectra, polarization of emitted light, and lifetimes. The instruments normally used for these types of measurements are *fluorometers* designed in accordance with the desired type of measurement.

Fluorescence measurements can be divided in two types: *steady-state* and *time resolved spectroscopy*.

In steady-state measurements the fluorophore is continually illuminated while the emission intensity is detected and recorded. The measurements yield a value related to the time integral of the time resolved intensity, $I(t)$, decay:

$$I(t) = I_0 e^{-\frac{t}{\tau}} \quad (2.4)$$

where I_0 represents fluorescence intensity at $t = 0$.

For time resolved measurements sources with very short light pulse (much shorter than the fluorescence lifetime) are used and the intensity decay is recorded.

2.3.1. Steady – state fluorescence

Steady-state measurements give spectral information (excitation and emission spectra) regarding the studied fluorescent molecules. Steady-state spectroscopy holds an advantage in the cheap instrumentation and in the simplicity of its operating system. At the same time, the major disadvantages can be counted, such as: the loss of information caused by the averaging process, and also errors caused by high concentrations and optical properties (Lakowicz 2006).

A typical fluorometer for steady state measurements has a light source (the most commune lamp sources are xenon arc lamp), the optical component, and a high sensitive detector (photomultipliers, most commonly used).

Besides of the excitation and emission spectra, anisotropy measurements can be performed on the same system if polarizers are set into the excitation and emission light paths.

When describing fluorescence anisotropy, we have to take into account the electromagnetic properties of light, especially its associated electric (E) and magnetic (B) field vectors. The two field vectors are oscillating in phase, perpendicularly to the direction of propagation, but as well to each other. Considering these properties, in the case of *natural light*, the electric field vector is randomly orientated, but for the *polarized light* a particular direction is selected.

For a molecule to be excited when the light is *linearly polarized* depends on the angle formed between the molecule absorption transition moment and the electric field vector. Thus, from a population of isotropic oriented molecules those with the transition dipole oriented parallel to electric field vector are preferentially excited. This *photoselection* phenomenon leads to an anisotropic distribution of the excited fluorophores so that the emitted fluorescence is unevenly distributed.

Any change in direction of the transition moment during the lifetime of the excited state will cause this anisotropy to decrease, i.e. will induce a partial (or total) *depolarization of fluorescence*.

For anisotropy measurements, the light is *vertically polarized* and the emission fluorescence is recorded through an analyzer with the principal axis oriented parallel or the perpendicular to the polarization of the excitation light. The *steady-state anisotropy*, r , can be described as:

$$r = \frac{I_{\parallel} - I_{\perp}}{I_{\parallel} + 2I_{\perp}} \quad (2.5)$$

where I_{\parallel} and I_{\perp} are fluorescence intensity components polarized parallel and perpendicular to the direction of incident light, respectively.

When polarized light is used to excite a molecule whose excitation dipole is oriented nearly parallel to the polarization of the excitation pulse, it is possible to separate the parallel and perpendicular components of the emitted fluorescence signal and to extract rotational diffusion constants.

Fluorescence polarization studies can offer important information with regard to the mobility and size of a molecule, fluidity/order of a medium (e.g., lipid membranes).

2.3.2. Time resolved fluorescence

Because of the short lifetimes of fluorophores, the Fluorescence lifetime measurements need detectors and signal processing electronics within sub-nanosecond resolution. There are two methods used to obtain information about the lifetime state which employ either the time or frequency domain.

In the *time domain*, a short light pulse is used to excite the fluorophore, usually on the timescale of ps or recently, fs. For time domain measurements, the *time-correlated single photon counting* (TCSPC) is the most common method used. This method relies on detecting the first emitted photon after an excitation pulse is applied and recording the time, t , at which it arrives at detector. The first photon arrival time is recorded and allocated in a corresponding bin of a *distribution histogram*. The procedure is repeated until enough photons have been detected and the histogram of the arrival of photons is constructed. After a sufficient number of photons are collected (at least, 10,000) we can say that the histogram represents the real fluorescence intensity decay allowing to determine the fluorescence lifetime.

Ideally, the pulse profile of a laser should be infinitively short (delta pulse), but practically it is not. Thus, for determining the fluorescence decay (lifetime) a deconvolution procedure is carried out considering the impulse response function (IRF).

In the *frequency domain*, the dye is excited this time by a steady state light source which is modulated by a high frequency. The fluorescence signal is modulated at the same frequency but, compared with the excitation signal, the phase is delayed and the amplitude demodulated. These differences in the signal contain the lifetime information of the dye.

Time resolved measurement can be used to discriminate between two fluorophores with similar emission spectra if their lifetimes are sufficiently separated. Furthermore, the contribution of each fluorophore will be known.

Another great advantage of time resolved spectroscopy is that fluorescence lifetimes are typically independent of concentration (Lakowicz 2006). This helps in eliminating errors arising from experimental mistakes as well as from changes of the probe concentration due to alterations induced by the environment (cellular imaging). Even though, time resolved spectroscopy instrumentation is expensive and requires a higher skill to operate, it does overcome the main problems associated with steady state spectroscopy.

2.4. Fluorescence microscopy

Microscopy is a powerful investigation technique which allows us to visualize the structure of living organism and to understand their functions. Microscopes can be used to record on living organism and trace different processes important for them. As the needs (a better imaging) increased over the years also the applications displayed a big growth in a variety of fields. Many types of microscopes can be used, each with distinct function and applications: bright field microscopy, epi-luminescence microscopy, confocal microscopy, etc.

Fluorescent microscopy proved to be very useful in the study of cells as is extremely sensitive and many dyes can stain specific structures or molecules inside the cell. Also using different fluorophores one can stain more biological structures, which can be simultaneously detected.

The fluorescence microscopy takes advantage on the fluorophores properties: emission light is shifted to longer wavelength than the excitation one. With this, the emission can be separated inside the microscope with the help of its optics: the excitation and emission filters and the dichroic mirror (Figure 2.5). The filters select only the needed wavelengths, while dichroic mirror allows the passage of light selectively: the excitation light is reflected, while the emission one is transmitted. The emission is collected through the emission filter with a CCD camera. The excitation sources can be lamps (halogen, xenon, etc.) or lasers.

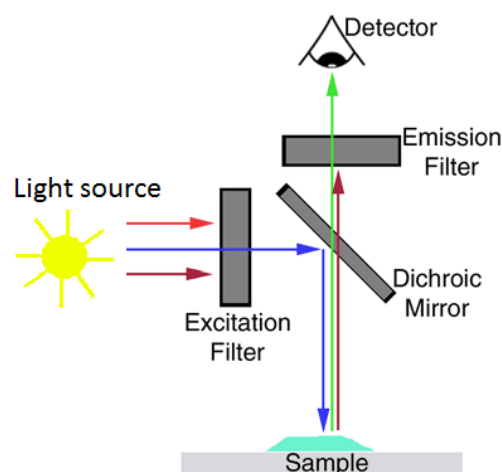


Figure 2.5. Schematic of an epi-fluorescence microscope

2.4.1. Confocal fluorescence microscopy

Compared with the conventionally optical microscopy, the confocal microscopy provides a higher resolution and a much thinner optical section, and thus could be used for 3D imaging by recording a z-stack.

The confocal microscope gives a better image by eliminating the out-of-focus light collected from the sample. This is achieved by adding a pinhole on both the excitation and emission light paths (Figure 2.6). The excitation sources are usually lasers and for the detection both CCD and PMTs can be used. The imaging of an optical section of the sample is obtained through scanning the specimen and recording the information from each pixel.

The microscope can be used in both transmission and reflection modes and also for fluorescence imaging. An advantage of using the fluorescence confocal microscope is the diminution of the damage (*photobleaching*) induced to the fluorophores.

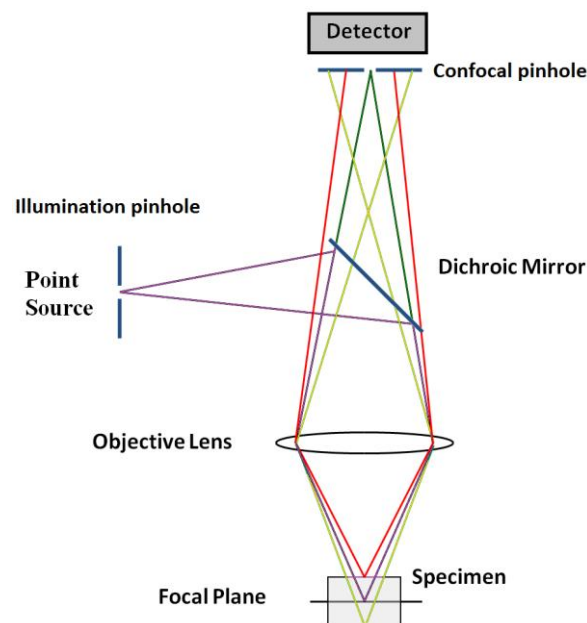


Figure 2.6. Schematic of a confocal microscope

2.4.2. Multiple-photon Excitation Fluorescence Microscopy

Another improvement was obtained through *multi-photon excitation fluorescence microscopy*. This is based on a particular property of a fluorescent dye. If two photons arrive almost simultaneously at a fluorophore, they can combine their energies and can promote the molecule from a ground state to an excited one (Figure 2.7). Because the energies of the photons that reach the molecule add and produce the effect of the ordinary (one-photon) excitation light, they can have a wavelength double of the needed one. The process is named *two-photon excitation* (TPE) and it constitutes the most common multi-photon fluorescence application in cell biology. The probability of two photons to arrive at the same time is higher in the focal point of the system, if the region imaged is thinner compared with the one obtained by OPE. Also, because the excitation light has a longer wavelength it can penetrate deeper into the specimens. Another advantage is the reduced photobleaching effect. TPE can be seen as an alternative to confocal microscopy. Because the multi-photon absorption process needs a very high density of photons, the excitation sources are usually ps-to-fs-pulsed lasers, the pulse width is in the range of 20 fs to 5 ps, with a high repetition rates of 10 -100 MHz. Because the majority of the dyes used are excitable in the near UV or visible range of the light spectrum the laser used are in the near-infrared region (Ti:Sapphire laser covers the spectral region from 700 to 1200 nm).

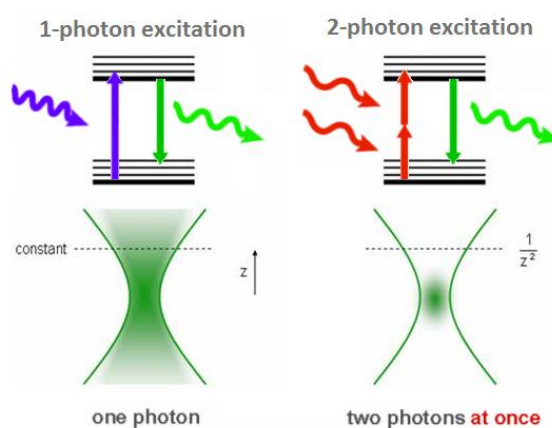


Figure 2.7. A schematic representation of Jablonski diagrams for OPE and TPE (Up). Schematics of the fluorescence emission in the microscope focus for OPE and TPE (down)

2.4.3. Fluorescence lifetime imaging. Two-photon Fluorescence Lifetime Imaging

An advantage of the pulsed lasers with MHz repetition rates is the capability of performing fluorescence lifetime imaging (FLIM). For FLIM the measurements are performed in TCSPC mode and from the images resulted additional information can be extracted as we obtain a spatially resolved distribution of the fluorescence lifetimes. By FLIM measurements one can obtain complementary information on the environment of the dye (fluidity, polarity, pH, etc.). The distinct lifetime of the dyes allows discriminating between regions which might have similar fluorescence intensity. Also, autofluorescence in living cells can be separated from the fluorescence of the fluorophores. A number of FLIM applications to cell biology have been reported: FLIM-FRET, calcium imaging, protein-protein interactions, etc (Becker 2012; Elangovan *et al.* 2002).

A disadvantage of FLIM is the time needed to record an image, which can take up minutes, and sometimes even tens of minutes. The interpretation of the lifetimes in proper biological and biochemical terms can be challenging.

CHAPTER 3

MATERIAL AND METHODS

3.1. Cell culture

3.1.1. OLN-93 cells

OLN-93 cells, derived from primary rat brain glial cell cultures, were obtained from Professor C. Richter-Landsberg (Department of Biology, Molecular Neurobiology, University of Oldenburg, Germany). To avoid changes of cells properties due to over-subculturing, the cells were used until the passage number 10 (Buckinx *et al.* 2007).

The cells were grown on poly-L-lysine (PLL) (50 µg/mL) coated glass cover slips (20,000 cells/24 mm cover slip) in Dulbecco's modified Eagle's medium (DMEM) (Invitrogen/Gibco, Carlsbad, CA, USA) with 10 % fetal calf serum (FCS), 100 U/mL penicillin and 100 µg/mL streptomycin (Invitrogen/Life Technologies) in a humidified incubator at 37 °C and 10 % CO₂.

To induce differentiation, OLN-93 cells were cultured for 24 h and after this period, the medium was removed and exchanged to medium with 0.5% FCS for another 48 h.

3.1.2. HEK293T cells

HEK293T cells (kindly provided by Dr. R. Konickx, Jessa Hospital, Hasselt, Belgium) were grown for two days on PLL (50 µg/mL) coated glass cover slips (20,000 cells/24 mm cover slip) in DMEM with 10 % FCS, 100 U/mL penicillin and 100 µg/mL streptomycin in a humidified incubator at 37 °C and 5 % CO₂.

3.1.3. Cell treatment

OLN-93 cells were treated with different concentrations of the lipophilic simvastatin (Calbiochem, Darmstadt, Germany) to induce different stages of Chol depletion. Initially four concentrations were tested 0.1, 1.0, 2.5 and 5.0 µM, from a stock solution of 10mM in DMSO to determine those that are not toxic for the cells. According with the results obtained and the ones presented in literature, the final concentrations selected are 0.1 and 1 µM (Buckinx *et al.* 2007). For concentrations higher than 2.5 µM, SV becomes toxic for the

cells changing very drastically their morphology and properties (Buckinx *et al.* 2007). The treatment started at the same time with the application of 0.5% FCS medium and lasted 48h before cell samples were studied.

Treatment of OLN-93 cells with the synthetic LXR agonist T0901317 (Cayman Chemical, Tallinn, Estonia) was done to induce Chol efflux from the membranes. Cells were treated for 72 h with 1 μ M or 10 μ M T0901317 (T09) from a stock solution of 10 mM in ethanol. These concentrations were previously proved to be non-toxic to cells from CNS (Whitney *et al.* 2002)

A more extreme depletion was obtained by treating both OLN-93 and HEK293T cells with 10 mM methyl- β -cyclodextrin (M β CD) for 90 min at 37 °C (Leventis and Silvius 2001).

3.1.4. Cell staining

Cells were washed with DMEM without phenol red (Invitrogen/Gibco) and then incubated for 30 min with Laurdan (10 mM in DMSO) at a final concentration of 5 μ M in DMEM without phenol red.

BNP was synthesized at was done at KULeuven by Volker Leen. For BNP staining of the membrane, the cells were incubated for 1h at 37°C, to a final concentration of 20 μ M. BNP stock solution concentration was 10 mM in DMSO. Finally, the cells were washed with HBSS (Hank's Buffered Salt Solution) and kept in HBSS during the performed measurements.

3.1.5. Determination of cell viability

Cells viability was assessed with a colorimetric CellTiter 96 AQueous One Solution Cell Proliferation Assay (MTS) kit (Promega, Madison, WI, USA). The samples were incubated at 37 °C for 4 h and after were measured at 490 nm with a Mithras LB 840 microplate reader from Berthold. The quantity of formazan processed by cells is directly proportional to the number of living cells in culture and the percentage of viable cells is determined by:

$$\% \text{ Viable cells} = (A_p - A_n) * 100 / (A_o - A_n),$$

where: A_p is the absorbance at 490 nm of the treated cells, A_n is the absorbance for the control cells and A_o is the absorbance for the blank.

3.1.6. Determination of apoptosis

Apoptosis was assessed with the Caspase-Glo 3/7 Assay kit, which can measure caspase-3/7 activities. The assay provides a proluminescent caspase-3/7 DEVD-aminoluciferin substrate which is cleaved by the caspase liberating the aminoluciferin. The aminoluciferin is consumed by the luciferase, generating a luminescent signal which is proportional to caspase-3/7 activity. The cells were incubated at room temperature for 2h and after that, the luminescence was measured with the Mithras LB 840 microplate reader.

3.2. Lipid vesicles

Biological membranes have a complex structure, due to hundreds of components (different types of lipids and proteins) from which they are composed. Therefore, using model systems, in which the composition of the membrane is controlled by the user, represents an easy way to study and understand specific biomembrane properties.

Model membranes are used mainly because, in this case, one can control the components used, the solutions and temperature, the membrane size and shape. They can be easily prepared in the laboratory, either from natural or synthetic lipids, they are reproducible with a high homogeneity, and they are stable during measurements. Model membranes can be easily used for spectroscopy and microscopy measurements. The organization adopted and the properties of lipid domains in different conditions (different composition, temperature, the absence/presence of other molecules: sterols, proteins) can be monitored using fluorescent lipid probes.

There are different types of model membranes, from *vesicles* (liposomes) to *lipid monolayers* and *planar lipid bilayers* (BLM). The type used in the studies depends on the parameters (properties), as all of them present advantages and disadvantages.

Liposomes can be prepared using different techniques resulting in vesicles of different sizes:

- SUVs (small unilamellar vesicles) obtained by sonication,
- LUVs (large unilamellar vesicles) obtained by extrusion, and
- GUV (giant unilamellar vesicles) obtained by electroformation.

In our studies, lipid vesicles with different compositions and sizes were used: LUVs for the spectroscopic studies and GUVs for the microscopic studies. Their preparation is presented below.

3.2.2. LUVs preparation

LUVs with different lipid composition were prepared by extrusion. Briefly, the appropriate amount of lipids from the stock solutions, prepared in chloroform, were mixed and dried under nitrogen flow. The lipid film was then hydrated with PBS, heated above the phase transition temperature (T_m) of the lipids used, and vigorously vortexed, resulting in a suspension of multilamellar vesicles (MLVs). The MLV suspension was subjected to 5 freeze-thaw cycles and extruded (15 times) through a 200 nm polycarbonate membrane using a standard extruder (Avanti Polar Lipids, Alabastre, AL, USA). The extrusion was performed at a temperature above T_m of the lipids used, resulting in a suspension of LUVs with a final lipid concentration of 50 μ M. Three types of liposomes were prepared: 100 % DMPC, 100 % DPPC, and a mixture of DMPC/Chol (4:1 weight ratio). After liposome preparation, Laurdan from a stock solution prepared in DMSO was added into the samples to a final lipid:probe molar ratio of 500:1.

3.2.3. GUVs preparation

Giant unilamellar vesicles (GUVs) with a diameter varying between 10 and 100 μ m were prepared by the electroformation method (Angelova and Dimitrov 1986) in a home-made closed holder using two square indium tin oxide (ITO) coated coverslips (Prazisions Glas & Optik GmbH, Iserlohn, Germany) separated by a 3 mm rubber spacer. Before each measurement, a fresh solution containing lipids (1.2 mM in chloroform) was mixed with the dye needed and a few drops (10 μ L) were placed on the surface of the bottom ITO-cover glass and the solvent was dried in an oven at 50 $^{\circ}$ C (15 min). After the chamber was assembled, Milli-Q water was added, at a temperature above T_m of the lipids used, and an AC voltage of 1.5 V amplitude at 10 Hz was applied for 30 min. GUVs images were recorded at room temperature. Three types of GUVs were prepared: 100 % DPPC, 100 % DOPC or a

mixture of DOPC/SM/Chol (1:2:1 molar ratio) with a probe:lipid ratio of 1:2,000 for all the dyes used.

3.3. Spectroscopy measurements

UV/VIS absorption spectra were recorded on a Cary-100 spectrophotometer from Varian between 300 and 480 nm. Measurements were performed in a 1 cm optical path length quartz cuvette on freshly prepared samples.

The solvents used for the spectroscopic measurements were: cyclohexane, benzene, chloroform (CHCl₃), toluene, ethyl acetate (EtOAc) acetone, acetonitrile (ACN), dimethylsulfoxide (DMSO), dimethylformamide (DMF), ethanol (EtOH), methanol (MeOH), butanol (BuOH), 2-propanol and acetic acid.

Steady-state fluorescence measurements were performed using a FluoroMax 3 spectrofluorimeter (Horiba Jobin Yvon, New Jersey, NJ, USA), equipped with a Peltier-thermostated cell holder. The excitation was performed at 378 nm and the spectra were recorded in the range of 400 nm to 600 nm with excitation and emission slits set at 3 nm. The spectra were corrected by subtracting the contribution of liposome suspension without Laurdan. The variation of the spectral sensitivity of the detector was taken into account.

Fluorescence lifetime measurements were performed using a home-made time-resolved fluorimeter based on time-correlated single-photon counting. For Laurdan the excitation light source was a sub-nanosecond pulsed LED head PLS 370 (380 nm, spectral width 15 nm, pulse width 600 ps) controlled with the PDL 800-D driver, both from PicoQuant (Berlin, Germany). The decay curves were recorded using the Time-correlated Single Photon Counting module TimeHarp 200 and a photomultiplier detector, PMA182-P-M also from PicoQuant. The fluorescence decays were measured at 440 nm and at 490 nm using filters with a band pass of 20 nm (Chroma Technologies, Bellows Falls, VT, USA). For BNP the excitation light source was a sub-nanosecond pulsed LED head PLS 8-2-522 (342 nm, spectral width < 20 nm, pulse width 500 ps) and the fluorescence decays was recorded at 490 nm using a filter with a band pass of 20 nm

The *instrument response function* (IRF) was obtained through the use of a scattering Ludox solution. The cuvette temperature (5 – 60) °C was controlled by a water bath thermostat. Fluorescence decay data were deconvoluted using the FluoFit 100 software package from PicoQuant.

3.4. Fluorescence microscopy measurements

3.4.1. FLIM

Fluorescence lifetime images (FLIM) were recorded using a confocal laser-scanning microscope (Zeiss LSM 510 META installed on a Zeiss Axiovert 200M; Zeiss, Jena, Germany). Two-photon excitation at 780 nm was with a Mai Tai Deep See laser (Spectra Physics, Newport). The excitation light was directed to the sample through a water immersion objective from Zeiss (LD C-Apochromat 40×/1.1 W Korr UV-VIS-IR) and separated from the emission with a KP 650 nm dichroic beam splitter from Zeiss. The emission was split into two channels using a dichroic beam splitter at 470 nm, a 405–455 nm filter for the blue channel and a 475–565 nm filter for the green channel. All filters are from Chroma. Two images of 128×128 pixels of optical cross-sections of GUVs and cells were simultaneously collected using the Becker & Hickl SPC830 card (Becker & Hickl GmbH, Berlin, Germany), allowing for time-correlated single photon counting. The intensity in each pixel was obtained by integrating the photons accumulated during the measurement. The IRF was obtained by recording the SHG signal obtained from KH_2PO_4 crystals. The fluorescence lifetime images were processed using SPCImage software from Becker & Hickl.

3.4.2. FRAP

Fluorescence recovery after photobleaching (FRAP) measurements were performed on the same experimental set-up used when performing FLIM measurements. The fluorescence light was detected in non-descanned mode through a BP 475-565 emission filter. The image size was typically set to 512 × 512 pixels with a pixel size ranging from 110 to 88 nm. The interval between the start of subsequent frames was determined as $1/3 \tau_D$. Each time series typically comprised 2 pre-bleach frames and 18 recovery frames. Measurements were performed at room temperature, on the top membrane (facing the bathing solution) of GUVs and on the bottom membrane of OLN-93 cells. Resulting time series were analyzed using custom written routines in a MatLab 9b software environment.

3.5. Data processing

Spectra were processed using Origin 8.0 (OriginLab Corporation, Northampton, MA, USA). GP values for spectrometric measurements were calculated using:

$$GP = \frac{I_{440} - I_{490}}{I_{440} + I_{490}} \quad (3.1)$$

where I_{440} and I_{490} are the emission intensities at 440 and 490 nm, respectively.

For microscopy measurements, GP values were calculated for each pixel using:

$$GP = \frac{I_{(405-455)} - g I_{(475-565)}}{I_{(405-455)} + g I_{(475-565)}} \quad (3.2)$$

where $I_{405-455}$ and $I_{475-565}$ are the emission intensities collected in the blue and green channel, respectively, and with g the *correction factor* specific for the experimental setup (Gaus *et al.* 2003):

$$g = \frac{I_{(405-455)}^{DMSO} (GP_{theo} - 1)}{I_{(475-565)}^{DMSO} (GP_{theo} + 1)} \quad (3.3)$$

where intensities of Laurdan emission in the specific channels were recorded for a sample of Laurdan in DMSO, under the same conditions as for cells; $GP_{theo} = 0.207$ and represents the known GP value of Laurdan in DMSO at 22 °C (Gaus *et al.* 2003).

Temperature dependence of GP and lifetimes values were fitted in Origin using a sigmoidal function and lipids T_m was estimated from the inflection point.

Images have been processed in MatLab 9b software (MathWorks, Natick, MA, USA) as follows. For GUVs, an *intensity based threshold* was used to discard the background pixels. For cells, two thresholds were used: the first threshold to discard the pixels related to the bathing solution (based on the intensity), and the second threshold (based on GP values) to discriminate the pixels from inside the cell with a lower GP . From the value distribution an average GP value over the membrane pixels (both GUVs and cells) was obtained for each recording. Lifetime images were processed likewise and an average lifetime over the membrane pixels was obtained for each channel. The average GP and lifetime values obtained for each image were used to calculate the averaged GP and lifetime over the GUVs and cells measured in the same conditions. When determining the angular dependence of GP and fluorescence lifetimes, with respect to the polarization of the incident light, pixel values

within a two degree angular step were binned. Data were analyzed using one-way-analysis of variance (ANOVA) with Bonferroni's Multiple Comparison Test.

CHAPTER 4

A NEW METHOD OF ANALYZING LAURDAN SPECTRA WHEN INSERTED IN LIPID MEMBRANES

Part of this chapter has been published as:

Bacalum, M., B. Zorilă and M. Radu

Fluorescence spectra decomposition by asymmetric functions – Laurdan spectrum revisited.

Anal Biochem. 2013 Jun 5. pii: S0003-2697(13)00263-7. doi: 10.1016/j.ab.2013.05.031

Bacalum, M., Bogdan Zorilă, M. Radu and A. Popescu

Laurdan solvatochromism: influence of solvent polarity and hydrogen bonds.

Optoelectronics and Advanced Materials – Rapid Communications vol. 7, iss. 5-6/2013

INTRODUCTION

The emission spectra of most fluorophores have a complex structure and usually have an asymmetric shape which can be analysed much better by log-normal (LN) distributions. Even so, only a few studies proposed this alternative, and the function mostly used to analyze them is a Gaussian one - a symmetric function. One of the procedures proposed by Siano and Metzler to describe the absorption spectra shape is based on a four parameter log-normal function (Siano and Metzler 1969). Later Burstein and his colleagues developed the procedure to analyze the emission spectra of a larger class of fluorophores (Burstein and Emelyanenko 1996) and validated it for analysis of the Tryptophan emission spectrum in proteins (Burstein *et al.* 2001). The procedure was extended to different fluorescent molecules, like Prodan and Acrylodan (Emel'ianenko *et al.* 2000), but to our knowledge it is far less used for Laurdan.

In this study, was proposed a new method to analyze the Laurdan complex spectrum in model lipid membranes (particularly LUVs) by decomposition of the spectra using LN functions. The procedure was calibrated for Laurdan using its spectra in homogeneous solutions of various solvents. A new parameter was proposed to evaluate Laurdan emission spectra with the prospect of acquiring a larger range of values than the classical *GP*.

In lipid bilayer, *GP* is calculated setting the blue and green channels at 440 nm and 490 nm, respectively. These values represent the peak positions reached in the two pure lipid phases: 440 nm for the gel phase and 490 nm for the liquid-crystalline phase. Because of the spectral overlapping of the emission from the relaxed and non-relaxed states, *GP* actually cannot reach these extreme values in lipid bilayer. Nevertheless, if the number of emitting molecules in each state would be used instead of I_{blue} and I_{green} , a more reliable parameter could be defined. Decomposition of the Laurdan spectrum in a superposition of elementary peaks can provide such information and instead of *GP*, the relative area of the elementary peaks was used as a quantitative global parameter characterizing changes in Laurdan spectrum as a function of temperature.

4.1. Solvent measurements and shape parameters relationships

To have the correct function first it needs to be made specific for Laurdan by finding the relationship between the ν_m, ν_{min} , and ν_{max} .

The first step was to record and evaluate the emission spectra of Laurdan in different solvents ranging from non-polar to polar protic ones (Table 4.1). These data are further used to calibrate the algorithm developed for the complex spectrum decomposition.

For this was used the LN mirror-symmetric form (in wavenumber scale) proposed to describe the emission spectra of organic fluorophores (Burststein and Emelyanenko 1996):

$$\begin{cases} I = I_m \exp\left[-\frac{\ln 2}{\ln^2(\rho)} \ln^2\left(\frac{a-\nu}{a-\nu_m}\right)\right] & \text{if } \nu < a \\ I = 0 & \text{if } \nu > a \end{cases} \quad (4.1)$$

where: I is the emission intensity, I_m is the maximum of intensity, ν is the wavenumber, ν_m is the position of the peak, $\rho = \frac{\nu_m - \nu_{min}}{\nu_{max} - \nu_m}$ is the asymmetry of the function (ν_{max} and ν_{min} are the wavenumber values at half intensity) and a is the limiting wave number: $a = \nu_m + \frac{(\nu_{max} - \nu_{min})\rho}{(\rho^2 - 1)}$

The influence of polarity on Laurdan emission spectra is presented in Figure 4.1 for three solvents, one from each class: non-polar, aprotic and protic. The shape of Laurdan spectra is clearly asymmetric and the asymmetry (ρ) has a slow trend to decrease with the increase of polarity (Table 4.1). The spectra were fitted very well for all the solvents by the LN function, with the residuals under 2 % (Table 4.1).

Table 4.1. Spectral characteristics of Laurdan emission solvents of varying polarities

	Solvent	ν_m / cm^{-1}	$\nu_{\min} / \text{cm}^{-1}$	$\nu_{\max} / \text{cm}^{-1}$	FWHM [*] / cm^{-1}	ρ	R ^{2**}
Non-polar	Cyclohexane	24,814	23,048	26,349	3,301	1.391	0.9978
	Hexane	24,752	23,025	26,416	3,390	1.393	0.9982
	Toluene	23,753	21,935	25,031	3,096	1.375	0.9996
	Benzene	23,641	21,884	24,948	3,064	1.374	0.9996
	CHCl₃	22,523	20,659	23,809	3,150	1.249	0.9999
Polar aprotic	EtOAc	23,095	21,238	24,392	3,154	1.286	0.9999
	THF	23,041	21,237	24,342	3,105	1.289	0.9998
	Acetona	22,272	20,517	23,644	3,127	1.232	0.9999
	DMF	21,786	20,038	23,117	3,078	1.226	0.9999
	ACN	21,692	20,024	23,130	3,106	1.200	0.9999
	DMSO	21,413	19,684	22,744	3,060	1.215	0.9999
Polar protic	2-propanol	20,704	19,101	22,082	2,981	1.183	0.9993
	Propanol	20,661	19,098	22,073	2,976	1.183	0.9993
	BuOH	20,492	18,836	21,843	3,007	1.178	0.9993
	EtOH	20,161	18,541	21,588	3,047	1.180	0.9996
	MeOH	19,763	18,121	21,164	3,044	1.167	0.9996

* Full width at half maximum of fitted spectrum.

** R² coefficient characterizing the quality of fit.

Laurdan is a solvatochromic fluorescent probe and the main characteristic is its red shift observed in the emission spectrum with the increase of solvent polarity (Figure 4.1). We can interpret the change of Laurdan spectrum directly in terms of the environment polarity because of the linear relationship between the peak position (ν_m) and the solvents polarity (expressed as E_T30 – data not shown).

The position of the two half maximum limits (ν_{\min} and ν_{\max}) were plotted against the peak position (ν_m), fitted to obtain the parameters used to restrain the shape of the elementary peaks in the LN function. This will reduce the number of the four parameters: the amplitude (I_m) and the shape parameters (ν_m , ν_{\min} , and ν_{\max}), to only two (intensity and peak position). The advantage is that the function will give a more robust fit and will force the selection of the peak shape according to the empirical calibration provided by the linear constraints.

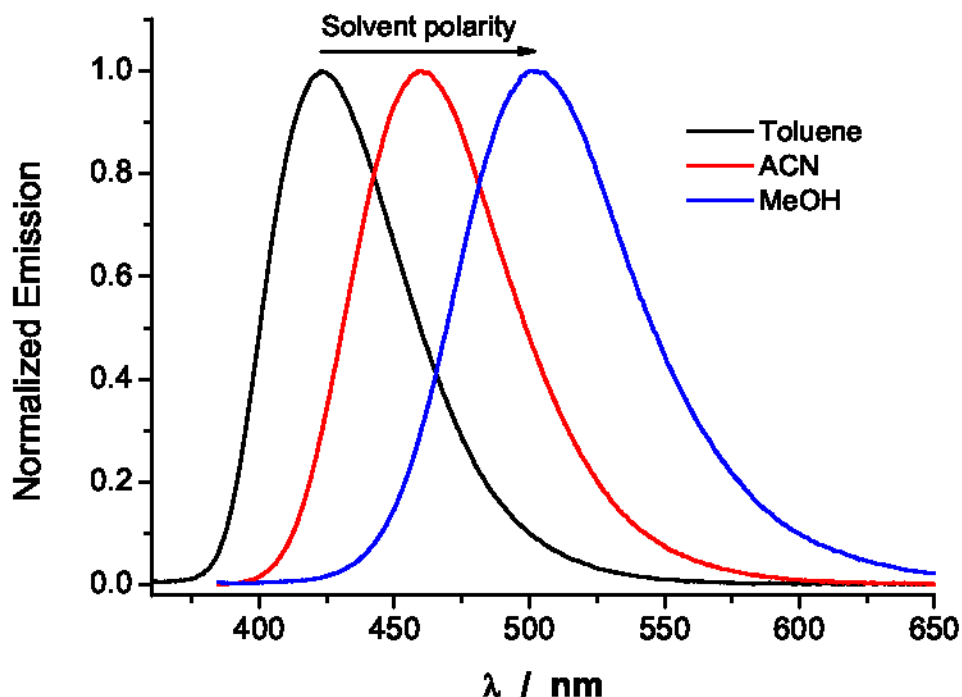


Figure 4.1. Normalized absorption and emission spectra of Laurdan in homogeneous solutions. One solvent for each category (non-polar - toluene, aprotic - ACN, and protic - MeOH) is presented in this graph.

4.2. Decomposition of emission spectra of Laurdan inserted in LUVs

After the function was particularized for Laurdan it was applied to the emission spectra recorded for Laurdan inserted into LUVs prepared from DMPC and DPPC. Laurdan complex spectrum was analyzed as a sum of two LN functions, one for each of the two excited states of Laurdan molecules: non-relaxed and relaxed state, respectively. An example of the spectrum decomposition by LN functions is presented in Figure 4.2 for two spectra recorded on DMPC LUVs, one at 10 °C (A) and the other one at 60°C (B).

The recorded spectra presented in Figure 4.2 show the typical pattern of Laurdan emission from LUVs with a high emission peak located at ~ 440 nm (at 10°C), and a smaller one located ~ 490 nm (at 60°C).

After the data were fitted with the LN function, we found that each spectrum can be deconvoluted in two emission bands, one that has a maximum at ~ 440 nm and the second at ~ 490 nm. From Figure 4.2, we can see that the spectra are highly asymmetric with an important emission in blue and green channels even in the extreme values of temperature

where the lipid bilayer is presumed to be in one phase (gel in Figure 4.2A or liquid-crystalline, in Figure 4.2B, respectively).

The ratio of the emission bands changes with increasing temperature. At lower temperature the blue peak prevails, but with increasing temperatures is reduced and the green peak becomes larger. This shows that even at low temperature (when the bilayer is in gel phase) some Laurdan molecules emit from a relaxed state.

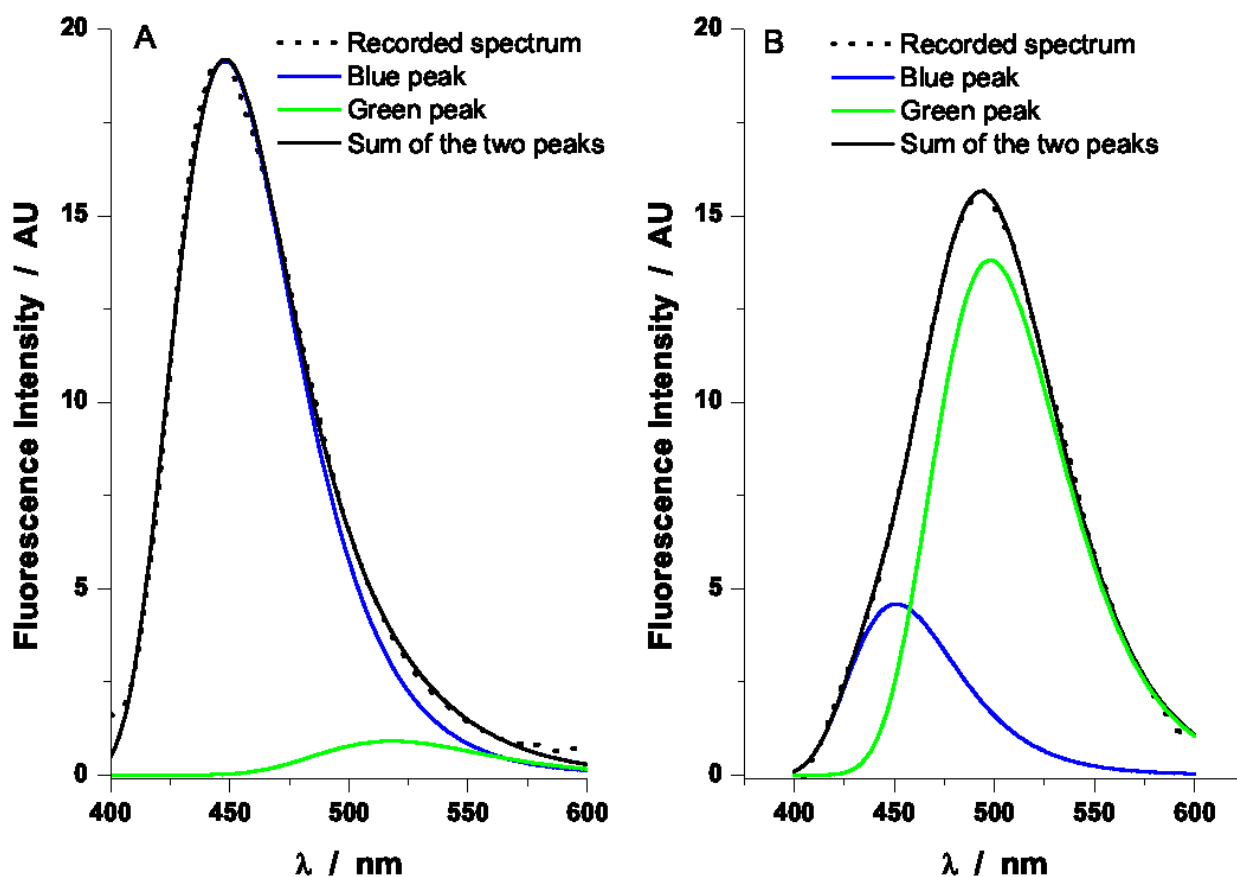


Figure 4.2. Decomposition of Laurdan spectra by LN function.

One example is given for a spectra recorded on DMPC LUV at (A) 10 °C – the gel phase and (B) 60°C – the fluid phase.

Based on the results obtained we can say that the transition starts in some localized sites where the water penetrates up to the Laurdan fluorescence moiety and saturates the relaxation process and Laurdan molecules switch from the non-relaxed to the relaxed state. The number of these sites increases with the temperature. Such a scenario is close to the coexisting phase domains of main phase transition as described for DPPC LUVs by

fluorescence spectroscopy (Metso *et al.* 2003) and by Monte-Carlo simulations (Ipsen *et al.* 1990).

The evolution of elementary peak areas of the data recorded for DMPC and DPPC LUVs is presented in Figure 4.3. The relative area of the peak in blue channel, emission from non-relaxed state, (Ar_B) is ~ 0.85 for DMPC LUVs and ~ 0.95 for DPPC LUVs at low temperatures, suggesting that the water molecules penetrate with great difficulty in the lipid bilayer since the bilayer is in the gel phase. Increasing the temperature, Ar_B decreases faster around the phase transition temperature and reaches, for both types of vesicles, ~ 0.25 , in the liquid-crystalline phase. The peak area for the emission from the relaxed state (Ar_G) has an opposite variation.

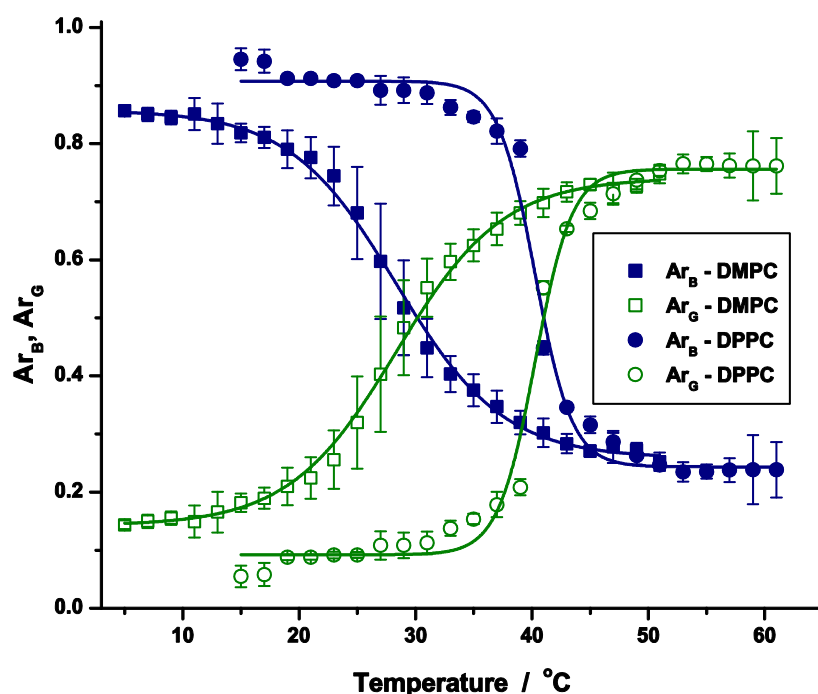


Figure 4.3. The relative areas resulted from the fitting with LN function.

Data were measured for LUVs prepared from DMPC and DPPC. The error bars are the standard deviations resulting from at least three repeated measurements for each condition.

The slightly lower value obtained for DMPC LUVs at lower temperatures can be explained by the difference in the length of the lipid chains. Because lipid chains DPPC have 16 carbons the membrane can accommodate better the Laurdan molecules and less water reaches them. Contrary, in the fluid phase, the length of the lipid chains is not important as the lipids become more mobile and for both types of LUVs similar environments are probed.

The point where the curve of the relative areas of the two peaks meet (the relative areas become equal) represents the experimental condition where the number of Laurdan molecules found in the gel and fluid phase is the same. Because this happens closely to the T_m of the lipids, we can use the plots from Figure 4.3 to determine the T_m for each of the lipids (Table 4.2).

Table 4.2. T_m of lipids obtained from the fitting with LN function

	DMPC	DPPC
Ar_B, Ar_G	28.35 ± 0.26^b	40.27 ± 0.22
ΔAr	28.18 ± 0.19	40.42 ± 0.24
[Ref.(Koynova and Caffrey 1998)]	23.6 ± 1.5	41.3 ± 1.8

If the relative areas of the elementary peaks are used, we can define a new parameter similar to GP , the difference of relative areas: $\Delta Ar = Ar_B - Ar_G$. This parameter depends on the fractions of emitting molecules in each state and, theoretically can range from -1 (emission from relaxed state only) to +1 (emission from non-relaxed state only). ΔAr for the recordings on DMPC and DPPC LUVs are plotted in Figure 4.4. The ΔAr values start from high values, ~ 0.7 for DPMC and ~ 0.9 for DPPC and drop to ~ -0.6 . The range covered by ΔAr is significantly larger than the one covered by GP , becoming a more sensitive parameter.

Using ΔAr we can also determine the T_m of the lipids used to prepare the LUVs (Table 4.2). The values determined using the 2 parameter described here give accurate values for DPPC, but slightly larger ones for DMPC.

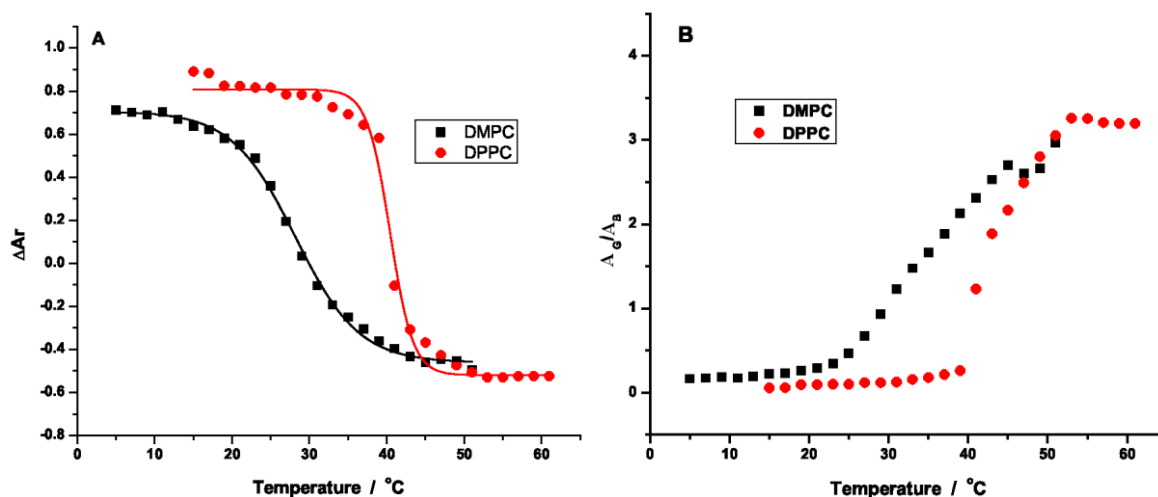


Figure 4.4. ΔAr -difference between relative areas of elementary calculated for Laurdan inserted in LUVs prepared from DMPC or DPPC (A). The ratio of the LN peak areas (A_G/A_B) for LUVs prepared from DMPC and DPPC (B).

Another parameter proposed in the literature (Ionescu and Ganea 2012) to characterize the changes in Laurdan spectrum is the ratio of elementary peak areas (A_G/A_B), and it is depicted in Figure 4.4 for our recordings on DMPC and DPPC LUVs analyzed by LN decomposition. This parameter has a sharp increase starting close to the phase transition temperature.

PARTIAL CONCLUSIONS

A new method to evaluate the complex spectrum of Laurdan inserted into the membrane of LUVs was proposed. This method is based on a decomposition algorithm that uses the asymmetric LN function as a validated analytical model for elementary peaks shape. An empirical calibration of the decomposition algorithm which relies on the relationships among the shape parameters of LN function as derived from analysis of Laurdan emission in homogeneous solutions of solvents with various polarities is generated. This procedure allows a better characterization of the hydration level at the Laurdan location, in good agreement with the literature data. The new parameter proposed to evaluate Laurdan emission spectra (ΔAr) proved to be a parameter more sensitive than *GP*. The method described here can be extended to more complex lipid systems.

CHAPTER 5

EXPLORING THE CORRELATION BETWEEN GENERALIZED POLARIZATION AND TIME-RESOLVED FLUORESCENCE OF LAURDAN IN LIPID MEMBRANES

Parts of this chapter will be mentioned in a report to be submitted:

Bacalum, M., N. Smisdom, A. Popescu, M. Radu and M. Ameloot

Exploring the correlation between Generalized Polarization and time-resolved fluorescence of Laurdan in lipid membranes.

INTRODUCTION

Model lipid membranes and natural membranes (HEK293T cells) were investigated using *GP* and the fluorescence lifetimes of Laurdan in both the blue and green channel and explore correlations between them. Different experimental conditions are considered, either by modulating the lipid composition of the membranes (changes in phospholipid type and Chol concentration) or by varying the temperature of the environment. Both spectrometry (steady-state and time-resolved fluorescence) and fluorescence microscopy techniques (two photon excitation and lifetime imaging) are used for observation in the blue and green part of the emission spectrum of Laurdan.

5.1. Measurement on LUVs

Fluorescence emission spectra of Laurdan inserted into DPPC, DMPC and DMPC/Chol LUVs were recorded as a function of temperature (Figure 5.1.A-C). The type of phospholipid does not influence the shape of Laurdan emission spectra for the S_0 and L_α phases, while adding Chol causes a broadening of the emission spectrum to shorter wavelengths for the L_α phase (Figure 5.1.D).

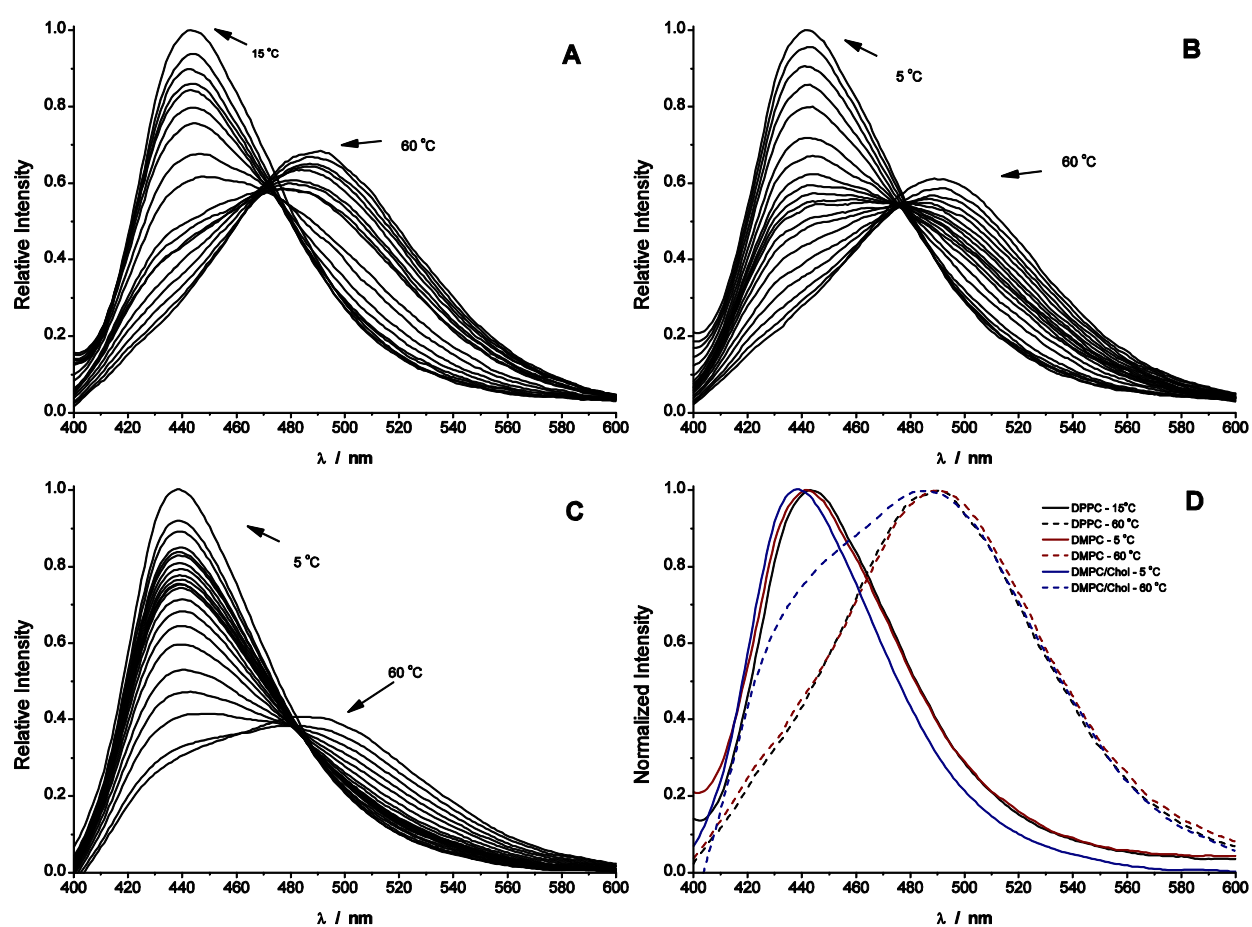


Figure 5.1. Fluorescence emission spectra of Laurdan inserted into the membrane of LUVs. LUVs were composed of DPPC (A), DMPC (B) and a mixture of DMPC/Chol (4:1 weight ratio) (C) at temperatures ranging from 5 to 60 °C (with a 5 °C step) (D) Peak normalized emission spectra of Laurdan in DPPC, DMPC and DMPC/Chol.

Membrane changes were assessed by GP values (Figure 5.2). LUVs prepared from DMPC or DPPC exhibit GP values higher than 0.4 below T_m , as it is expected for lipid membranes in a S_o phase. The GP values decrease with increasing temperature and reach values smaller than -0.4 at 60 °C, when the lipids are in the L_α phase. In the case of the LUVs prepared from a mixture of DMPC and Chol, the shape of the curve is very different from the other two. Compared to the LUVs composed of DMPC only, there is an overall increase of GP values with a less steep decline of the curve with increasing temperature. A higher increase was observed at temperatures higher than T_m .

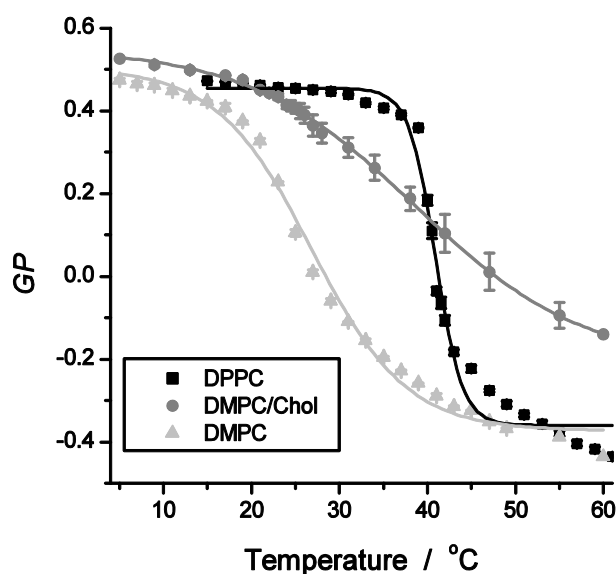


Figure 5.2. Variation of GP values with temperature.

Laurdan was inserted in the membrane of LUVs prepared from DMPC, DPPC and a mixture of DMPC/Chol (4:1 weight ratio). The error bars correspond with the standard deviation resulting from three repeats.

Values for T_m based on the temperature dependence of GP observed for DMPC and DPPC LUVs (Table 5.1) are in close agreement with those reported in the literature (Koynova and Caffrey 1998). For LUVs prepared from DMPC/Chol we can observe that the phase transition becomes broader and that the apparent transition temperature is increased as compared to DMPC LUVs.

Addition of Chol to membranes increases the GP values over the investigated temperature range. The presence of Chol reduces the membrane hydration (Parasassi *et al.*

1994; Parasassi *et al.* 1995), which is translated in a blue shift of the emission spectra of Laurdan (Figure 5.1), and therefore, to an increase of GP (Figure 5.2) (Harris *et al.* 2002). The change is more pronounced in the L_α phase where the packing effect of Chol is more efficient. (Aguilar *et al.* 2012; McMullen *et al.* 2004) The apparent transition temperature determined for this mixture is higher than that for the pure DMPC liposomes (Table 5.1). This is expected because Chol tends to reduce the difference between the L_α and S_o phases (McMullen *et al.* 2004) and to increase the lipid order for temperatures above T_m (Harris *et al.* 2002).

The fluorescence lifetime of Laurdan incorporated in LUVs was recorded in the blue (440 nm) and the green (490 nm) channel at different temperatures for each type of vesicle composition (Figure 5.3). In the blue channel (Figure 5.3), the lifetime was about 5-6 ns, for the S_o phase and about 2 ns, for the L_α phase. The lifetimes in the green channel (Figure 5.3) were somewhat larger, about 6-7 ns, for the S_o phase and about 3.5 ns for the L_α phase. The temperature dependence of the lifetimes in the two channels for the LUVs displays a similar behaviour as shown for GP and the same procedure was followed for the determination of T_m (Table 5.1). The changes in the lifetimes observed in the blue channel are more pronounced than those in the green channel. Therefore T_m is better determined for the blue channel.

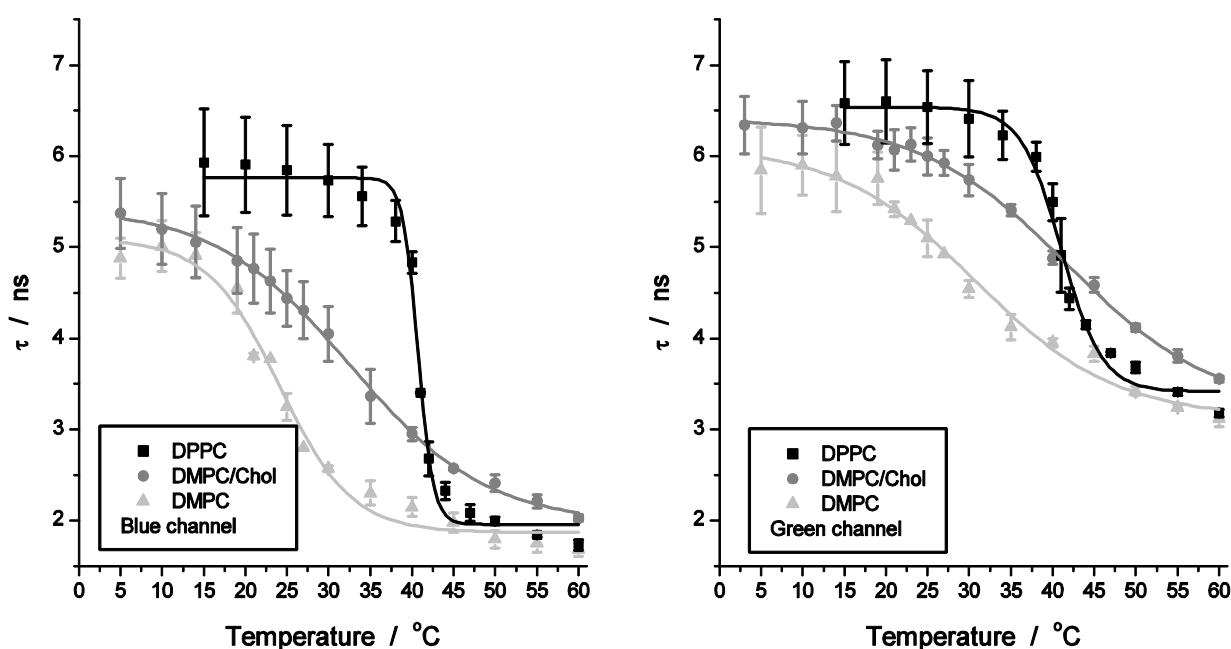


Figure 5.3. Fluorescence lifetimes of Laurdan.

Fluorescence lifetime was recorded in the blue (left) and green (right) channels for Laurdan inserted in the membrane of LUVs prepared from DMPC, DPPC and a mixture of DMPC/Chol (4:1 weight ratio). Error bars indicate the standard deviations resulting from three repeats.

From Figure 5.3, we can observe that the LUVs composed from DMPC yield a smaller lifetime value in comparison to those made with DPPC. In the blue channel, a lifetime of ~ 5 ns was recorded for DMPC and ~ 6 ns for DPPC, while in green channel the lifetimes were ~ 6 ns and ~ 6.8 ns, respectively. However, in the L_{α} phase the observed lifetimes were essentially independent of the chain length, and take values of ~ 2 ns in the blue channel and ~ 3.5 ns in the green channel.

Table 5.1. Transition temperatures (in $^{\circ}\text{C}$) obtained by analyzing the temperature dependence of GP and lifetimes

	DMPC	DPPC	DMPC/Chol ^a
<i>GP</i>	$26.8 \pm 0.5^{\text{b}}$	40.9 ± 0.2	38.6 ± 0.4
τ_{blue}	24.1 ± 0.7	40.7 ± 0.2	32.6 ± 0.5
τ_{green}	30.8 ± 1.3	41.1 ± 0.4	41.8 ± 0.9
[Ref.(Koynova and Caffrey 1998)]	23.6 ± 1.5	41.3 ± 1.8	-

^aApparent transition temperature.

^bUncertainties are standard errors obtained from the fit parameters.

For comparison, the fluorescence lifetime of $1 \mu\text{M}$ Laurdan in different solvents (DMSO, ethanol and cyclohexane) was recorded. The lifetimes were solvent dependent but no significant difference was observed between the fluorescence lifetimes recorded in the blue and green channel for each solvent (Table 5.2).

Table 5.2. Fluorescence lifetimes of Laurdan in solvents (room temperature)

	Cyclohexane	DMSO	Ethanol
$\tau_{\text{blue}} / \text{ns}$	$0.28 \pm 0.02^{\text{a}}$	3.37 ± 0.11	3.13 ± 0.03
$\tau_{\text{green}} / \text{ns}$	0.31 ± 0.02	3.60 ± 0.10	3.24 ± 0.11

^aUncertainties are standard deviations obtained from the fit parameters.

Figure 5.4 shows the relation between GP values (Figure 5.2) and the lifetimes in the blue and in the green channel (Figure 5.3). While the lifetime in the green channel is always larger than the lifetime in the blue channel at the corresponding GP value, both lifetimes increase almost linearly with GP . In the pure phospholipid systems the lifetimes are essentially independent of the phospholipid type for negative GP values (L_α) within each of the two channels. For highest observed GP values (S_o) the lifetimes are influenced by the phospholipid type. Apart from the highest GP values, the DMPC/Chol system exhibits lower lifetimes in each of the two emission channels at corresponding GP values in comparison to pure DMPC or DPPC systems.

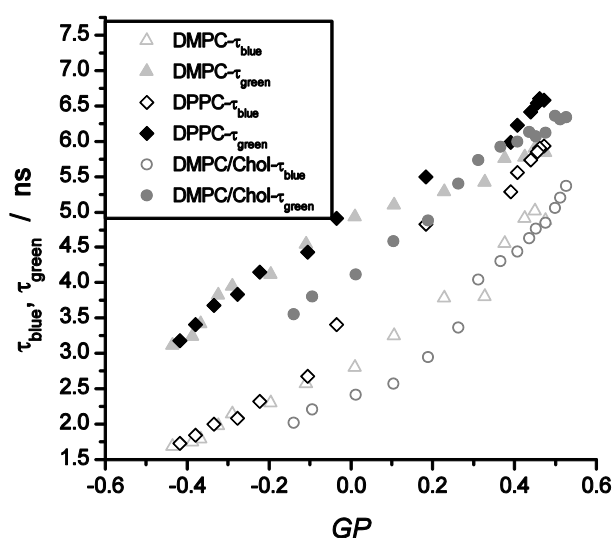


Figure 5.4. Fluorescence lifetimes in the blue and green channel recorded for Laurdan in LUVs (Figure 5.3) versus GP values (Figure 5.2) at corresponding temperatures.

5.2. MEASUREMENTS ON GUVs

Spatial variation of GP and lifetimes can be monitored in GUVs. Microfluorimetric measurements were performed at room temperature on GUVs that exhibit different phases: S_o phase (DPPC), L_α phase (DOPC) or L_o/L_d phase separation (for a mixture of DOPC/SM/Chol). Both GP and fluorescence lifetime images were obtained. The fluorescence relaxation within each pixel was well fitted by a single exponentially decaying function. The reduced χ^2 value was smaller than 1.2 for the majority of the pixels.

As the excitation light is linearly polarized, the photoselection effect is observed in the fluorescence intensity images. This effect is stronger when the lipids are in the S_o phase (Figure 5.5) in comparison to the L_α phase, where the intensity is more evenly distributed (Figure 5.6).

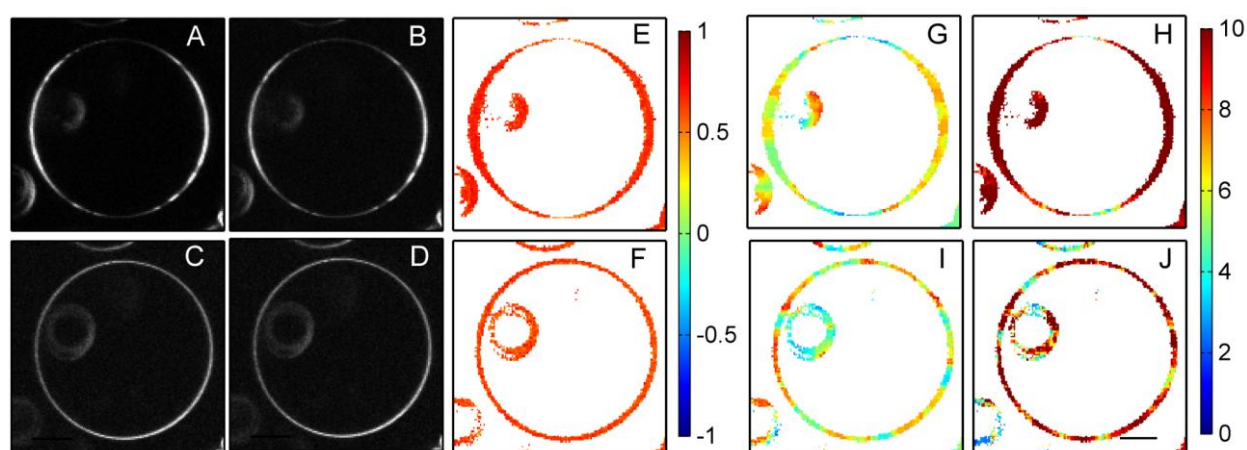


Figure 5.5. Laurdan measurements on GUVs prepared from DPPC.

Fluorescence intensity images of Laurdan recorded in the blue channel (A and C) and in the green channel (B and D) with linearly polarized light (first row) and circularly polarized excitation light (second row) for GUVs prepared from DPPC (S_o phase- room temperature). GP images (E and F) and fluorescence lifetime images (G-J) recorded in the blue channel (G and I) and green channel (H and J). The color code bar in the middle reflects the GP values and the bar on the right indicates the lifetime values in ns. The orientation of the linear polarization of the excitation light is horizontal for the images presented in the top row. The photoselection effect occurs only when the light is linearly polarized. The fluorescence lifetimes in the membrane regions oriented parallel to the polarization direction of the incident light are characterized by values lower than the ones recorded from the regions oriented perpendicularly to this direction. The images show a smaller GUV is enclosed by a larger GUV. The size of the scale bar (panel J) is $10\ \mu\text{m}$ applied to all images.

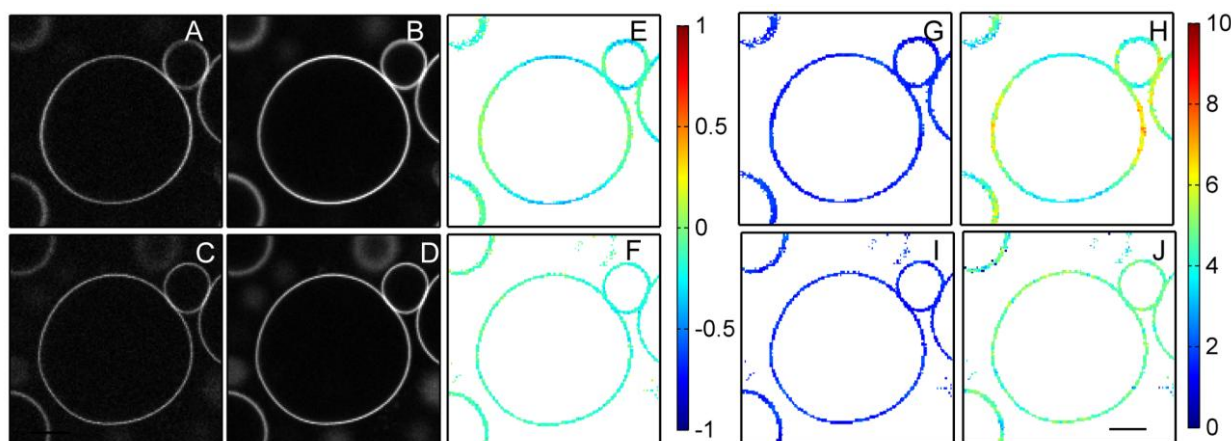


Figure 5.6. Laurdan measurements on GUVs prepared from DOPC.

Fluorescence intensity images of Laurdan recorded in the blue channel (A and C) and in the green channel (B and D) with linearly polarized excitation light (first row) and circularly polarized light (second row) for GUVs prepared from DOPC (L_α phase – room temperature). GP images (E and F) and fluorescence lifetime images (G-J) recorded in the blue channel (G and I) and green channel (H and J). The color code bar in the middle reflects the GP values and the bar on the right indicates the lifetime values in ns. The orientation of the linear polarization of the excitation light is horizontal for the images presented in the top row. No pronounced photoselection effect can be observed in the intensity images. However, in the GP and fluorescence lifetime images, the membrane regions oriented parallel to the polarization direction of the incident light are characterized by values lower than the ones recorded from the regions oriented perpendicularly to this direction. In the case of circularly polarized light this distinction is not observed. The size of the scale bar (panel J) is $10\ \mu\text{m}$ applied to all images.

For both phases, the membrane regions where the Laurdan molecules are aligned perpendicular to the direction of polarization of the exciting light yield lower GP values and lower lifetime values (Figures 5.5 and 5.6; see also Figure 5.7). The effect of the membrane orientation on GP and lifetimes disappears under circularly polarized excitation light (Figures 5.5 and 5.6).

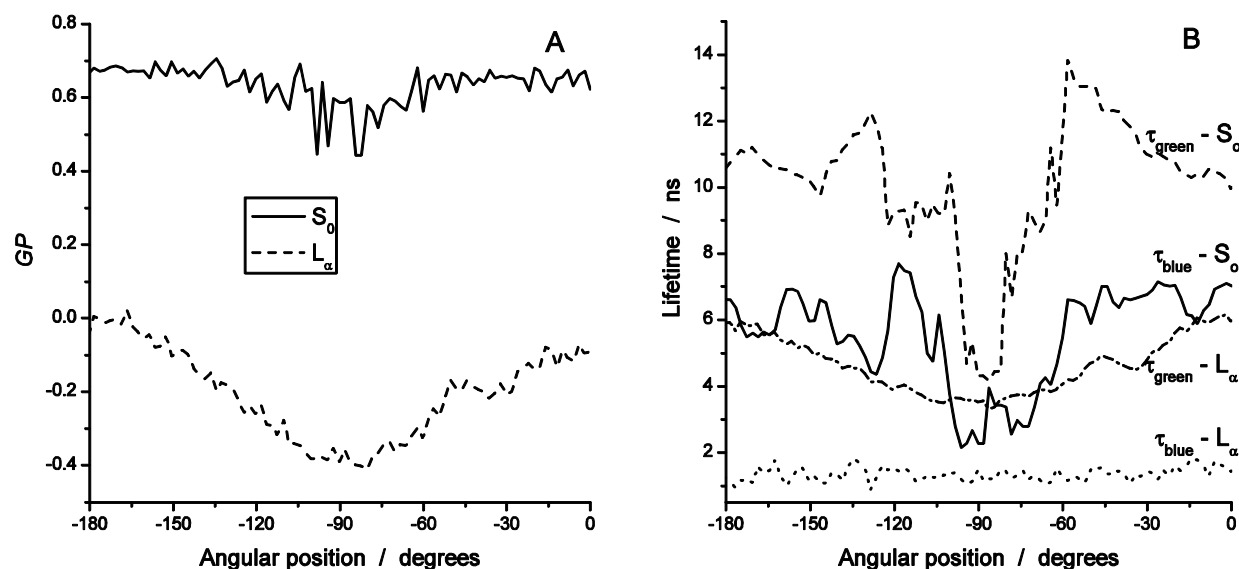


Figure 5.7. Angular dependence of *GP* and fluorescence lifetimes of Laurdan

GP (A) and lifetimes (B) as a function of their position on the circumference of a *GUV* prepared from *DPPC* (S_0 phase) or *DOPC* (L_α phase). The angular position of 90° is perpendicular to the linear polarization of the incident light. The plots were obtained for the *GUVs* presented in Figure 5.5 and 5.6. Measurements were performed at room temperature.

Figure 5.7 shows the *GP* values and lifetimes in the blue and the green channel as a function of the angular position of the pixels on the circumference of *GUVs* prepared from *DPPC* (S_0 phase) or *DOPC* (L_α phase). *GP* values for the L_α phase exhibit a much stronger angular dependence as compared to the S_0 phase (Figure 5.7.A). However, in contrast, the lifetime values collected in the green channel for the S_0 phase display a pronounced variation within a narrow range of angular positions (Figure 5.7.B). Though, the angular range of lifetime variation in the green channel is somewhat narrower and more pronounced compared with the blue channel. For the L_α phase, the angular dependence of the lifetime in the green channel shows a variation over a much broader angular range, while the lifetime in the blue channel is essentially independent of the angular position.

The photoselection effect on the values of *GP* and the fluorescence lifetimes is observed also in *GUVs* exhibiting L_0/L_d phase (Figure 5.8). *GP* values of this type of *GUVs* are between 0.4 and 0.8 for the L_0 phase and between -0.4 and 0.4 for the L_d phase (Figure 5.8.A). The two phases exhibit significantly different lifetimes, both in the blue and green channel as shown in Figure 5.8.C and 5.8.D. The difference in the lifetimes in the L_0 and L_d phases is more pronounced in the blue channel, with an average lifetime of 2 ns for the L_d phase and of 5 ns for the L_0 phase (Figure 5.8).

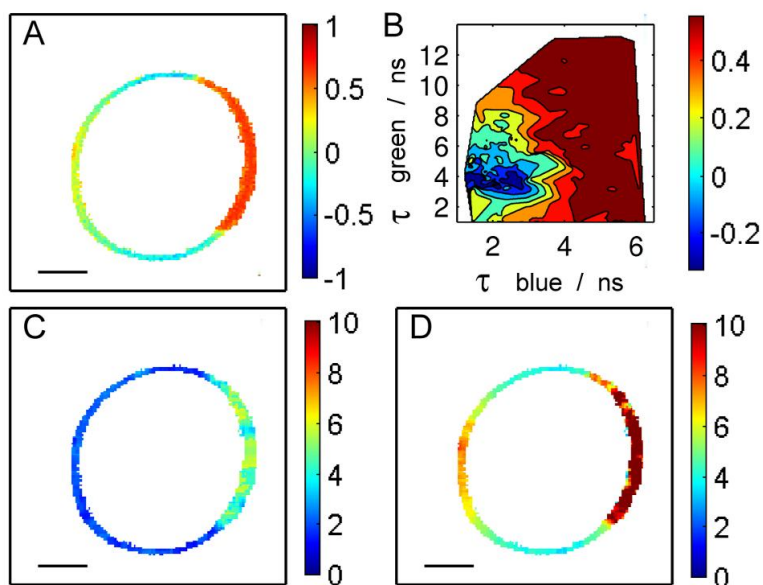


Figure 5.8. Laurdan in GUVs with L_o/L_d phase separation observed with horizontally, linearly polarized excitation light.

Measurements were performed at room temperature on GUVs prepared from DOPC/SM/Chol (1:2:1 molar ratio). GP (A) and fluorescence lifetimes images (C – blue channel and D – green channel). The values of GP and the lifetime (in ns) are represented by the corresponding colour bars. (B) Correlation map between GP and fluorescence lifetimes. GP is shown by colour coded values. This representative GUV was selected because the two phases are well represented in the optical cross-section and the photoselection effect can be observed for the L_d phase, which is recognized by low GP values. Scale bar is 10 μm .

GP and fluorescence lifetimes images for GUVs with L_o/L_d phase separation obtained with circularly polarized light are shown in Figure 5.9.

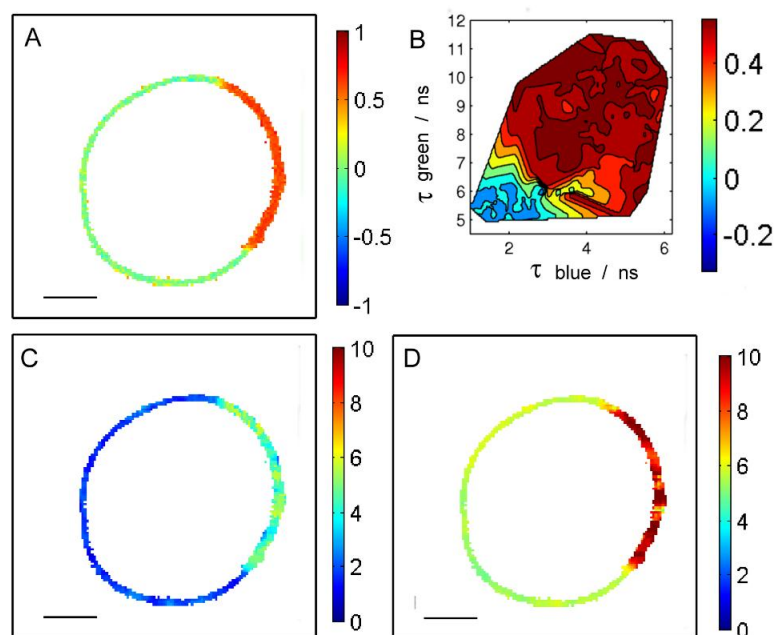


Figure 5.9. Laurdan in GUVs with L_0/L_d phase separation observed with circularly polarized excitation light.

Measurements were performed at room temperature on GUVs prepared from DOPC/SM/Chol (1:2:1 molar ratio). GP (A) and fluorescence lifetimes images (C – blue channel and D – green channel). The values of GP and the lifetime (in ns) are represented by the corresponding colour bars. (B) Correlation map between GP and fluorescence lifetimes. GP is shown by colour coded values. This representative GUV was selected because the two phases are well represented in the optical cross-section and the photoselection effect can be observed for the L_d phase, which is recognized by low GP values. Scale bar is 10 μm .

A comparison between the data recorded on GUVs with either linearly polarized excitation light or circularly polarized excitation light is shown in Figure 5.10. Independent of the polarization of the excitation light, the lifetimes for DPPC GUVs in the blue and green channel display a rather wide distribution for a narrow distribution of GP, while the opposite is true for DOPC GUVs (Figure 5.10). The same observations can be made for the two phases in the DOPC/SM/Chol GUVs (Figure 5.10). The distribution of the lifetimes in the L_d phase is somewhat narrower for the circularly polarized excitation although the distribution of GP values is not affected. Overall, it can be stated that a low lifetime in both the blue and green channel correlate with a low GP value, and that a high lifetime in both the blue and green channel correlate with a high GP value. Both GP values and lifetimes in the blue and green channel are smaller in the L_d phase than in the L_0 phase.

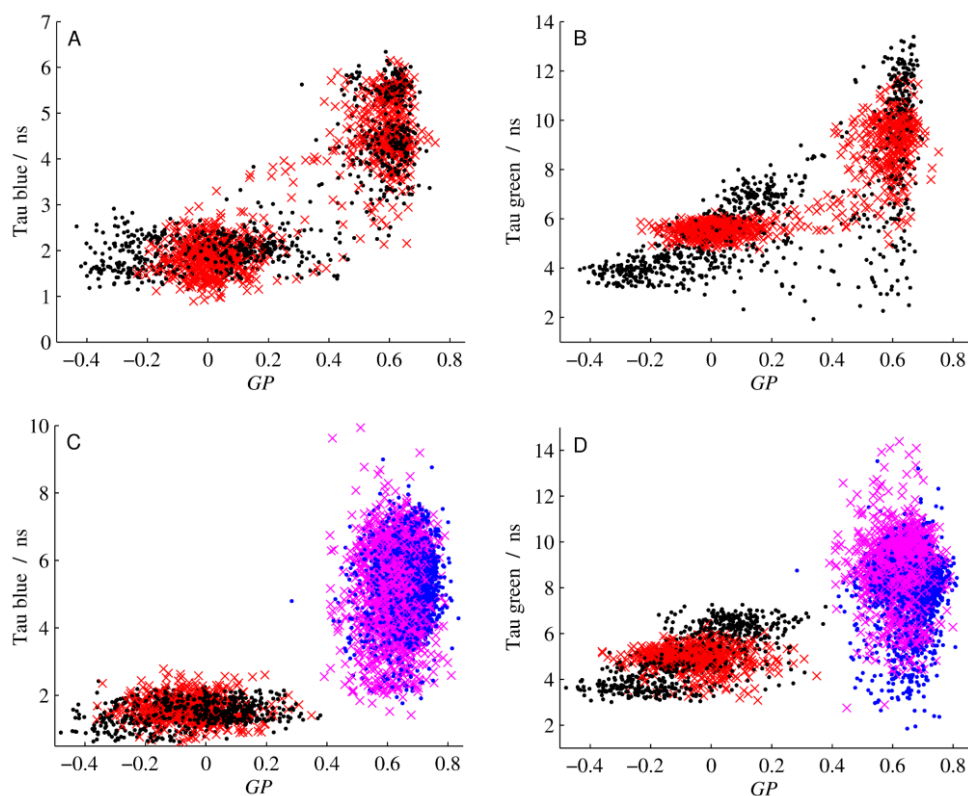


Figure 5.10. Distribution of the pixelwise correlation between lifetimes and GP for Laurdan in GUVs. *DOPC/SM/Chol (1:2:1 molar ratio)* (A, B); *DOPC (red and black in C and D) and DPPC (magenta and blue in C and D)* were recorded with linearly polarized excitation light (black and blue) and circularly polarized excitation light (red and magenta). Experiments were performed at room temperature.

The pixelwise correlation between GP values and fluorescence lifetimes for *DOPC/SM/Chol* GUVs can be represented in a topographic map (Figure 5.8.B). The topographic maps of a single component GUVs are presented in Figure 5.11. Although the lifetime values have a wide distribution for both phases, a correlation between the lifetimes and GP values can be observed for each phase.

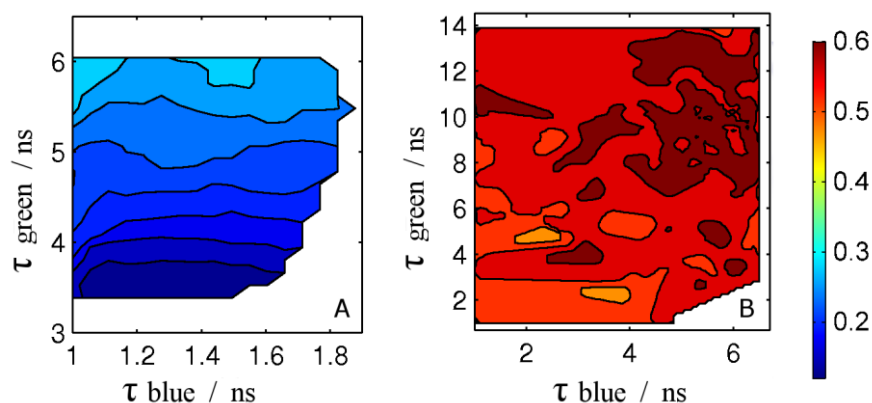


Figure 5.11. Correlation map between GP and fluorescence lifetimes for homogenous GUVs.

Fluorescence was collected with linearly polarized excitation light at room temperature for Laurdan in DOPC GUVs - the L_d phase (A) and DPPC GUVs - S_o phase (B). GP is shown by color coded values.

Figure 5.12 shows the pixel distributions of GP and fluorescence lifetimes for GUVs of DPPC, DOPC and DOPC/SM/Chol at room temperature.

Overall, higher GP values are observed for the S_o phase (around 0.6) as compared to the L_α phase (around 0.2). Also, the lifetimes in the S_o phase, are larger as compared to those in the L_α phase, and this for both channels of observation. The average lifetimes recorded in the blue channel (around 2 ns for the L_α phase and around 5 ns, for the S_o phase) are smaller than the lifetimes in the green channel (around 4 ns for the L_α phase and around 8 ns, for the S_o phase).

In the case of DOPC/SM/Chol, the two phases can be clearly discriminated both by the GP values and the lifetimes in the blue and the green channels. Figure 5.12.B shows that the average GP and lifetime values obtained for L_o and L_d are significantly different. For all three parameters, GP and the lifetimes in the two channels, the values for the pure L_α phase (DOPC) are lower than those obtained for the L_d phase. Comparing the S_o phase (DPPC) with respect to the L_o phase, only the GP values and the lifetimes recorded in the blue channel are higher, while the lifetimes recorded in the green channel are rather similar for both phases (Figure 5.12.B). While all parameters indicate that the L_d phase is more ordered than the L_α phase, only GP values and the lifetimes in the blue channel indicate that the L_o phase is less ordered than S_o phase. Similar distributions and correlations are found when using circularly polarized excitation light (Figure 5.13.A and 5.13.B).

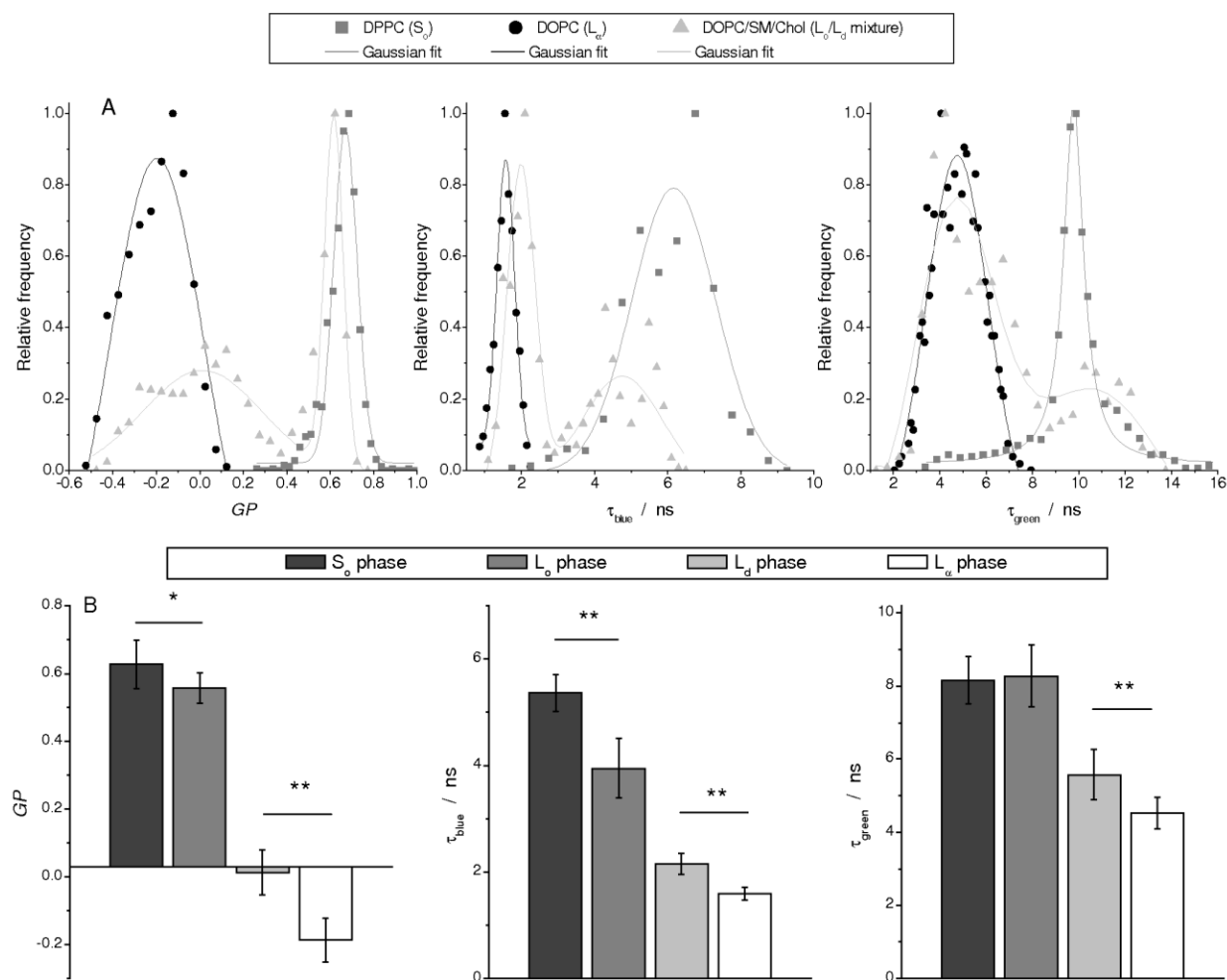


Figure 5.12. Laurdan in GUVs observed with linearly polarized excitation light at room temperature. (A) Pixel distribution of GP values and lifetimes in the blue and the green channel from a representative GUV for each of the various lipid phases: L_α phase (circles), mixture of L_o and L_d phases (triangles) and S_o phase (squares). Distributions are fitted to a Gaussian or a sum of Gaussians. (B) Average GP and fluorescence lifetimes for the different phases. The error bars are the standard deviations resulting from at least seven GUVs measured for each condition. The data were analyzed using one-way-analysis of variance (ANOVA) with Bonferroni's Multiple Comparison Test with significance level: * significant at $P < 0.05$, ** significant at $P < 0.01$.

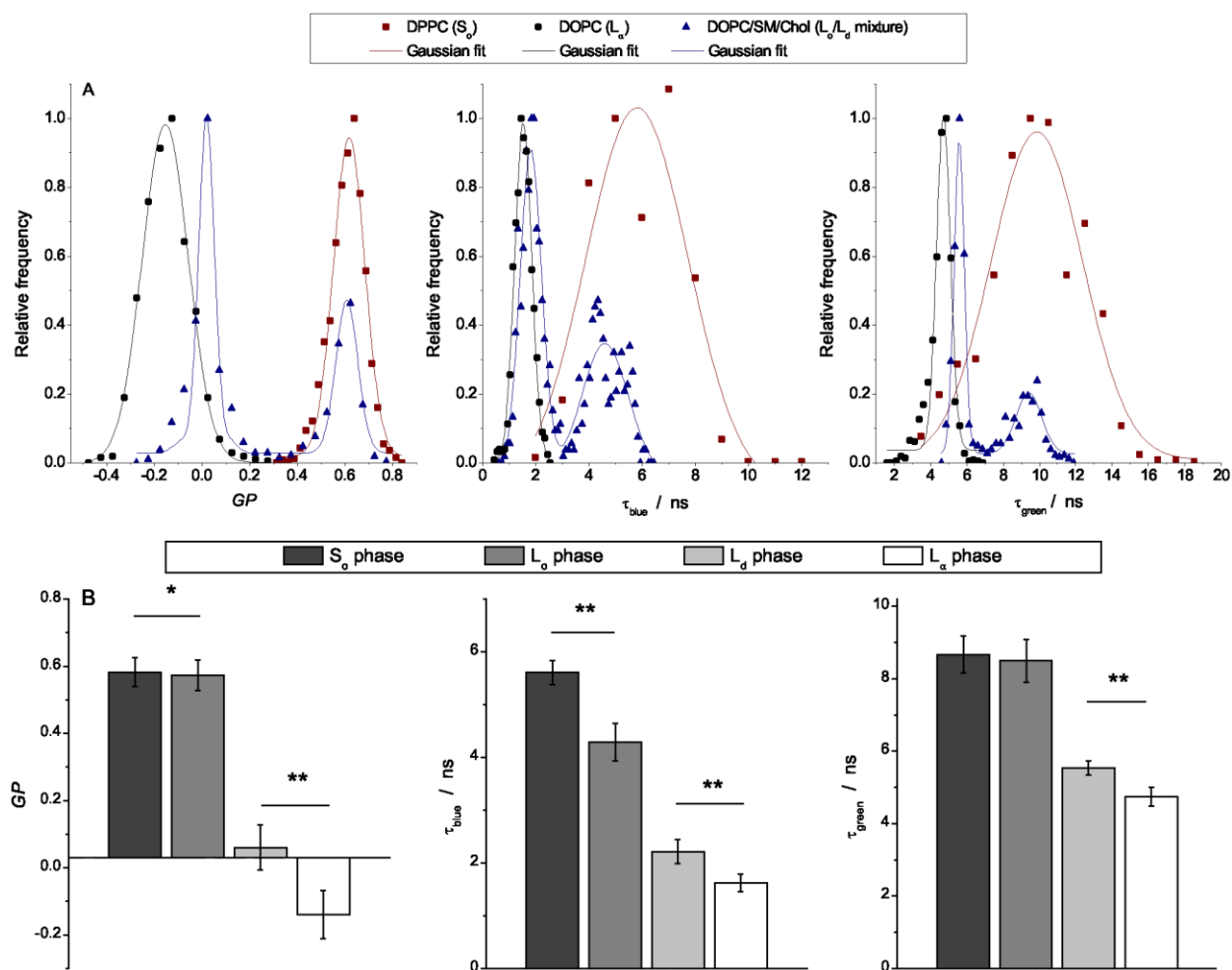


Figure 5.13. Laurdan in GUVs observed with circularly polarized excitation at room temperature.

(A) Distribution of the GP values and the lifetimes in the blue and the green channel for various lipid phases: L_α phase (black), mixture of L_o and L_d phases (blue) and S_o phase (red). Distributions are fitted to a Gaussian or a sum of Gaussians. (B) Average GP and fluorescence lifetimes for the different phases. The error bars are the standard deviations resulting from at least seven GUVs measured for each condition. The data were analyzed using one-way-analysis of variance (ANOVA) with Bonferroni's Multiple Comparison Test with significance level: * significant at $P < 0.05$, ** significant at $P < 0.01$.

5.3. Measurements on HEK293T cells

Determination of *GP* and fluorescence lifetimes in the blue and the green channels were performed on HEK293T cells at 21 °C and 37 °C, before and after Chol depletion with M β CD. Autofluorescence of unstained cells was evaluated under the same conditions and no contribution arising from the plasma membrane could be detected (data not shown).

A typical result obtained by applying to the plasma membrane segmentation procedure, described in the Materials and Methods section, is shown in Figure 5.14.

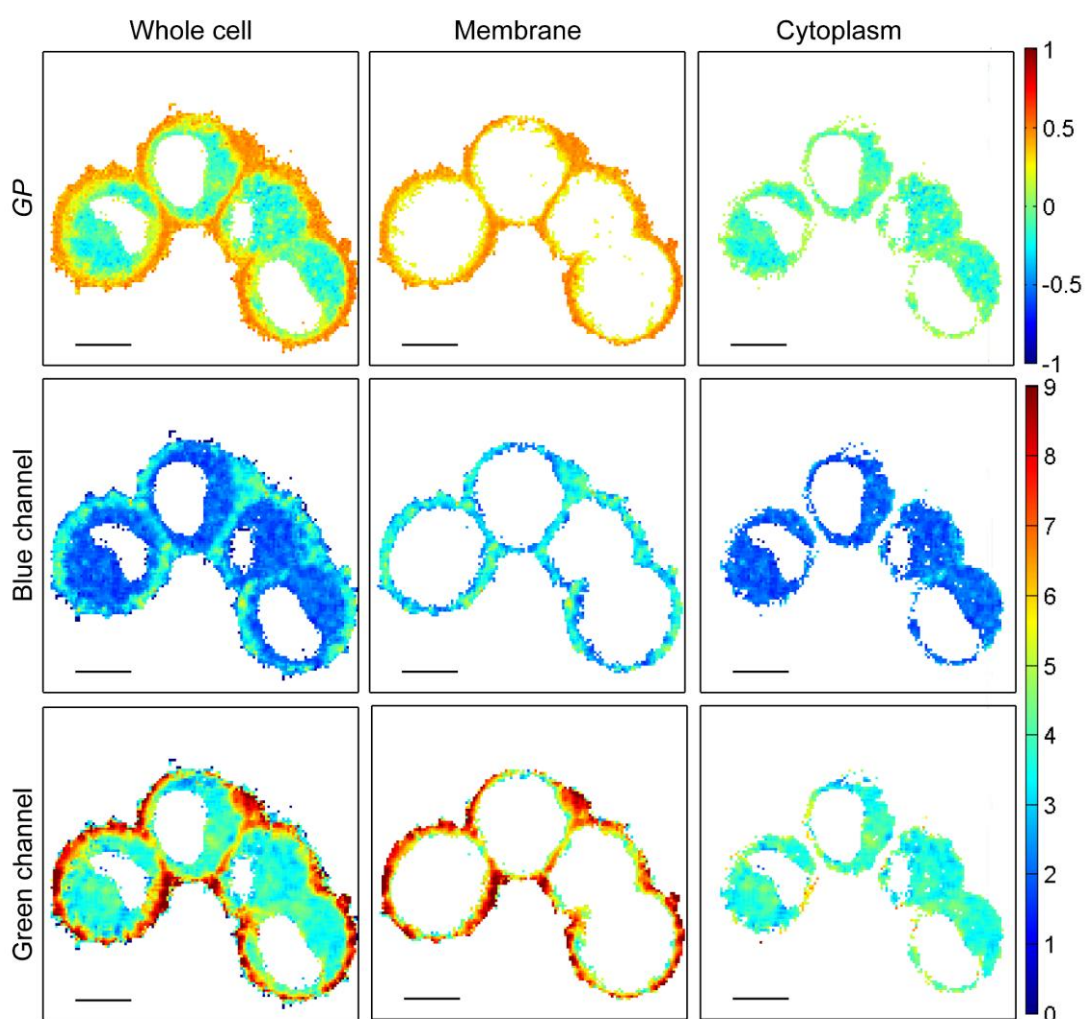


Figure 5.14. *GP* and fluorescence lifetime images obtained for Laurdan in HEK293T cells at 21 °C. Applying a mask to the whole cell (left), we can separate the plasma membrane (middle) from the cell cytoplasm (right). Note that Laurdan does not stain the nucleus. Excitation light is horizontally polarized. The size of the scale bar is 10 μ m for all images.

The mapping of *GP* and lifetime values over the plasma membrane region is shown in Figure 5.15.

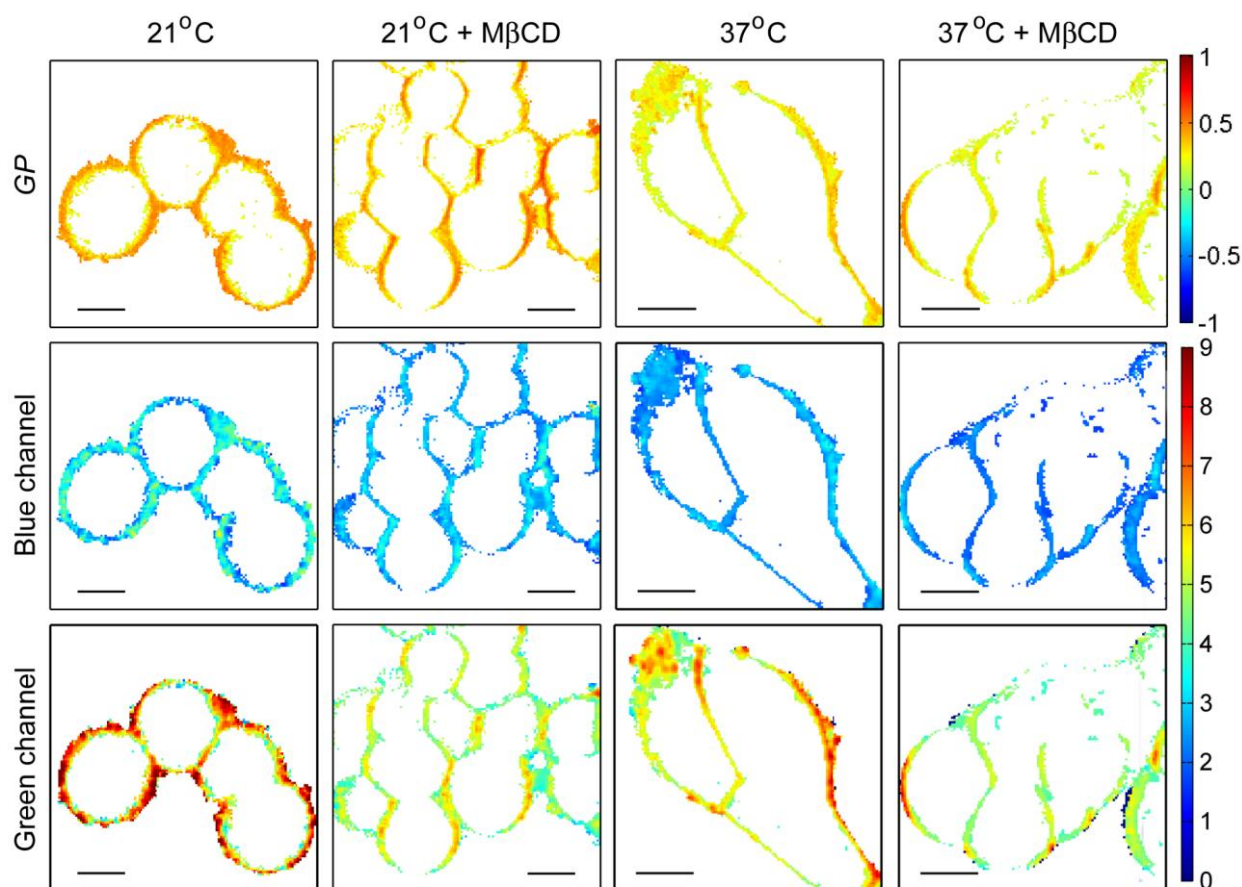


Figure 5.15. Laurdan in the plasma membrane of HEK293T cells.

Mapping of GP and fluorescence lifetimes (color coded lifetime values in ns) in the blue and the green channels. Chol depletion was achieved by application of M β CD. Note that some plasma membranes are no longer visible after the membrane segmentation procedure. The orientation of the linear polarization of the excitation light is horizontal. The size of the scale bar is 10 μ m for all the images.

Correlation maps between *GP* values and fluorescence lifetimes for Laurdan in the plasma membrane of HEK293T cells are presented in Figure 5.16. Although there are no distinct phases, low lifetime values for both channels correlate with low *GP* values. Similarly, high lifetime values for both channels correlate with high *GP* values. The correlation is most pronounced for cells treated with M β CD.

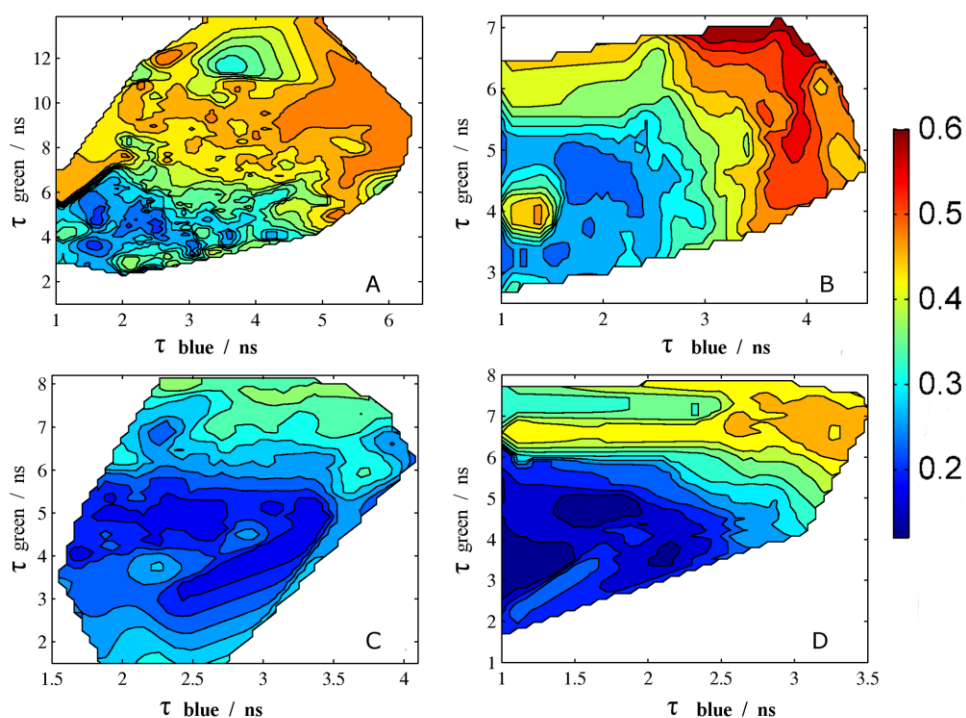


Figure 5.16. Topographic maps of Laurdan in the plasma membrane of HEK293T cells. Measurements performed at 21 °C: untreated (A) and treated with M β CD (B). Measurements performed at 37 °C: untreated (C) and treated with M β CD (D). GP is shown by color coded values. The excitation light is horizontally polarized.

The distribution of GP and lifetime values over the pixels related to the membrane depends on temperature and Chol content (Figure 5.17). These histograms are between those obtained for the L_o and L_d phases of the GUVs. The histograms of the lifetimes are better defined in comparison to the GP histograms. However, it can be observed that the maximum of the GP distribution is shifted to lower values upon temperature increase or Chol depletion. The lifetime distribution in the blue channel is shifted to smaller values with both temperature and Chol modulation, while in the green channel the shift is better observed after Chol depletion. A narrowing of the lifetime distributions is observed in both channels upon increasing temperature or Chol depletion.

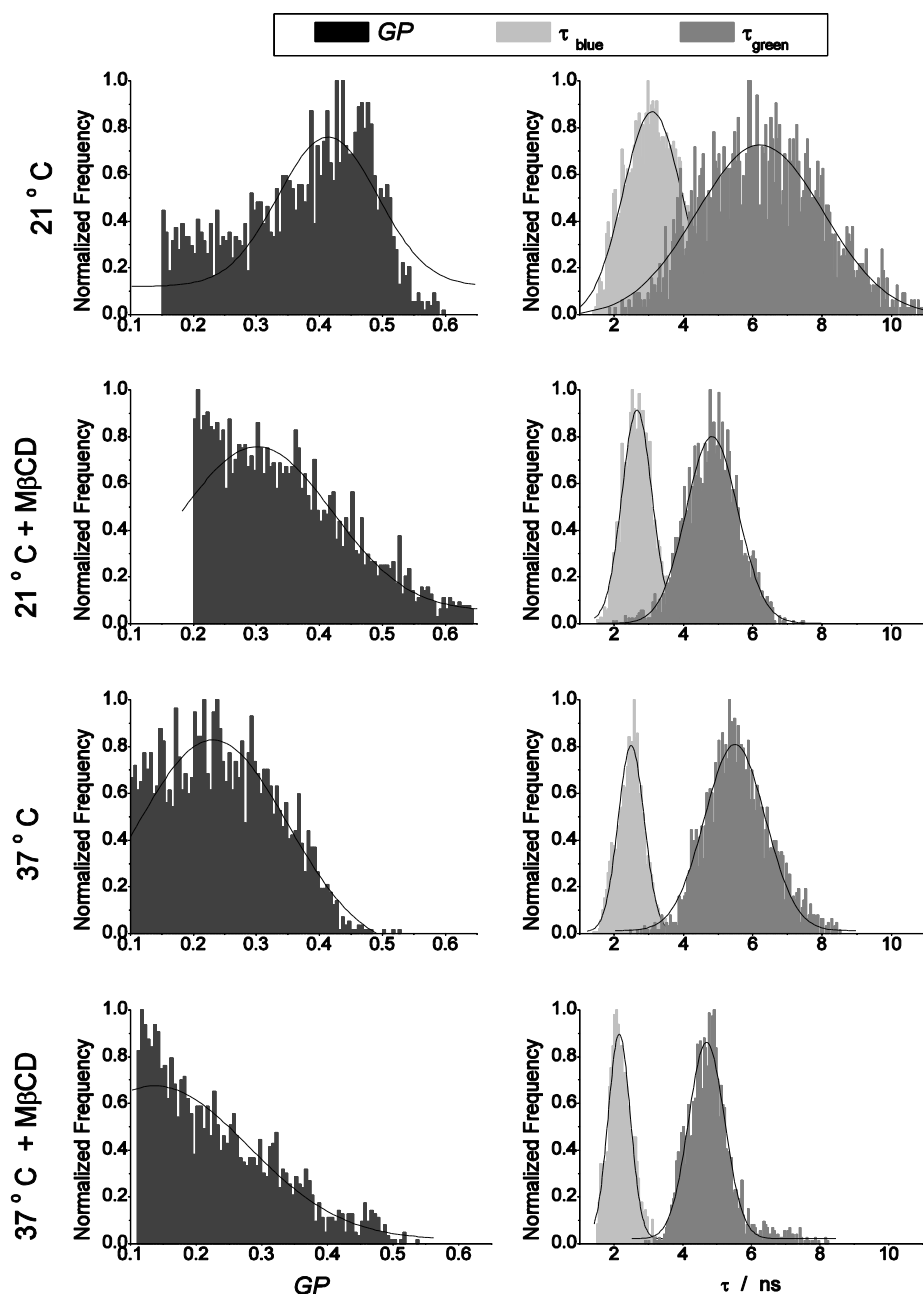


Figure 5.17. Histogram of GP and fluorescence lifetime values for Laurdan in the plasma membrane of HEK293T cells.

The histograms are for the cells shown in Figure 5.15. Because we used a threshold based on GP values to separate the plasma membrane from the rest of the cell, GP distributions show an abrupt stop at lower values.

The average values for GP and lifetimes in the blue and green channel for the images recorded in each of the conditions considered, are shown in Figure 5.18. The average GP value decreases significantly with temperature from 0.39 at 21 °C to 0.28 at 37 °C for

untreated cells, while after M β CD treatment, the average GP value changed from 0.35 at 21 °C to 0.23 at 37 °C. GP values obtained for the treated cells are also significantly smaller than those obtained for the untreated cells recorded at the same temperature. Compared with the GP behaviour, the lifetime changes recorded in the two channels were less pronounced. The average lifetime recorded in the blue (green) channel for the untreated cells decreased from ~ 2.9 ns (~ 6 ns) at 21 °C to ~ 2.5 ns (~ 5.4 ns) at 37 °C, and for the cells treated with M β CD from ~ 2.7 ns (~ 4.9 ns) at 21 °C to ~ 2.2 ns (~ 4.8 ns) at 37 °C. A statistically significant decrease of the average lifetime was observed after Chol depletion in each channel for both temperatures.

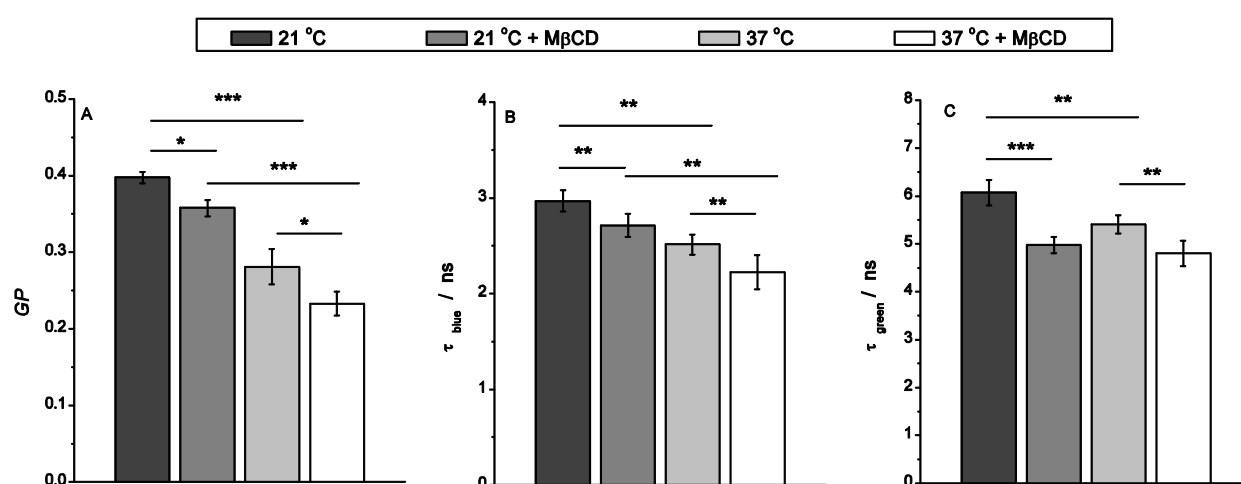


Figure 5.18. Average values of GP and fluorescence lifetime for Laurdan in the plasma membrane of HEK293T cells.

Average GP values (A), average fluorescence lifetimes in the blue (B) and green (C) channels. The data were analyzed using one-way-analysis of variance (ANOVA) with Bonferroni's Multiple Comparison Test with significance level: *significant at $P < 0.05$, ** significant at $P < 0.01$, *** significant at $P < 0.001$. The error bars are standard deviations resulting from at least 11 measurements for each condition.

The data for Laurdan in HEK293T cells can be analyzed from the perspective of GUVs exhibiting the L_o/L_d phase separation. The experiments on the GUVs indicated that L_o and L_d phases can be discriminated using GP threshold values of about 0.3, and this in correspondence with the literature (Bagatolli and Gratton 2000). A similar approach has been suggested for the plasma membrane of living cells (Gaus *et al.* 2003).

We applied the 0.3 *GP*-threshold value to the pixels related to the plasma membrane of the HEK293T cells. Average *GP* and lifetime values were calculated for the two classes of pixels defined in this way (Table 5.3). We calculated the fraction of the membrane related pixels with *GP* values higher than 0.3. This fraction is decreasing with increase in temperature and M β CD treatment, as expected.

Table 5.3. Average *GP* and lifetimes for pixels related to the plasma membrane of the HEK293T cells with *GP* < 0.3 and with *GP* > 0.3

Conditions	<i>GP</i> > 0.3			<i>GP</i> < 0.3			% of pixels with <i>GP</i> > 0.3
	<i>GP</i>	τ_{blue} (ns)	τ_{green} (ns)	<i>GP</i>	τ_{blue} (ns)	τ_{green} (ns)	
21 °C	0.43 ± 0.01 ^a	2.99 ± 0.06	6.3 ± 0.30	0.26 ± 0.01	2.50 ± 0.09	5.4 ± 0.10	80 ± 8
21 °C + M β CD	0.43 ± 0.02	2.9 ± 0.10	5.0 ± 0.20	0.25 ± 0.02	2.33 ± 0.09	4.6 ± 0.10	61 ± 13
37 °C	0.39 ± 0.02	2.6 ± 0.10	5.7 ± 0.30	0.25 ± 0.02	2.24 ± 0.11	4.9 ± 0.20	56 ± 15
37 °C + M β CD	0.39 ± 0.04	2.4 ± 0.10	5.2 ± 0.40	0.18 ± 0.03	1.98 ± 0.08	4.5 ± 0.10	27 ± 15

^aUncertainties are standard deviations.

5.4. Discussion

Laurdan can be used to detect and assess changes in both model and natural membranes due to its solvatochromic properties (Bagatolli 2006; Bagatolli and Gratton 2000). In the current view the shifts in the spectra are ascribed to the relaxation of the polar solvent molecules around the increased dipole moment of the probe in the excited state (Jurkiewicz *et al.* 2012). The change in dipole moment can be quite large for solvatochromic probes that exhibit intramolecular charge transfer from a donor to an acceptor region of the molecule (Marini *et al.* 2010). In the case of Laurdan, this charge transfer is between the dimethylamino group (electron-donor) and the carbonyl group (electron-acceptor) located at the opposite sites of the naphthalene moiety (Sanchez *et al.* 2007).

The fluorescence properties of Laurdan inserted into lipid membranes depend on the relaxation of the water molecules near the excited naphthalene moiety, which is generally considered to be located at the level of the glycerol backbone (Bagatolli 2006; Jurkiewicz *et al.* 2006). As the lipid phase modulates the accessibility of water molecules to the naphthalene moiety, the state of the lipid phase can be assessed by the fluorescence characteristics of Laurdan (Parasassi *et al.* 1990). For a membrane with a higher order of lipid packing (S_o), only a few water molecules can reach the naphthalene moiety of Laurdan, implying a small effect of dipolar reorientation. Conversely, the L_α phase of the membrane is characterized by a poor lipid packing allowing more water molecules to penetrate the outer region of the membrane. Thus the emission maximum of Laurdan shifts from around 440 nm in the S_o phase to around 490 nm in the L_α phase (Bagatolli 2006; Bagatolli and Gratton 2000; Sanchez *et al.* 2007). Unlike lipid membranes, Laurdan in solvents is completely surrounded by solvent molecules and only changes in polarity of the solvent can lead to a spectral shift.

However, the large spectral shift of Laurdan cannot be explained only by the increase of the Laurdan dipole moment with 5-8D upon excitation (Mukherjee and Chattopadhyay 2005; Parisio *et al.* 2011; Tomin *et al.* 2003). For Laurdan both a non-hydrogen and a hydrogen bonded form have to be considered (Marini *et al.* 2010). The few reports modeling the large spectral shift of Laurdan due to hydrogen bonding (Klymchenko *et al.* 2004) are mostly based on molecular dynamics simulations (Jurkiewicz *et al.* 2012; Parisio *et al.* 2011). The models differ in the origin of the water molecules with which the Laurdan molecules are interacting: a) with water molecules of the hydrated lipids found at the level of the probe (Jurkiewicz *et al.* 2012), or b) with water molecules that penetrate the membrane (Parisio *et*

al. 2011). In these simulation studies it is stated that the blue emission occurs from a population less accessible to water, while the green emission comes from a population located closer to the surface of the membrane. Jurkiewicz *et al.*, showed that the molecules embedded more into the membrane emit at a shorter wavelength, while the molecules closer to membrane surface emit at longer wavelengths (Jurkiewicz *et al.* 2006).

However, for the Laurdan probe it is difficult to discriminate experimentally between dipole-dipole and specific H-bonding interactions (Klymchenko *et al.* 2004).

5.4.1. Lifetimes are more sensitive to lipid composition than *GP*

GP values are usually used to quantify membrane changes (Bagatolli 2006; Parasassi *et al.* 1998). Although *GP* can take values from -1 to +1, the experimental values reported in the literature for Laurdan in a lipid environment range from - 0.40 to 0.65 (Bagatolli *et al.* 1999; Esquembre *et al.* 2007; Parasassi *et al.* 1998; Periasamy and Winter 2006). The *GP* values obtained for LUVs in this study (Figure 5.2) for the S_o and L_α phase are essentially independent of the phospholipid type and in agreement with the literature (Parasassi *et al.* 1991). Previous studies on liposomes showed that the phase transition temperature of the lipids can be accurately determined by the temperature dependence of *GP* (Bagatolli *et al.* 1999; Parasassi *et al.* 1991). The data presented in Figure 5.2 and Table 5.1 yield transition temperatures that are consistent with those reported in the literature (Koynova and Caffrey 1998).

Beside spectral changes the fluorescence lifetimes of Laurdan depend on the environment (Parasassi *et al.* 1991; Tomin *et al.* 2003) (Table 5.2). Relatively few reports discuss the lifetime of Laurdan in a lipid environment. It was reported that the lifetime of Laurdan takes a larger value (> 5 ns) in the S_o phase than in the L_α phase (< 4 ns) (Aguilar *et al.* 2012; Bagatolli *et al.* 1998; Bagatolli *et al.* 1997; Bagatolli *et al.* 1999) However, in these studies the time-resolved emission comprised simultaneous contributions from both blue and green channels.

Very recently, Owen *et al.* (Owen *et al.* 2012) combined the phasor approach (Digman *et al.* 2008) with FLIM measurements of Laurdan in sonicated vesicles in which a long-pass filter (430 nm) was used. Single lifetimes were found for single phase ordered and disordered membranes. Phasor plots revealed that membranes with co-existing phases gave rise to biexponential decays.

The impact of the emission wavelength interval of observation in time-resolved measurements has been pointed out by Stefl *et al.* (Stefl *et al.* 2011). A single fluorescence relaxation time has been observed for Laurdan in DMPC small unilamellar vesicles (SUVs) at 25 °C for measurements over the entire Laurdan emission. However, when using a 470 nm long pass filter a more complex decay is observed. These observations have been interpreted as that the nonrelaxed state determines the overall emission, while the time-resolve data collected at the longer wavelengths are indicative of dipolar relaxation.

In our LUV experiments the fluorescence decays were well described ($\chi^2 < 1.2$) by a single exponentially decaying function in both the blue and green channel in a relevant temperature range. The lifetime recorded in the blue channel is generally lower than in the green channel.

An interesting observation is the effect of the type of lipid on the lifetime values which is limited only for the S_o phase, but not for the L_α one. This result shows that the lifetime, unlike the GP, is sensitive to the lipid type in homogeneous model membranes. In spite of the similar structure of the lipid head groups, the length of fatty acid chains influences the accessibility of water molecules to the naphthalene moiety. The longer lifetime determined for DPPC can suggest that Laurdan is less accessible to water as compared to DMPC.

In a recent study of Barucha-Kraszewska *et al.* (Barucha-Kraszewska *et al.* 2010), the time-resolved relaxation of the excited state of Laurdan in water and in DOPC membranes was analyzed. Their results show four relaxations time constants: two shorter ones (on a picosecond time scale), associated with the rotation and translation of water molecules, while the two longer ones (on a nanosecond time scale) are considered to be caused by reorganization of the lipids after changes in hydration of the membrane. The two longer relaxation times reported by Barucha-Kraszewska *et al.* (Barucha-Kraszewska *et al.* 2010) are similar to the lifetimes recorded by us in the blue and green channel for both LUVs and GUVs found in a L_α phase.

Upon addition of Chol to DMPC both GP and lifetimes in each of the channels increase above and below the phase transition temperature (Figure 5.2, Figure 5.3). This observation is somewhat at variance with the results obtained by Aguilar *et al.* (Aguilar *et al.* 2012) upon the addition of Chol to DPPC LUVs. They studied the influence of Chol on the single relaxation time of Laurdan determined over the whole emission band. The single relaxation time increased if the DPPC LUV was initially in the L_α state and decreased when the system was in the S_o state.

The temperature dependence of the lifetime can be used to determine the lipid T_m values. Apart from the T_m value derived from the lifetime values in the green channel for DMPC, the values are consistent with those derived from GP curves and those reported in literature (Table 5.1). The relative decrease of the lifetimes upon the transition from the S_o phase to the L_α phase is larger in the blue channel than in the green channel (Figure 5.3). As the molecules emitting in the green channel are in a more relaxed environment, one can assume that the increased exposure of Laurdan to water molecules has reduced the sensitivity of the green channel to changes in the membrane structure. This reduction can be larger for DMPC assuming that the Laurdan molecules reside closer to the water interface and could explain the difference in the estimated value of T_m .

A strong correlation between GP and the fluorescence lifetimes in the blue and green channel is observed (Figure 5.4). For temperatures lower than the phase transition temperature the lifetimes for Laurdan in DMPC and DPPC coincide in each channel at the same GP value. This means that Laurdan is essentially probing the same environment in these systems. At higher GP values the lifetimes obtained for DMPC and DPPC can be different at the same GP value. When Chol is added to DMPC the lifetimes in each of the channels are lower than in the pure DMPC system at the same GP value, apart from the situation at higher GP values where they become essentially equal. It can be concluded that Laurdan is not necessarily probing the same local environment in the different systems at lower GP values.

5.4.2. Correlations between GP and lifetimes differentiate coexisting lipid phases in GUVs

Because of the inherent spatial averaging in spectroscopy measurements, microscopy experiments were performed on GUVs to obtain both GP values and fluorescence lifetime based images. To our knowledge, no FLIM images, but only GP images (Bagatolli and Gratton 1999; Bagatolli and Gratton 2000; Sanchez *et al.* 2011) for Laurdan in GUVs are reported in the literature. In our study, GUVs at room temperature exhibiting either S_o (DPPC) or L_α (DOPC) phases, or coexistent L_o/L_d phases (DOPC/SM/Chol) were characterized by GP and FLIM images. Independent of the polarization of the excitation light, we found that both S_o and L_α phases are characterized by average GP values around 0.6 and -0.2, respectively, in line with the values obtained for LUVs in this report and for the GUVs in the literature (Bagatolli and Gratton 2000; Parasassi *et al.* 1997). Because the

L_o phase is considered to be an intermediate state between S_o and L_α phases, it was expected that the GP values found are smaller than those recorded in the S_o phase. While the L_d and L_α phases are considered to be similar as both of them represent the disordered phase (McMullen *et al.* 2004), the GP values we obtained suggest that the L_d phase is more ordered as compared with the L_α phase. This behaviour is consistent with the data previously reported in literature (Kaiser *et al.* 2009).

The lifetime distribution recorded in the blue and the green channel for both the S_o and L_α phases are independent of the polarization of the incident light (Figure 5.10; Figures 12 and 13). The average lifetime obtained for DPPC at room temperature (S_o phase) in the blue channel compares well with that obtained for the corresponding LUV, while the average lifetime in the green channel is somewhat higher for the GUV than for the LUV. The average lifetimes in the blue and green channel obtained for DOPC GUVs at room temperature (L_α phase) are essentially equal to the lifetimes obtained for the DMPC and DPPC LUVs well above the transition temperature. The average lifetimes in the two channels and the average GP values are consistent with the relation obtained for LUVs (Figure 5.4).

In the case of L_o/L_d phase coexistence, the lifetime recorded in the blue channel is significantly smaller for the L_o phase than for the S_o phase, while for the green channel no significant difference was observed. On the other hand, the lifetimes recorded for the L_d phase are for both channels higher than the ones recorded in the L_α phase. Analyzing the results obtained for the different phases, it can be stated the lifetime images recorded in the blue channel are more sensitive to coexistent phases.

The correlation between GP and lifetime values was explored on GUVs with L_o/L_d phase coexistence. We found that high GP and lifetime values characterize the L_o phase while smaller values of GP and lifetimes are obtained for the L_d phase. This is better illustrated in the topographic map not only for a GUV with L_o/L_d phase coexistence (Figure 5.8), but also for the one component GUVs (Figure 5.11). A topographic map for GUVs with L_o/L_d phase coexistence measured with circularly polarized light was also obtained (Figure 5.9). Comparing the two maps of GUVs with L_o/L_d phase coexistence we can see a stronger correlation for the data obtained with circularly polarized light. In the absence of a pronounced photoselection effect, GP and lifetime values obtained for the two phases are better separated, giving a narrower distribution and thus a stronger correlation. This effect can be easily observed for the lifetimes recorded in the green channel. The correlation between GP and fluorescence lifetimes observed for the GUVs with circularly polarized light is in line with the correlation obtained for LUVs (Figure 5.4).

We performed experiments on Laurdan in GUVs in which GP and lifetimes are determined as a function of the angle between the polarization direction of the incident excitation light and the position on the circumference of the GUV. The angular dependence of GP shown in Figure 5.7 is consistent with earlier observations (Bagatolli *et al.* 2003). Although photoselection results in angular variation of the intensities, GP can remain constant because of its ratiometric nature. Assuming an elongated shape for Laurdan, Bagatolli *et al.* (Bagatolli *et al.* 2003) interpreted the relation between GP and angular position in terms of intrinsic microheterogeneity for the fluid phase which is absent in the gel phase. In the gel phase the Laurdan molecules have their axis mostly along the normal to the membrane, while in the liquid-crystalline phase a much wider distribution is observed (Gasecka *et al.* 2009). The fluorescence intensities in the gel phase can be expected to exhibit a stronger angular dependence than in the liquid-crystalline phase. If there is no microheterogeneity and the orientation of the reporter molecule does not influence the wavelength of emission, the observed GP is independent of the position on the circumference of the GUV. In the case of microheterogeneity, the contribution of the membrane regions with the normal parallel to the polarization of the incident light will be mainly due to a more ordered phase, while in the perpendicular direction a less ordered phase contributes the most. We also investigated the angular dependence of the fluorescence lifetimes in the blue and green channel for the gel and liquid-crystalline phase (Figure 5.7).

The lifetime in the green channel for the gel phase decreases abruptly around 90° but shows a gradual change with the angle for the liquid-crystalline phase. Also the lifetime in the blue channel exhibits a strong angular dependence around 90° in the gel phase but is essentially constant in the liquid-crystalline phase. We observed a corresponding photoselection effect in the L_o/L_d system. As a fluorescence lifetime does not depend on the actual number of emitting fluorophores this angular dependence of the lifetimes requires further exploration.

The strong angular dependence around 90° for the green channel in the gel phase suggests that photoselection reveals a particular subpopulation of Laurdan with a shorter lifetime. This can be a population of elongated molecules with their axis around 90° with the normal to the membrane. Although this has been observed for the neutral and apolar membrane probe DPH (1,6-Diphenyl-1,3,5-hexatriene) in artificial membranes above the phase transition (Ameloot *et al.* 1984), this is unlikely to be the case for Laurdan in the gel phase. Fluorescence polarimetry imaging shows a Gaussian distribution for Laurdan around the normal to the membrane for both the gel and the liquid-crystalline phases (Gasecka *et al.*

2009). The width of the Gaussian distribution in the gel phase predicts a very small excitation probability at 90° .

Recently Parisio *et al.* (Parisio *et al.* 2011) suggested different conformations of Laurdan in a lipid bilayer based on quantum mechanical electronic structure calculations and molecular field theory. They showed that Laurdan in the liquid-crystalline phase can take an elongated form and an L-shaped form in which the fluorescent moiety makes an angle with the hydrocarbon chain of the probe. It was suggested that in the gel phase the elongated conformer prevails. Also Barucha-Kraszewska *et al.* (Barucha-Kraszewska *et al.* 2013) found through MD and quantum mechanical simulations that Laurdan has a high probability for the L-shape in the liquid-crystalline phase (DOPC at room temperature).

The L-shaped conformers in the gel phase must have a different position along the normal to the membrane as the elongated conformer because of the lipid organization in the gel phase. The L-shaped conformers have a larger exposure to the water phase than the elongated conformer. The kinetics in this environment of the L-shaped conformer might be faster than for the more buried elongated conformers so that a shorter lifetime can be expected.

The lifetime in the blue channel for the gel phase also shows a strong variation around 90° albeit somewhat reduced in comparison the green channel. The shorter lifetimes in the blue channel can be interpreted as being related to the locally excited state.

The lifetimes in the green channel in the liquid-crystalline phase show a more gradual angular variation. This can be modeled by a decreased difference between the two conformers. The change in lipid packing allows for a wider orientation distribution of the elongated conformer and for different vertical positions of the L-shaped conformer. However, around 90° the contribution of the L-shaped conformer with the shorter lifetime is still somewhat more important.

The lifetime in the blue channel in the liquid phase takes a small value and is independent of the position on the circumference of the GUV. This indicates that Laurdan in the liquid phase probes an environment for which the locally excited state of the elongated and L-shaped conformers are essentially the same.

5.4.3. *GP*-lifetime topographical maps reveal complex organization of the plasma membrane of the living cell

In this chapter we reported on the spatial distribution of *GP* and fluorescence lifetimes of Laurdan in the plasma membrane of HEK293T cells. Because of the diversity of the lipids and the proteins constituting the plasma membrane and the restricted experimental spatial resolution, prohibiting the detection of local lipid unmixing giving rise to the so-called lipid membrane rafts (Pike 2003), it is unlikely to get values corresponding to the extreme phases (S_o and L_a). Nevertheless, *GP* values of Laurdan can be used to monitor membrane changes (Gaus *et al.* 2003; Harris *et al.* 2002; Jaureguiberry *et al.* 2010; Parasassi *et al.* 1997). The membrane organization can be modulated either by modifying the temperature or by altering the lipid composition of the membranes, mostly accomplished by M β CD Chol depletion (Brejchova *et al.* 2011; Jaureguiberry *et al.* 2010; Mukherjee and Chattopadhyay 2005; Ohki 2005; Wheeler and Tyler 2011). The clear photoselection effect we observed for Laurdan in GUVs with linearly polarized excitation light is reduced because of the membrane convolutions and because the cross sections are not circular (Gaus *et al.* 2006).

A somewhat limited number of papers report *GP* images obtained on cells. Yu *et al.* found an average *GP* of 0.3 for a mouse fibroblast culture at room temperature (Yu *et al.* 1996). Kim *et al.* (Kim *et al.* 2007), working on A431 cells, described *GP* distributions with two subpopulations, one with *GP* \sim 0.5 and the other with *GP* \sim 0.2. However, the analysis was done on the entire cell image, including intracellular positioned pixels. On the other hand, Schneckenburger *et al.* reported smaller values of *GP* for Chinese hamster ovary (CHO) cells recorded at 24 °C: \sim 0.095 in the plasma lemma and \sim 0.03 for the whole cell image (Schneckenburger *et al.* 2004). The average *GP* value for untreated cell membranes reported in this work is \sim 0.4. Consistent with the literature, *GP* values recorded in the present experiments decrease with temperature increase (Gaus *et al.* 2003; Ohki 2005), and also with the decrease of Chol concentration for cells treated with M β CD (Brejchova *et al.* 2011; Wheeler and Tyler 2011). *GP* values of intracellular membranes (Figure 5.14) are smaller than those of plasma membranes, in agreement with the literature (Schneckenburger *et al.* 2004).

Only few papers report on fluorescence lifetime imaging of Laurdan embedded in cellular membranes (Owen *et al.* 2012; Schneckenburger and Wagner 2005; Schneckenburger *et al.* 2004; Yu *et al.* 1996). Yu *et al.* (Yu *et al.* 1996), found that the lifetimes in the plasma membrane are higher ($>$ 4.3 ns) compared to those in the nuclear

membrane (< 2.7 ns). Schneckenburger *et al.* studied CHO cells (Schneckenburger and Wagner 2005; Schneckenburger *et al.* 2004) and obtained values of ~ 5 ns in young cells and of ~ 3 ns in aged cells when the Laurdan emission was recorded in a broad spectral band (420-800) nm (Schneckenburger *et al.* 2004). When measurements were performed within narrow bands, 454 ± 20 nm and 497 ± 20 nm, the lifetime recorded with the shorter wavelength band decreased by 20–30 % when increasing the temperature from 24 °C to 41 °C, whereas the lifetime in the longer wavelength band remained almost constant (Schneckenburger *et al.* 2004). Owen *et al.* (Owen *et al.* 2012) performed FLIM measurements of Laurdan in HeLa cells at 37 °C using a 430 long-pass filter and applied the phasor approach. The actual lifetimes were not given but the plasma membrane at room temperature was estimated to have an ordered:disordered ratio of 80:20. This ratio compares well with the ratio of membrane related pixels we obtained when grouped on the basis of *GP* (Table 5.3).

In the present study, the average lifetime values of Laurdan in HEK293T cells are in the range of $\sim 2 - 3$ ns in the blue channel and in the range of $\sim 5 - 6$ ns in the green channel. Both the increase in temperature and Chol depletion induced a decrease of the lifetime in the blue and green channel. However, the two lifetime channels react differently to the changed conditions. While the lifetimes in the blue channel are more sensitive to temperature changes, the lifetimes in the green channel are only affected by the change in Chol concentration. It can be stated that, although the magnitude of the decrease for the lifetimes is less pronounced compared with the *GP* values, one can still use them to detect changes in the membrane.

The distribution of *GP* values of DOPC/SM/Chol GUVs (Figure 5.12) indicate that L_o and L_d areas can be separated with a *GP* threshold value of 0.3, in correspondence with suggestions in the literature (Bagatolli and Gratton 2000; Gaus *et al.* 2003). We used this value to group the membrane pixels and to calculate the corresponding average value of *GP* and the lifetimes in the blue and green channel (Table 5.3). The resulting averages can be compared with the correlation obtained from the LUV experiments (Figure 5.4). For the pixel group with $GP > 0.3$, the lifetime in the green channel is to some extent compatible with the average *GP* value but the lifetime in the blue channel is too small, even after Chol depletion at the higher temperature. This is also the situation for the pixel group with $GP < 0.3$. Although the percentage of pixels with $G > 0.3$ follows the expected trend upon Chol depletion and temperature increase (Table 5.3), the deviated lifetime in the blue channel indicates that assignments based on *GP* alone should be interpreted with some cautiousness. In the case of GUVs, the lipid domains are substantially larger than the optical resolution of

the system and their GP and lifetime values are clearly separated. Cell membranes are more difficult to analyze because of their heterogeneity in composition and because the lipid domains are believed to be of the order of a few tenths of nanometers (Simons and Vaz 2004). The pixel value for GP and lifetimes will therefore be averages of the environment covered by the point spread function of the optical system. Furthermore, the photoselection could bias the observation to regions with high GP (Parasassi *et al.* 1997), although this effect is probably not severe for cell membranes.

As could be expected the correlation between GP and lifetimes in each of the channels is less clear as for the GUVs. For the untreated cells at 21 °C the topographic map (Figure 5.16.A) comprises a large lifetime region with high GP values. This suggests the presence of L_o -like regions in the plasma membrane as this part of the topographic map is consistent with the observations for DPPC GUVs at room temperature: a narrow range of values for high GP and a wide interval for the lifetime values (Figure 5.10.C and 5.10.D). The lower left quadrant of the topographic map (Figure 5.16.A) covers a rather wide range of GP values for a more restricted range of lifetimes in the two channels. This resembles the situation as obtained for DOPC GUVs at room temperature, albeit with a much broader range of GP values. It can be concluded that the untreated cells at room temperature contains a variety of membrane areas with different properties.

Overall, the topographic map (Figure 5.16.A) of the untreated cells at room temperature contains a high number of structures. These structures largely disappear when the temperature is increased and Chol depletion is applied (Figure 5.16.D). This can be interpreted as that the membrane has a more homogeneous organization under these conditions.

When the temperature is increased or Chol depletion is applied, the area in the lifetime plane of the topographic map decreases substantially although the range of GP values is only a bit smaller (Figure 5.16). The topographic map is essentially reduced to the lower left quadrant of the topographic map obtained for the untreated cells. The topographic map shown in Figure 5.16.D still reflects membrane heterogeneity but to a reduced extent. It is clear from the topographic maps that grouping pixels using a threshold of $GP = 0.3$ can only be a first approximation to get a representation of the membrane properties. The native membrane organization at room temperature cannot be modeled as a combination of L_o and L_d areas. The less ordered domains cannot be labeled as disordered as the GP -lifetimes signature is not compatible with the L_d domains. More elaborated models are required. Recently, Sanchez *et al.* (Sanchez *et al.* 2012) presented an elegant method in which the time

fluctuations of Laurdan GP in cell membranes are analyzed. These fluctuations can be interpreted in terms of a membrane model in which high- GP domains with different size and mobility move in a background of low- GP .

PARTIAL CONCLUSIONS

In this chapter, we demonstrated that *GP* and fluorescence lifetimes are indicative of membrane characteristics of both model and natural membranes.

Fluorescence lifetimes were recorded in two channels, allowing us to characterize Laurdan molecules emitting from two different states: locally excited (LE) where the molecules are not affected by dipole relaxation and charge transfer (CT) where the molecules are affected by dipole relaxation. For the measurements performed on model membranes we were able to detect changes in the lipid packing order of the membrane using *GP* values, while using the lifetimes we were able to distinguish among the phospholipids we used. The lifetimes have a similar behavior as *GP*, decreasing with increasing temperature, thus the T_m assessed by *GP* and lifetimes are similar to those previously reported. Using the lifetimes we can characterize the behavior of the two populations, unlike when using the *GP* values. Therefore, we observed that the molecules emitting from the LE state are more sensitive to membrane changes than the one emitting from the CT state.

Measurements performed on different types of GUVs strengthen the image obtain from the LUVs measurements. First, the photoselection effect was observed for the lifetimes not only for the *GP* values, which allowed us to learn more about Laurdan molecules. Using linearly polarized light we can obtain information regarding the orientation of Laurdan molecules, but also about the microheterogeneity of the phospholipids. We showed that there is a correlation between the *GP* values and the lifetimes in both blue and green channel: high *GP* are correlated with high lifetime values and are characteristic for a more ordered membrane, while lower *GP* and lifetime values are obtained for a less ordered membrane.

The behaviour of Laurdan in lipid membranes is quite complex as different conformers have to be considered. Although the use of *GP* is very useful some cautiousness is appropriate, especially when mapping *GP* over the cell surface. Topographic maps of *GP* and lifetimes reveal the complex situation in biological membranes when information at the pixel scale is used.

CHAPTER 6

**MEMBRANE ORGANIZATION OF OLIGODENDROCYTES WHEN
SUBJECTED TO CHOLESTEROL MODULATION FACTORS**

INTRODUCTION

Because Chol is essential for normal brain development alteration of its biosynthesis and transport can caused CNS autoimmune diseases.

Although in the recent years, statins are more and more use in treatment of these diseases there are not always effective, as a number of studies reported report no significant changes or even an increase in the disease development.

Therapeutic effects in different diseases, like atherosclerosis, diabetes, or inflammatory diseases were observed also for T09.

In this study, Chol modulating factors (SV and T09) were used on OLN-93 cells and the morphological changes they induced were assessed by Laurdan *GP* values and fluorescence lifetimes.

Both SV and T09 cause morphological changes to OLN-93 cells and interfere with the Chol from the plasma membrane, but their mechanisms are different. SV inhibits the synthesis of Chol from an early stage and thus the content of Chol in the membrane decreases. On the other hand, T09 activated LXR which leads to Chol efflux from the cells by activating the Chol transporters found in the cells. It is thought that after T09 treatment, Chol and sphingomyelin are redistributed from rafts to non-rafts and the excess of Chol is transported out of the cells.

6.1. Simvastatin effects on OLN-93 cells membrane

Simvastatin effects on OLN-93 cells and particularly their membrane was investigated using Laurdan fluorescence.

OLN-93 cells grown in medium with 0.5% show a big arborization similar with the pre-mature OLs (Figure 6.1A). When subjected to SV treatment (0.1 and 1 μM) the morphology of the cells changes. The number of branches reduces until the majority of the cells have a bi-polar morphology (Figure 6.1C).

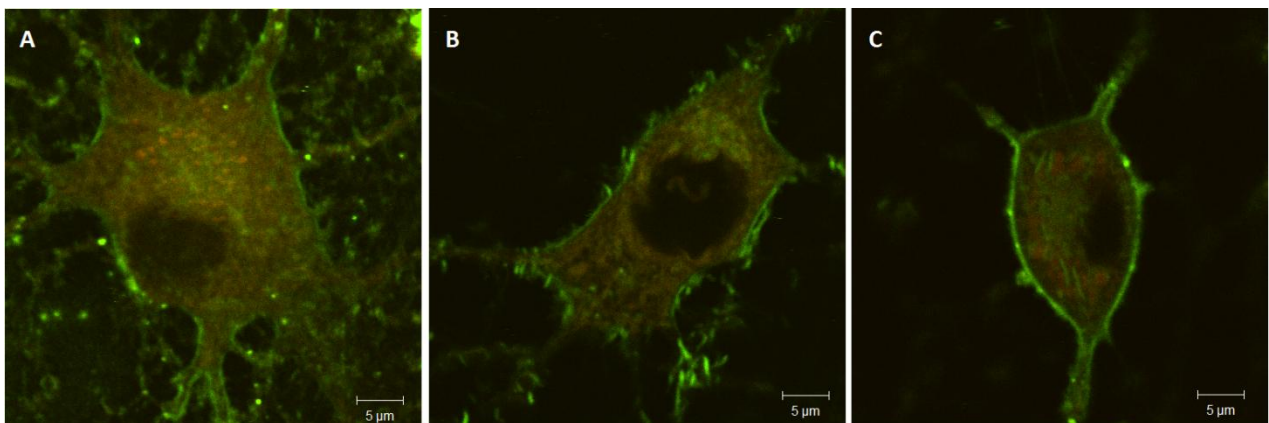


Figure 6.1. Morphological changes of OLN-93 cells.

Fluorescence images of the OLN-93 cells grown under different condition: (A) control cells, (B) cells treated with 0.1 μM SV and (C) cells 1 μM SV. The morphology of the cells changes with increasing SV concentration. Each image is obtained after the images recorded in the two channels were superimposed: the green represents the fluorescence of Laurdan recorded in the blue channel and the red the one recorded in the green channel.

In Figure 6.2 is presented an untreated cell recorded at 21 $^{\circ}\text{C}$. The *GP* values from the membrane are higher than the ones obtained inside the cell. Similar results are obtained for the fluorescence lifetimes recorded in the blue and green channel.

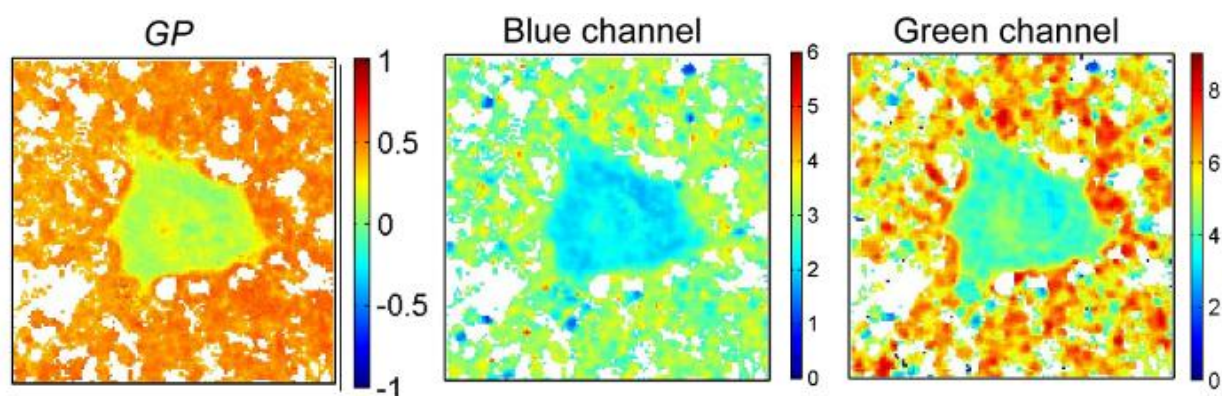


Figure 6.2. OLN-93 cell recorded at 21 °C.

GP image (A) and fluorescence lifetime image (lifetimes in ns) in the blue (B) and green (C) channels.

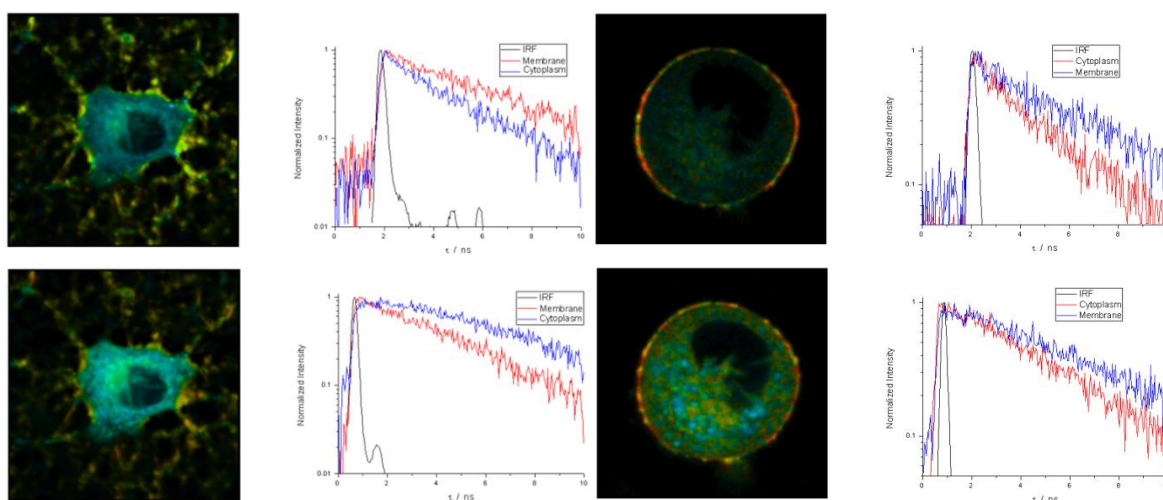


Figure 6.3. FLIM measurements on OLN-93 cell recorded at 21 °C.

Decays recorded for the untreated cells (left) and 10 mM M β CD treated cells (right) in the blue (up) and green (low) channels. The colors represent the fluorescence lifetimes obtained with the B&H software-SPCImage.

In Figure 6.3 are presented the FLIM images for the untreated cells and cells treated with 10 mM M β CD recorded at 21 °C. The decays for the membrane and cytoplasm obtained for the two channels are exemplified. A lower lifetime is recorded in the cytoplasm compared with the plasma membrane and also in the blue channel compared with the green one.

The images recorded on untreated and treated cells loaded with Laurdan were processed to obtain *GP* and fluorescence lifetime images in the blue and the green channels. All conditions were recorded at 21 °C and 37 °C. Autofluorescence of unstained cells was evaluated under the same conditions and no contribution arising from the plasma membrane could be detected (data not shown).

After applying the procedure described in the Materials and Methods section, only the plasma membrane was extracted and analyzed. The mapping of *GP* and lifetime values over the plasma membrane region for a representative cell from each condition measured at 21 °C is shown in Figure 6.4.

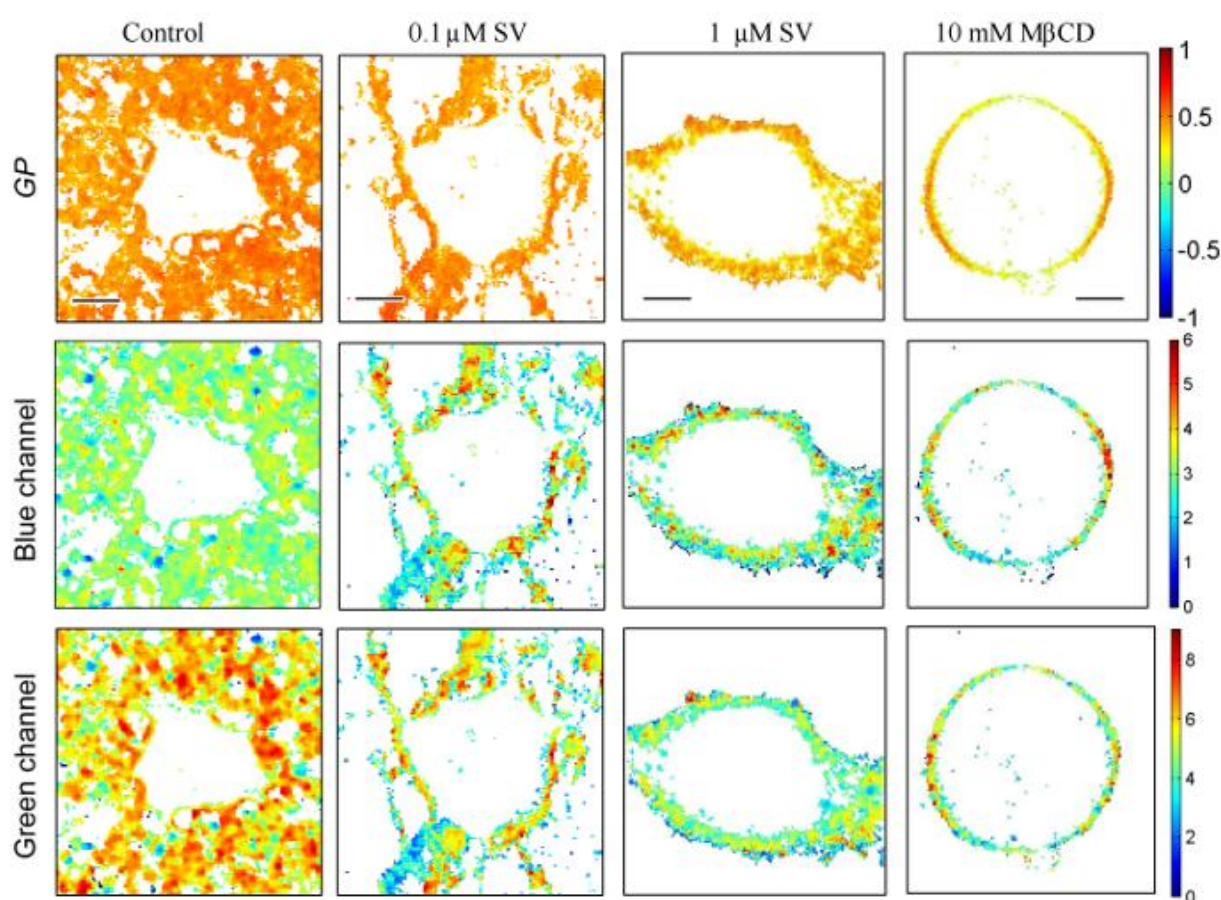


Figure 6.4. Laurdan in the plasma membrane of OLN-93 cells recorded at 21 °C.

Mapping of GP and fluorescence lifetimes (color coded lifetime values in ns) in the blue and the green channels. Chol depletion was achieved by application of SV and MβCD. The orientation of the linear polarization of the excitation light is horizontal. The size of the scale bar is 10 μm for all the images.

As observed from Figure 6.4, the *GP* values and fluorescence lifetimes in the blue and the green channels are decreasing with the increase of Chol depletion.

In Figure 6.5 are presented representative cells from each condition measured at 37 °C. Compared with the results obtained at 21 °C, the values are lower both for the *GP* values and the fluorescence lifetimes.

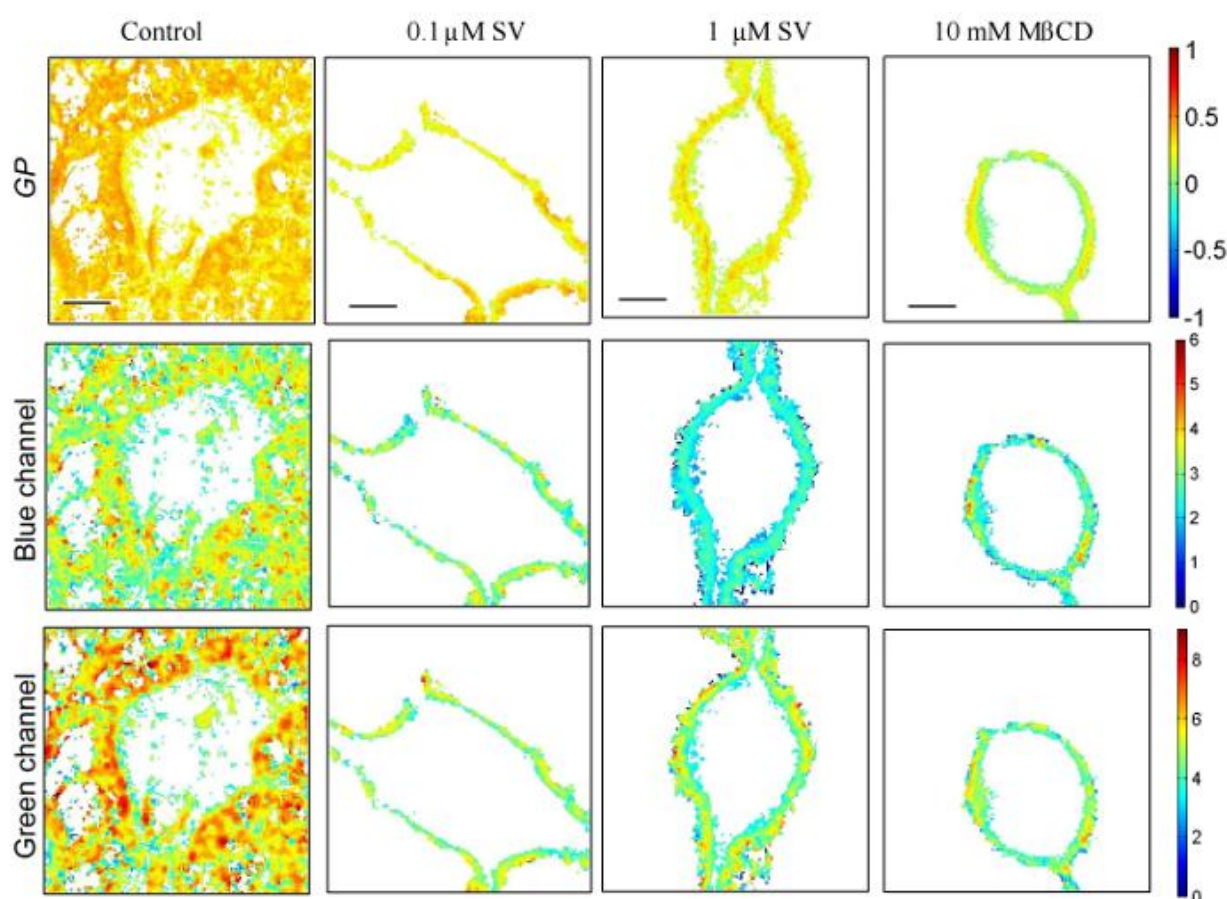


Figure 6.5. Laurdan in the plasma membrane of OLN-93 cells recorded at 37 °C.

Mapping of GP and fluorescence lifetimes (color coded lifetime values in ns) in the blue and the green channels. Chol depletion was achieved by application of SV and MβCD. The orientation of the linear polarization of the excitation light is horizontal. The size of the scale bar is 10 μm for all the images.

The average *GP* values for the cells recorded in each of the conditions considered are shown in Figure 6.6. *GP* values obtained for the cells grown in similar conditions but recorded at 37 °C are significantly smaller than those obtained for the cells recorded at 21 °C. Also, *GP* values obtained for the MβCD treated cells, which extracts up to 70% of the

membrane Chol, are smaller than those obtained for the untreated cells recorded at the same temperature. Thus, the average *GP* values for untreated cells are 0.43, at 21 °C and 0.31, at 37 °C, while for treated cells, the average *GP* value changed from 0.25 at 21 °C to 0.13 at 37 °C.

For the cells treated with SV and recorded at 21 °C, *GP* values are decreasing with increasing concentration, from 0.42 for 0.1 μM SV to 0.38 for 1 μM SV. For the same conditions recorded at 37 °C, the average *GP* values are 0.3 for 0.1 μM SV and 0.23 for 1 μM SV. In the case of SV treatment only the concentration of 1 μM SV induced a significant decrease of the average *GP* values at both temperatures.

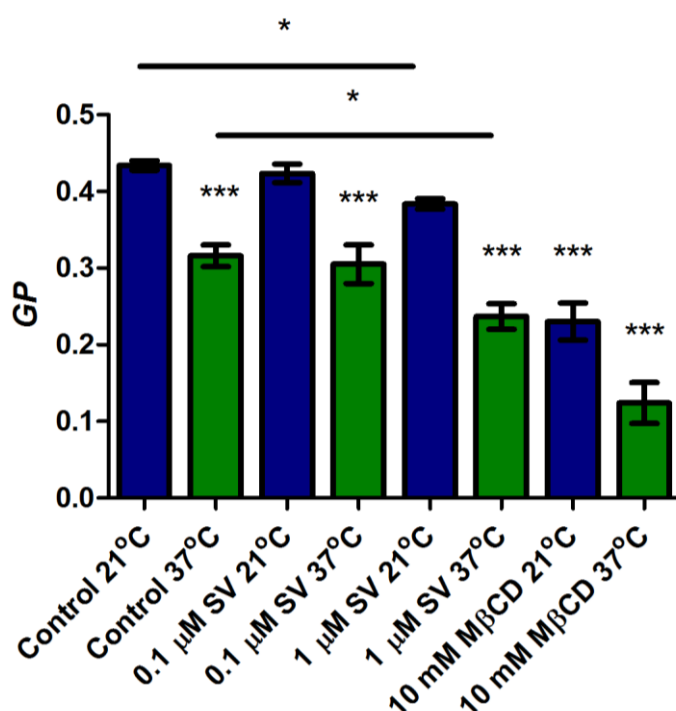


Figure 6.6. Average *GP* values for each experimental condition.

OLN-93 cells treated with SV (0.1 or 1 μM) or 10 mM MβCD were recorded at 21 or 37 °C. The error bars are standard deviations resulting from at least 20 cells measured for each condition. The data were analyzed using one-way-analysis of variance (ANOVA) with Bonferroni's Multiple Comparison Test with significance level: * significant at $P < 0.05$, *** significant at $P < 0.001$. Increasing temperature and MβCD treatment caused a significant change of *GP*.

The average fluorescence lifetimes in the blue and green channel for the images recorded in each of the conditions considered are shown in Figure 6.7 and Figure 6.8,

respectively. Compared with the *GP* behaviour, the lifetime changes recorded in the two channels were less pronounced.

A statistically significant decrease of the average lifetime was observed with increasing temperature for each experimental condition. The average lifetime recorded in the blue channel for the untreated cells decreased from ~ 3.24 ns at 21°C to ~ 2.75 ns at 37°C , and for the cells treated with $\text{M}\beta\text{CD}$ from ~ 2.49 ns at 21°C to ~ 2.09 ns at 37°C .

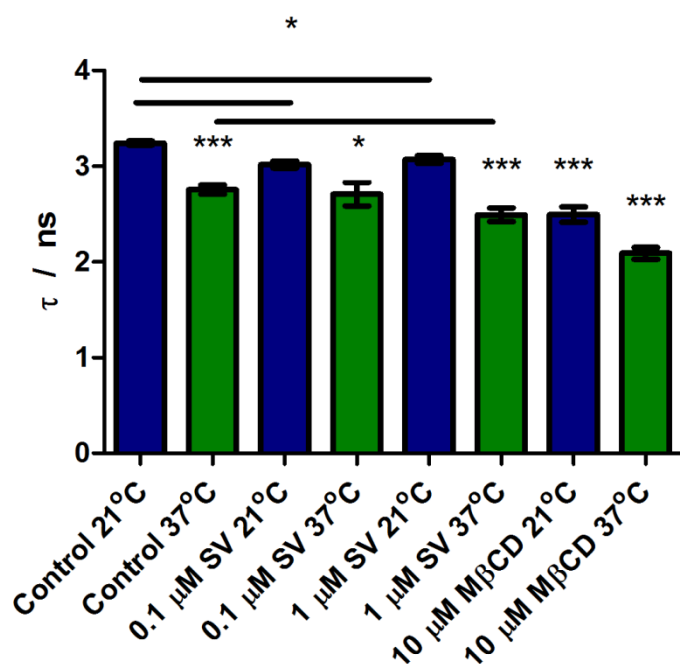


Figure 6.7. Average values of fluorescence lifetime recorded in the blue channel.

OLN-93 cells treated with SV (0.1 or 1 μM) or 10 mM $\text{M}\beta\text{CD}$ were recorded at 21 or 37°C . The error bars are standard deviations resulting from at least 20 cells measured for each condition. The data were analyzed using one-way-analysis of variance (ANOVA) with Bonferroni's Multiple Comparison Test with significance level: * significant at $P < 0.05$, *** significant at $P < 0.001$. Increasing temperature and $\text{M}\beta\text{CD}$ treatment caused a significant change of the lifetimes.

For the cells treated with the SV and recorded at 21°C , fluorescence lifetime values are ~ 3 ns for 0.1 μM SV and ~ 3.07 ns for 1 μM SV, while for the ones recorded at 37°C the average fluorescence lifetime values are ~ 2.7 ns for 0.1 μM SV and ~ 2.49 ns for 1 μM SV. A significant decrease was observed for cells treated with 1 μM SV at both temperatures, as for treatment with 0.1 μM SV was observed only at 21°C .

For the fluorescence lifetime recorded in the green channel the temperature did not caused a statistically significant decrease in any of the experimental conditions. The average lifetime recorded at 21 °C decreased from ~ 5.43 ns for the untreated cells to ~ 4.29 ns at 37°C for the cells treated with M β CD and from ~ 5.25 ns to ~ 4.13 ns for the cells recorded at 37 °C.

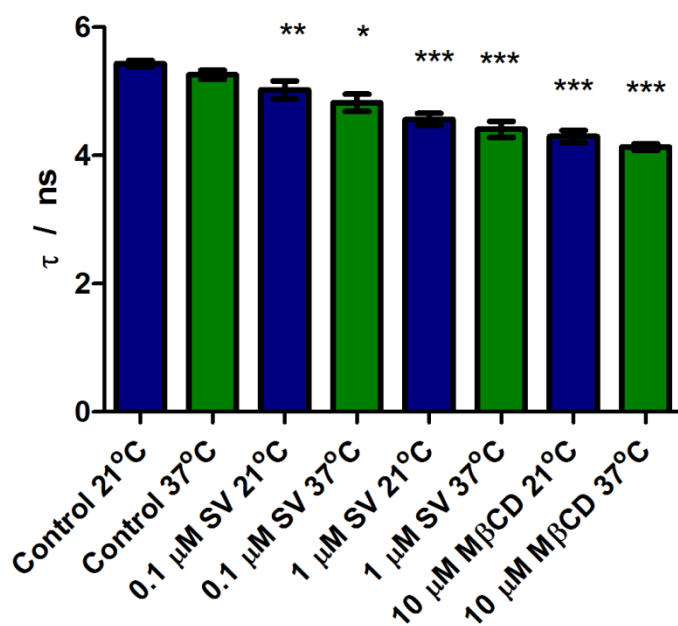


Figure 6.8. Average values of fluorescence lifetime recorded in the green channel.

OLN-93 cells treated with SV (0.1 or 1 μ M) or 10 mM M β CD were recorded at 21 or 37 °C. The error bars are standard deviations resulting from at least 20 cells measured for each condition. The data were analyzed using one-way-analysis of variance (ANOVA) with Bonferroni's Multiple Comparison Test with significance level: * significant at $P < 0.05$, ** significant at $P < 0.01$, *** significant at $P < 0.001$. Only Chol depleting treatment caused a significant change of the fluorescence lifetimes.

For the cells treated with the SV and recorded at 21 °C, fluorescence lifetime values are ~3 ns for 0.1 μ M SV and ~ 3.07 ns for 1 μ M SV, while for the ones recorded at 37 °C the average fluorescence lifetime values are ~2.7 ns for 0.1 μ M SV and ~ 2.49 ns for 1 μ M SV. A significant decrease was observed for cells treated with either 0.1 or 1 μ M SV at both temperatures studied.

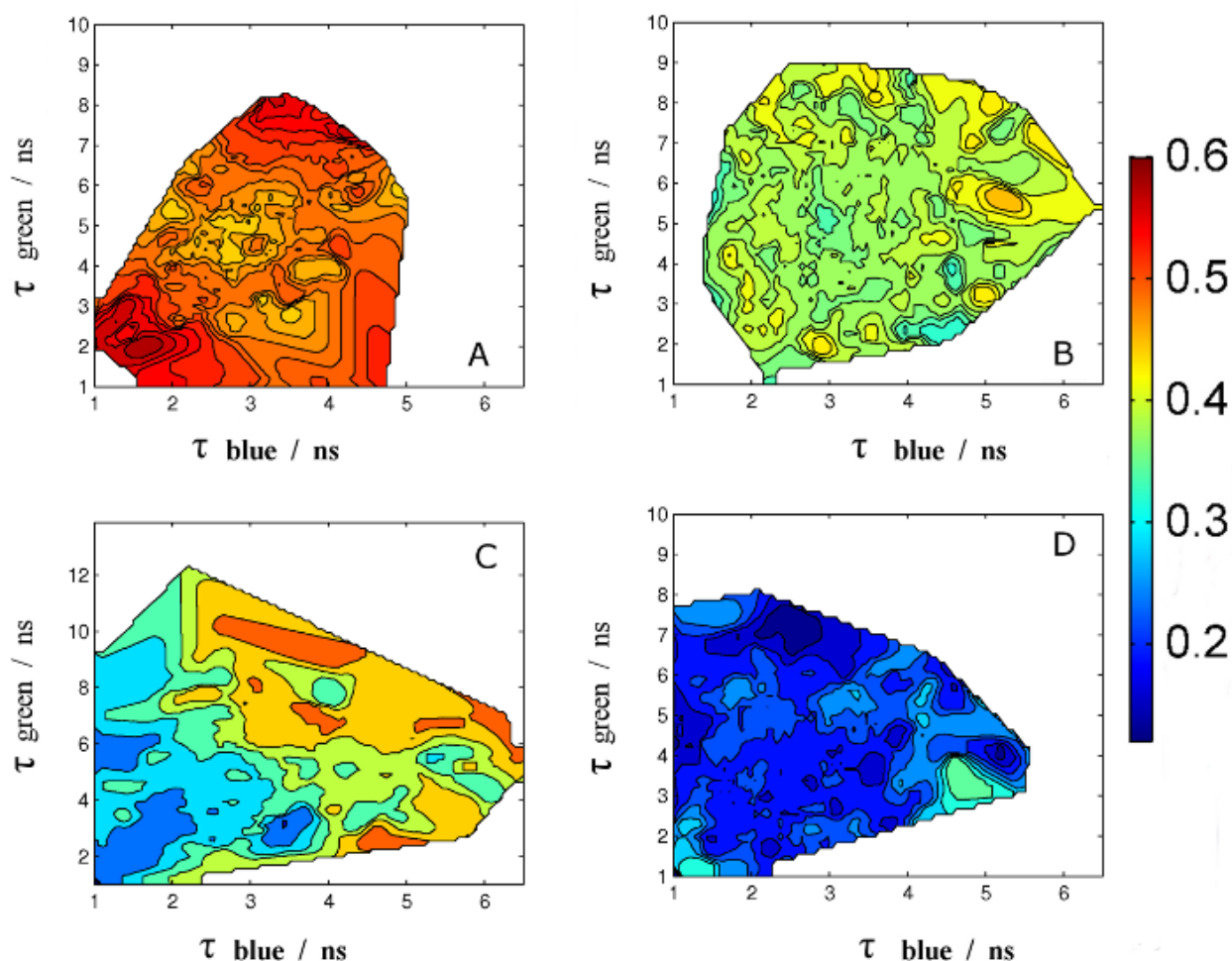


Figure 6.9. Topographic maps of Laurdan in the plasma membrane of OLN-93 cells.

Measurements performed at 21 °C: untreated (A) and treated with M β CD (C) and at 37 °C: untreated (B) and treated with M β CD (D). GP is shown by color coded values. The excitation light is horizontally polarized.

Correlation maps between GP values and fluorescence lifetimes for Laurdan in the plasma membrane of untreated and M β CD treated cells are presented in Figure 6.9. Although there are no distinct phases, low lifetime values for both channels correlate with low GP values. Similarly, high lifetime values for both channels correlate with high GP values. If for the untreated cells the values obtain show a more uniform distribution for the GP value independent of the variation of the lifetimes, for the cells treated with M β CD a more pronounced correlation is observed.

The topographic maps for the cells treated with SV are presented in Figure 6.10. A better correlation is observed for the cells recorded at 37 °C.

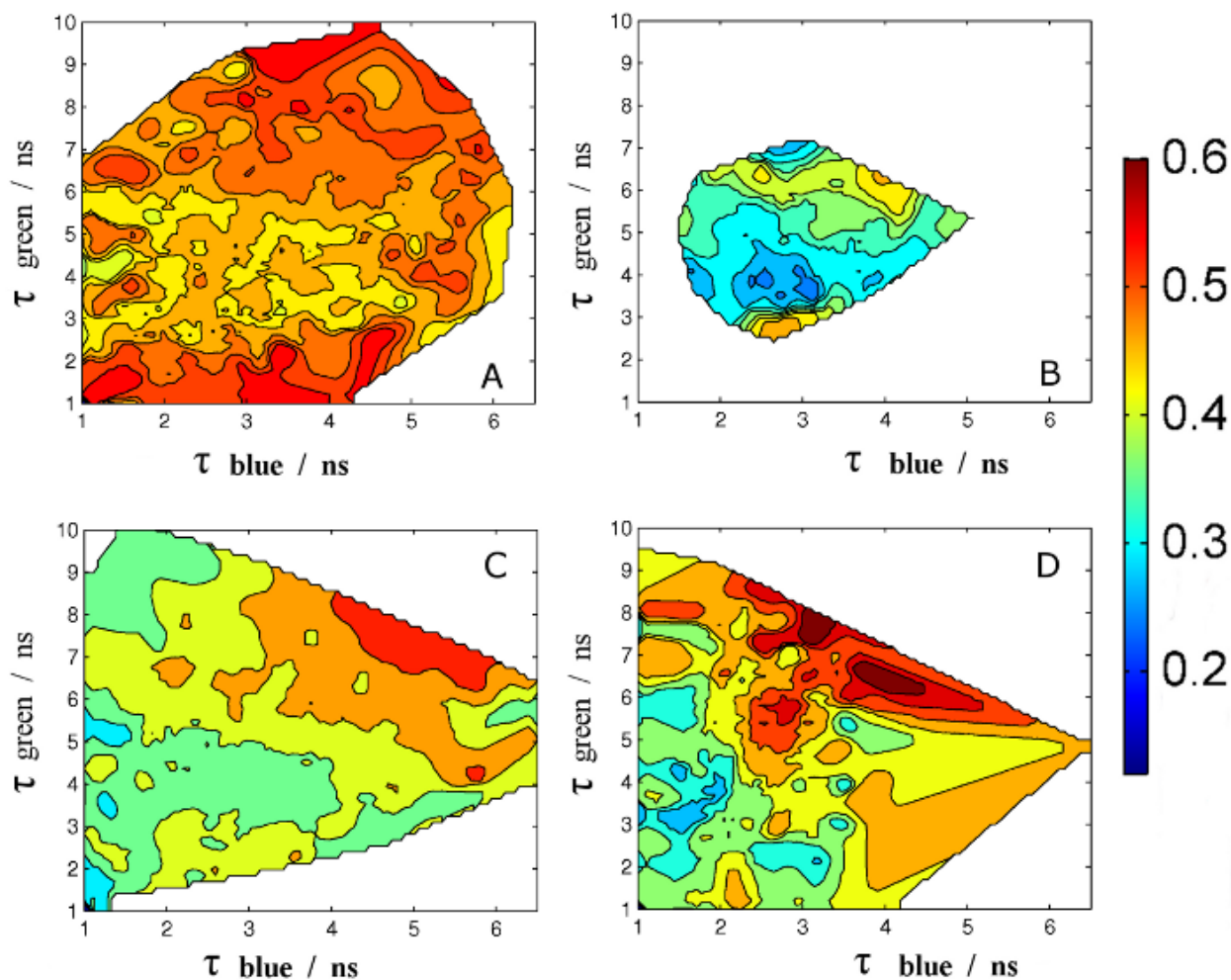


Figure 6.10. Topographic maps of Laurdan in the plasma membrane of SV treated OLN-93 cells. Measurements performed at 21 °C: 0.1 μM (A) and 1 μM (C) SV treatment and at 37 °C: 0.1 μM SV (B) and 1 μM SV (D) SV treatment. GP is shown by color coded values. The excitation light is horizontally polarized.

6.2. T09 effects on OLN-93 membrane

Similar to SV treatment, T09 treatment affects OLN-93 cells morphology. For the tested conditions (1 and 10 μM) OLN-93 cells lose their arborization (Figure 6.11).

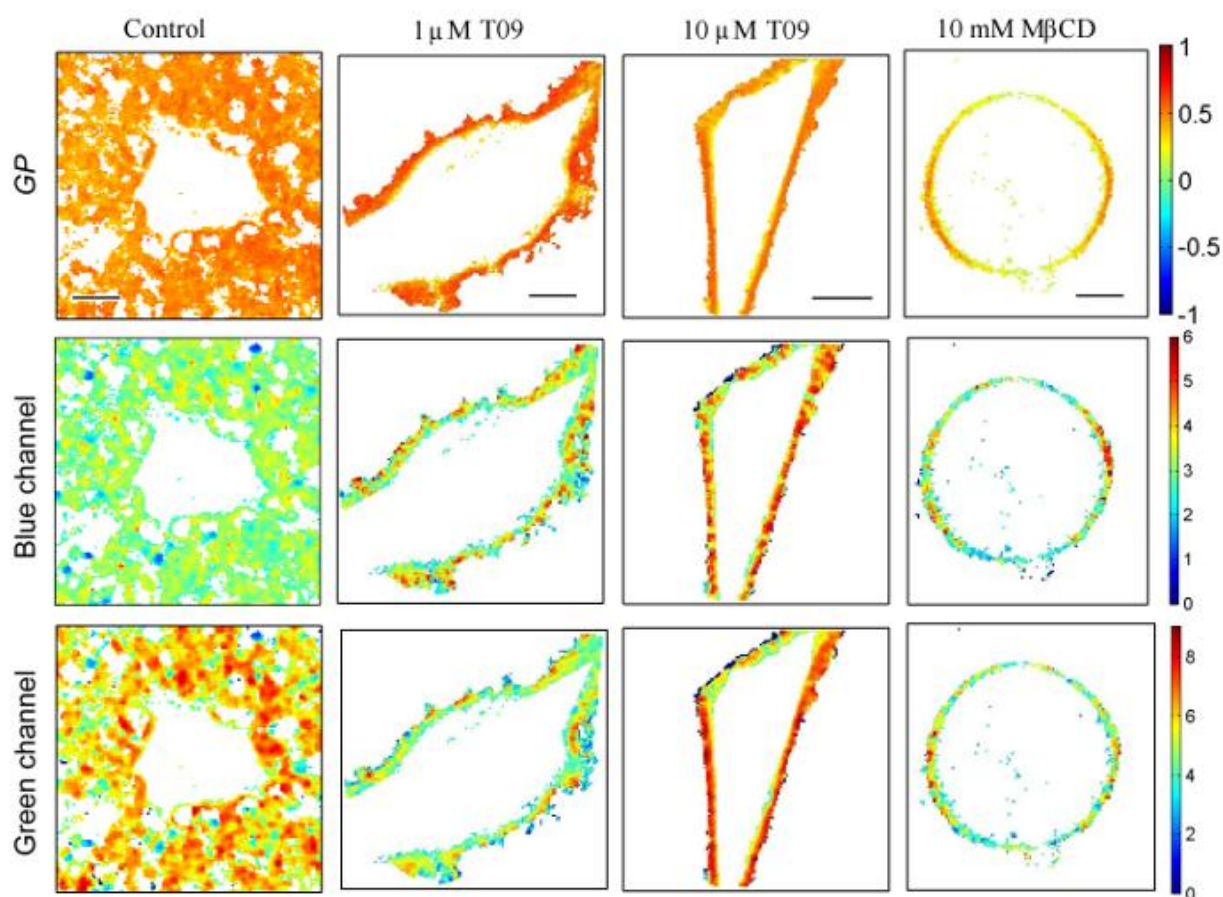


Figure 6.11. Laurdan in the plasma membrane of OLN-93 cells recorded at 21 °C.

Mapping of GP and fluorescence lifetimes (color coded lifetime values in ns) in the blue and the green channels. Chol depletion was achieved by application of T09 and M β CD. The orientation of the linear polarization of the excitation light is horizontal. The size of the scale bar is 10 μm for all the images.

A mask was applied to select only the membrane and the final image was processed to obtain average GP and lifetime values and an example from each condition is presented in Figures 6.11 and 12.

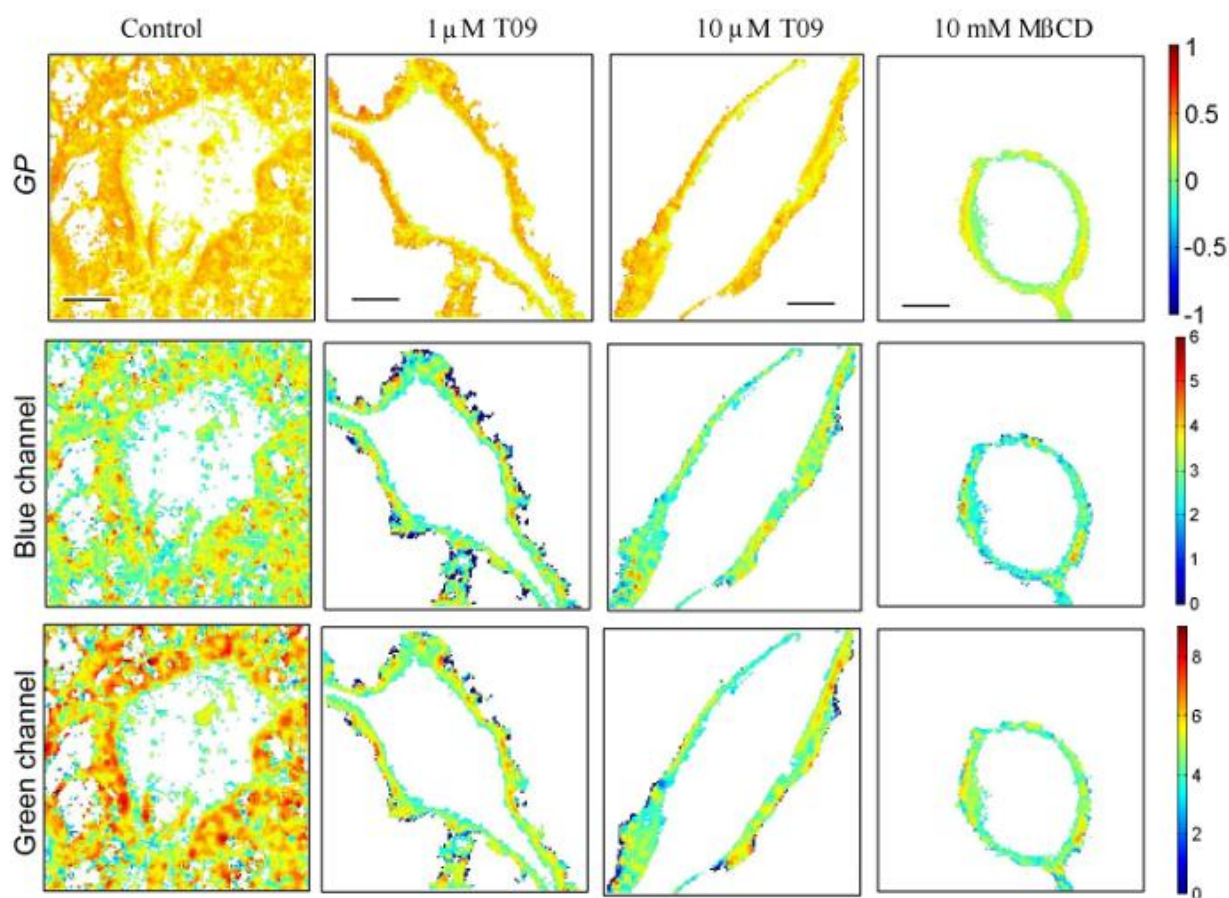


Figure 6.12. Laurdan in the plasma membrane of OLN-93 cells recorded at 37°C.

Mapping of GP and fluorescence lifetimes (colour coded lifetime values in ns) in the blue and the green channels. Chol depletion was achieved by application of T09 and MβCD. The orientation of the linear polarization of the excitation light is horizontal. The size of the scale bar is 10 μm for all the images.

The average GP values for the cells recorded in each of the conditions considered are shown in Figure 6.13. GP values obtained for the cells grown in similar conditions but recorded at 37 °C are significantly smaller than those obtained for the cells recorded at 21 °C, but the T09 treatment did not produce any significant change to the GP. Thus, the average GP values obtained at 21 °C are 0.43 for untreated cells, 0.44 for cells treated with 1 μM T09 and 0.45 for cells treated with 10 μM T09. While, the average GP value obtained at 37 °C are 0.31 for control cells, 0.31 for cells treated with 1 μM T09 and 0.31 for cells treated with 10 μM T09.

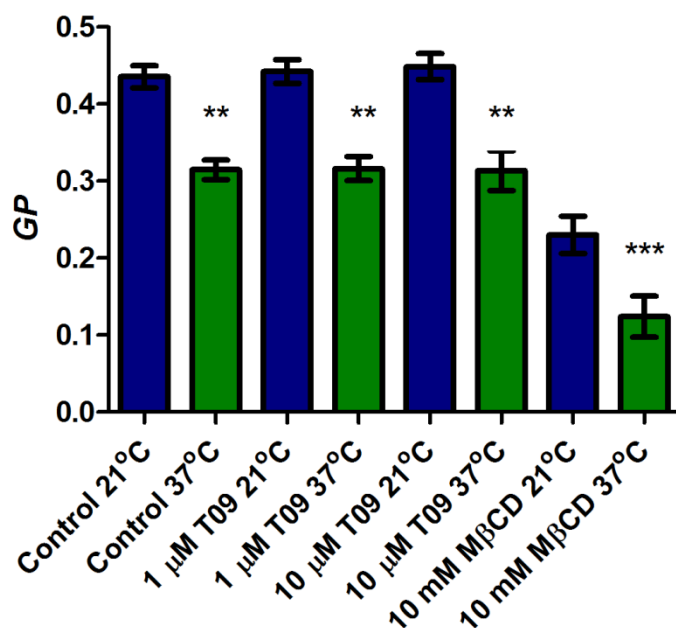


Figure 6.13. Average GP values recorded for each experimental condition.

*OLN-93 cells treated with T09 (1 or 10 µM) or 10 mM MβCD were recorded at 21 or 37 °C. The error bars are standard deviations resulting from at least 20 cells measured for each condition. The data were analyzed using one-way-analysis of variance (ANOVA) with Bonferroni's Multiple Comparison Test with significance level: * significant at $P < 0.05$, ** significant at $P < 0.01$, *** significant at $P < 0.001$. Increasing temperature and MβCD treatment caused a significant change of GP.*

The average fluorescence lifetimes in the blue channel for the images recorded in each of the conditions considered are shown in Figure 6.14. Similar with the GP behaviour, only increasing temperature caused a significant decrease of the fluorescence lifetime.

The average lifetime recorded in the blue channel at 21 °C are increasing with increasing treatment: ~ 3.27 ns for the untreated cells, ~ 3.28 ns for cells treated with 1 µM T09 and ~ 3.51 for cells treated with 10 µM T09. The lifetimes recorded at 37 °C are decreasing with increasing treatment: ~ 2.91 ns for the untreated cells, ~ 2.80 ns for cells treated with 1 µM T09 and ~ 2.73 for cells treated with 10 µM T09.

Although a strange behaviour of the lifetimes is observed at the two different temperatures, only treatment with 10 µM T09 at 21 °C caused a statistically significant increase of the average lifetime.

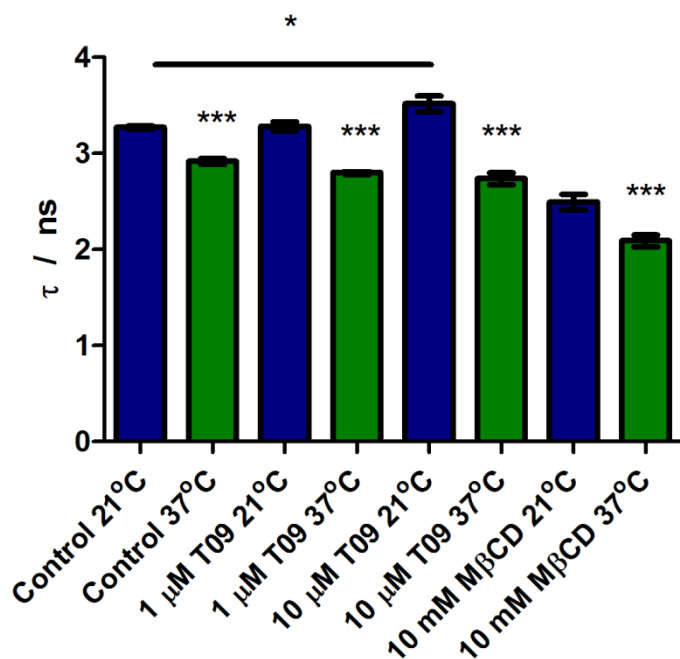


Figure 6.14. Average values of fluorescence lifetime recorded in the blue channel.

*OLN-93 cells treated with T09 (1 or 10 μ M) or 10 mM M β CD were recorded at 21 or 37 $^{\circ}$ C. The error bars are standard deviations resulting from at least 20 cells measured for each condition. The data were analyzed using one-way-analysis of variance (ANOVA) with Bonferroni's Multiple Comparison Test with significance level: * significant at $P < 0.05$, *** significant at $P < 0.001$. Increasing temperature and M β CD treatment caused a significant change of the fluorescence lifetime.*

The average fluorescence lifetimes in the green channel for the images recorded in each of the conditions considered are shown in Figure 6.15. The lifetime recorded in this channel is less sensitive to changes in membrane fluidity.

The average lifetime recorded in the green channel at 21 $^{\circ}$ C are increasing with increasing treatment: ~ 5.39 ns for the untreated cells, ~ 5.25 ns for cells treated with 1 μ M T09 and ~ 5.69 for cells treated with 10 μ M T09, while those recorded at 37 $^{\circ}$ C are decreasing with increasing treatment: ~ 5.08 ns for the untreated cells, ~ 4.69 ns for cells treated with 1 μ M T09 and ~ 4.59 for cells treated with 10 μ M T09.

Similarly with the lifetime recorded in the blue channel, only treatment with 10 μ M T09 at 21 $^{\circ}$ C caused a statistically significant increase of the average lifetime.

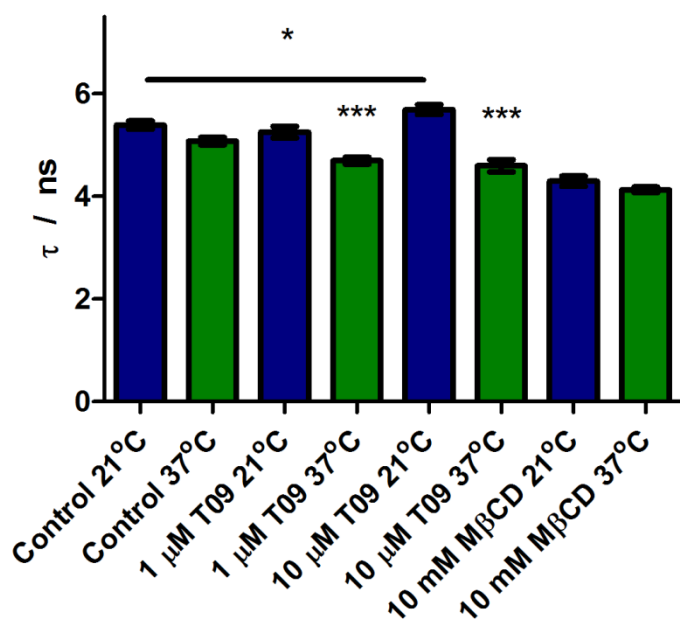


Figure 6.15. Average values of fluorescence lifetime recorded in the green channel.

*OLN-93 cells treated with T09 (1 or 10 μ M) or 10 mM M β CD were recorded at 21 or 37 °C. The error bars are standard deviations resulting from at least 20 cells measured for each condition. The data were analyzed using one-way-analysis of variance (ANOVA) with Bonferroni's Multiple Comparison Test with significance level: * significant at $P < 0.05$, *** significant at $P < 0.001$. Increasing temperature and M β CD treatment caused a significant change of the fluorescence lifetime.*

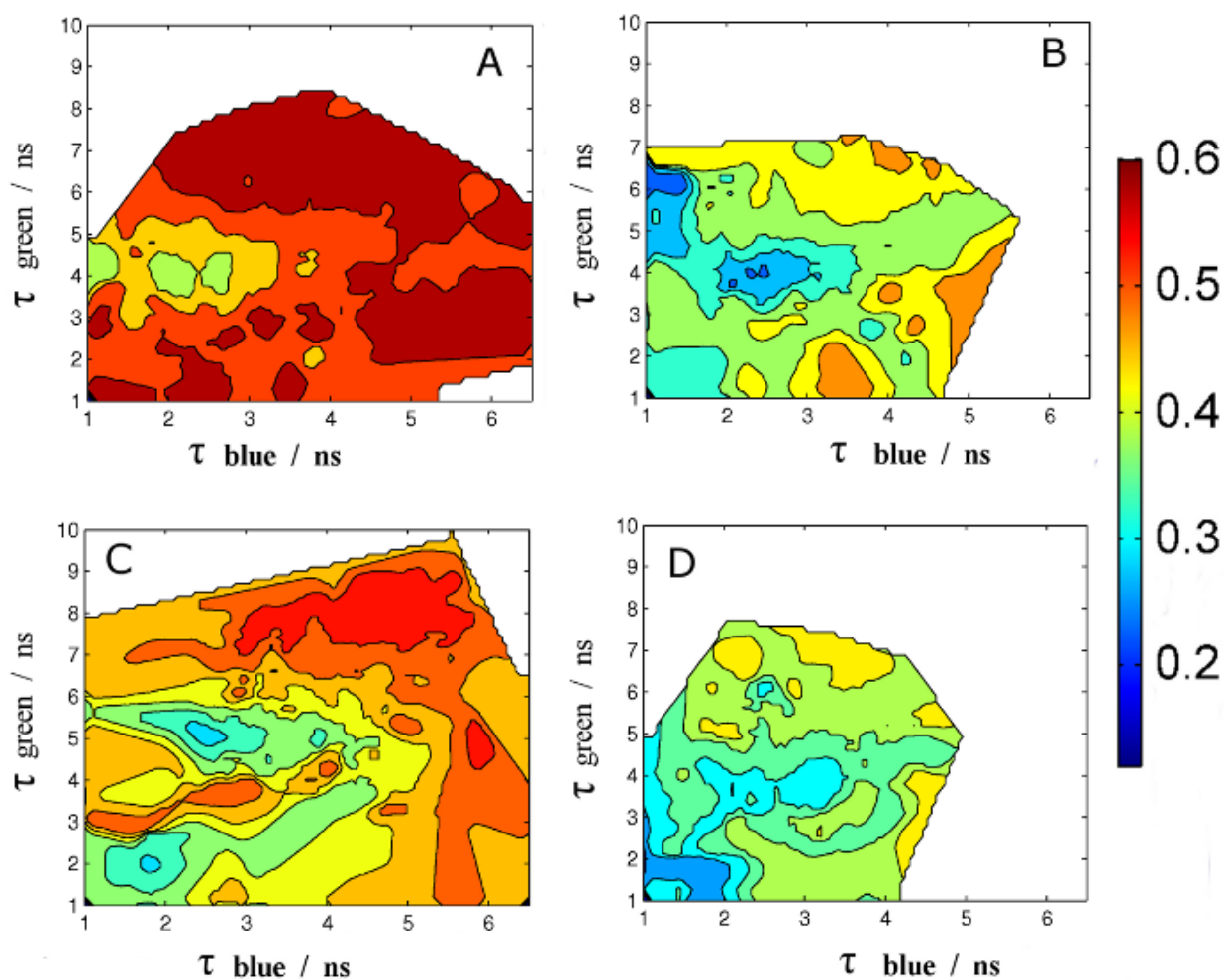


Figure 6.16. Topographic maps of Laurdan in the plasma membrane of T09 treated OLN-93 cells. Measurements performed at 21 °C: 1 μ M (A) and 10 μ M (C) T09 treatment and at 37 °C: 1 μ M SV (B) and 10 μ M SV (D) T09 treatment. GP is shown by colour coded values. The excitation light is horizontally polarized.

Topographic maps for the cells treated with T09 are presented in Figure 6.16. Contrary to the cells treated with SV, for the cells treated with T09 the correlation between GP and fluorescence lifetimes is observed for all conditions recorded.

6.3. Discussion

Statins inhibit HMG-CoA reductase activity thereby reducing the synthesis of mevalonate, a precursor not only for Chol but also for a group of proteins involved in the pathways related to the cell proliferation (Chapman-Shimshoni *et al.* 2003; Gullu *et al.* 2005). The reduced Chol synthesis modifies the organization of the membranes and in particular of lipid rafts. This might restrict the activity of receptors associated with membrane rafts.

These membrane changes can be detected with the fluorescent dye, Laurdan, a membrane probe sensitive to polarity changes. When Chol is extracted from the membrane, the fluidity of the membrane changes so that the probability for water molecules around Laurdan increases.

The most common parameter used to detect these changes is *GP*, but as we showed in the previous chapter, that also the fluorescence lifetimes can be used to detect changes in membrane fluidity, induced either by the change of temperature or by Chol composition.

The untreated cells recorded at 37 °C were used as a control. Normally, at 37 °C, the plasma membrane of the cells is characterized by a fluid phase. At 21 °C we expect that the membrane is in a more rigid state. The Laurdan measurements showed that at 21 °C the plasma membrane is indeed in a more rigid state than at 37 °C.

For the lowest SV concentration recorded at 37°C no changes were observed, but at 1 µM SV the fluidity of the membrane decreased. At 21 °C a similar behaviour was observed. Fluorescence lifetimes in the blue and green channel can also be used to detect the changes in membrane fluidity. If the lifetimes in the blue channel behave similarly with *GP*, the lifetimes in the green channel are less sensitive to changes in temperature but can detect changes induced by Chol treatment.

T09, another Chol modulator was used because it has a different mode of action. Contrary to SV which reduces the synthesis of Chol, T09 redistributes the Chol from the rafts to the non-rafts. If the appropriate receptors are present Chol is then exported from the cells.

In this case, at 37 °C the same effects as for the SV treatment were observed after the treatment: a decrease in the fluidity of the membrane and both *GP* values and fluorescence lifetimes were able to detect them. Unexpectedly, at 21 °C an increase of the rigidity of the membrane is observed with increasing T09 concentration, for both *GP* values and fluorescence lifetimes.

The correlation maps between *GP* and lifetimes in each of the channels were determined for each experimental condition. For the untreated cells at 21 °C the topographic map (Figure 6.9.A) we observe high *GP* values over all the range of lifetimes, but a also a high number of structures. The topographic map for this cells is similar with the L_o region observed on the DPPC GUVs map (Figure 5.10), suggesting that at this temperature most of the OLN-93 cell membrane is similar with L_o phase. Similar behaviour is observed for the untreated OLN-93 cells recorded at 37 °C (Figure 6.10.B. Although the *GP* decrease they are still higher than the ones obtained for the L_d phase on the DOPC GUVs. This suggests that due to the high content of Chol in the plasma membrane the OLN-93 cells are found mostly in a rigid state.

When M β CD treatment was applied, the maps change very much. For the cells treated and recorded at 21 °C, the topographic map is similar with the one obtained for the GUVs with a phase coexistence suggesting that some of the existent structures were destabilized and the proposition of the regions similar with L_d phase in the detriment of the L_o ones. The effect is more pronounced for the treated cells recorded at 37 °C.

Overall, the topographic map of untreated cells, independent of the temperature has a more homogenous organization mostly similar to L_o phase. After M β CD treatment, more structures can be observed ranging from rigid L_o phase like ones, to more fluid L_d phase like. We can conclude that with decrease of Chol the cells contain a variety of membrane areas with different properties.

Topographic maps were also made for the cells treated with SV. For cells treated with 0.1 μ M SV the maps are similar with the ones recorded for the untreated cells, but with slightly more regions with different characteristics. When treated with 1 μ M instead, the maps change showing a wider range for *GP* values (Figure 6.10). Similar observations can be made for the cells treated with T09.

PARTIAL CONCLUSIONS

The use of Laurdan provides not only evidence concerning the changes in membrane fluidity induced by changes in Chol composition and distribution inside the plasma membrane of OLN-93, but also shows that cells respond differently to the treatment by SV and T09.

For cells treated with SV, both *GP* values and the fluorescence lifetimes are decreasing with increasing treatment independent of the temperature at which they were measured.

On the other hand, for the T09 treatment, both *GP* values and the fluorescence lifetimes are decreasing with increasing treatment for measurements performed at 37 °C, but a small increase of both *GP* and the lifetimes was observed for the cells recorded at 21 °C and treated with the highest concentration of T09.

CHAPTER 7

A BLUE EMITTING BODIPY BASED LIPID PHASE SENSITIVE PROBE

Parts of this chapter will be mentioned in a report to be submitted:

Bacalum, M., L. Wang, V. Leen, P. Yuan, N. Smisdom, E. Fron, W. Dehaen, N. Boens, S. Knippenberg, G. Fabre, P. Trouillas, D. Beljonne and M. Ameloot
A blue emitting BODIPY based lipid phase sensitive probe.

INTRODUCTION

In this chapter we introduce a BODIPY based lipid probe (Figure 7.1) that emits in the blue part of the spectrum (Figure 7.2). As previously reported, attaching in the meso-position of an amino group, shifts the absorption band in the blue part of the spectra still maintaining high quantum yields (Banuelos *et al.* 2011). This allows us to use single-photon excitation with CW lasers and two-photon excitation with pulsed lasers at a not too long wavelength. Additionally, the design is such that we expect the excitation transition moments to be parallel to the lipid membrane upon insertion. This allows to image top or bottom membrane of a GUVs or a cell under the microscope. Furthermore, the probe can detect various lipid phases (i.e. S_o , L_d and L_o (van Meer *et al.* 2008)) by preferentially partitioning into them.

Photophysical properties of the probe in a variety of solvents were investigated using UV/Vis absorption, steady-state and time-resolved fluorescence techniques. The probe behaviour in lipid systems was investigated in different types of lipid vesicles. The results showed that the photophysics of the probe are not dependent on the polarity of the solvent or of the lipid phase of liposomes. Partition into binary (DOPC/DPPC) and ternary lipid mixtures (DOPC/SM/Chol) was analyzed by fluorescence microscopy, and a similar behaviour to the DiI-C18 probe was observed. Using computational studies we were able to determine that the probe core is located at the interface between the hydrophobic region and the polar surface of the DOPC lipid bilayer. Contrary to our expectations the dipole moment is not perpendicular to the surface of the membrane but adopts a slightly smaller angle which may vary with strong thermal fluctuation.

Although fluorescence lifetime measurements showed no changes of the lifetime within different lipid phases, diffusion measurements have proved useful in characterizing them. Fluorescence recovery after photobleaching (FRAP) was used to monitor BNP diffusion in both GUVs membranes and plasma membranes of OLN-93 cells. We found that there is a difference of one order of magnitude for the diffusion coefficient obtained for the DOPC and DPPC lipid membranes, while BNP behaviour in plasma membrane of OLN-93 cells is similar with the one observed for the fluid phase of GUVs.

7.1. Fluorescence properties of BNP in organic solvents

The photophysical properties of BNP (Figure 7.1) were studied in 14 organic solvents, including apolar, polar and protic solvents. A selection of normalized UV/Vis absorptions and fluorescence excitation and emission spectra of BNP in solvents are presented in Figure 7.2. For clarity, only a limited number of spectra are shown. Spectroscopic properties of BNP dissolved in all the studied solvents are reported in Table 7.1.

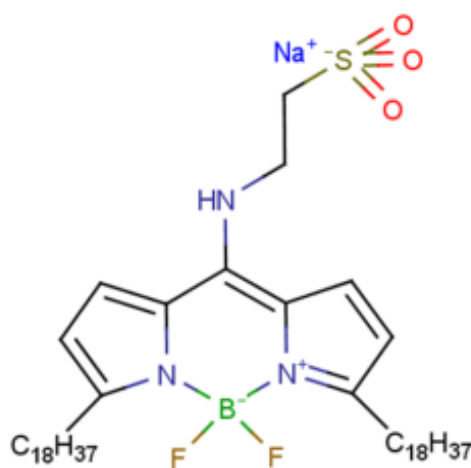


Figure 7.1. Chemical structure of the BNP

The spectra show a strong absorption band that can be assigned to the $S_0 - S_1$ transition, with the maximum positioned between 415 nm (in ACN) and 428 nm (in CHCl₃). Compared with the classic BODIPY probes the emission is blue shifted with ~ 80 nm (Arbeloa *et al.* 2005). There is no shoulder observed at shorter wavelengths and the absorption band is wider. Similarly to other BODIPY probes, changes in the polarity of the solvent causes only a small shift, of only 13 nm, of the absorption maximum. The full width at half-maximum of the main absorption band (FWHM_{abs}) is wider compared to the common BODIPY probes, but is nearly independent of solvent.

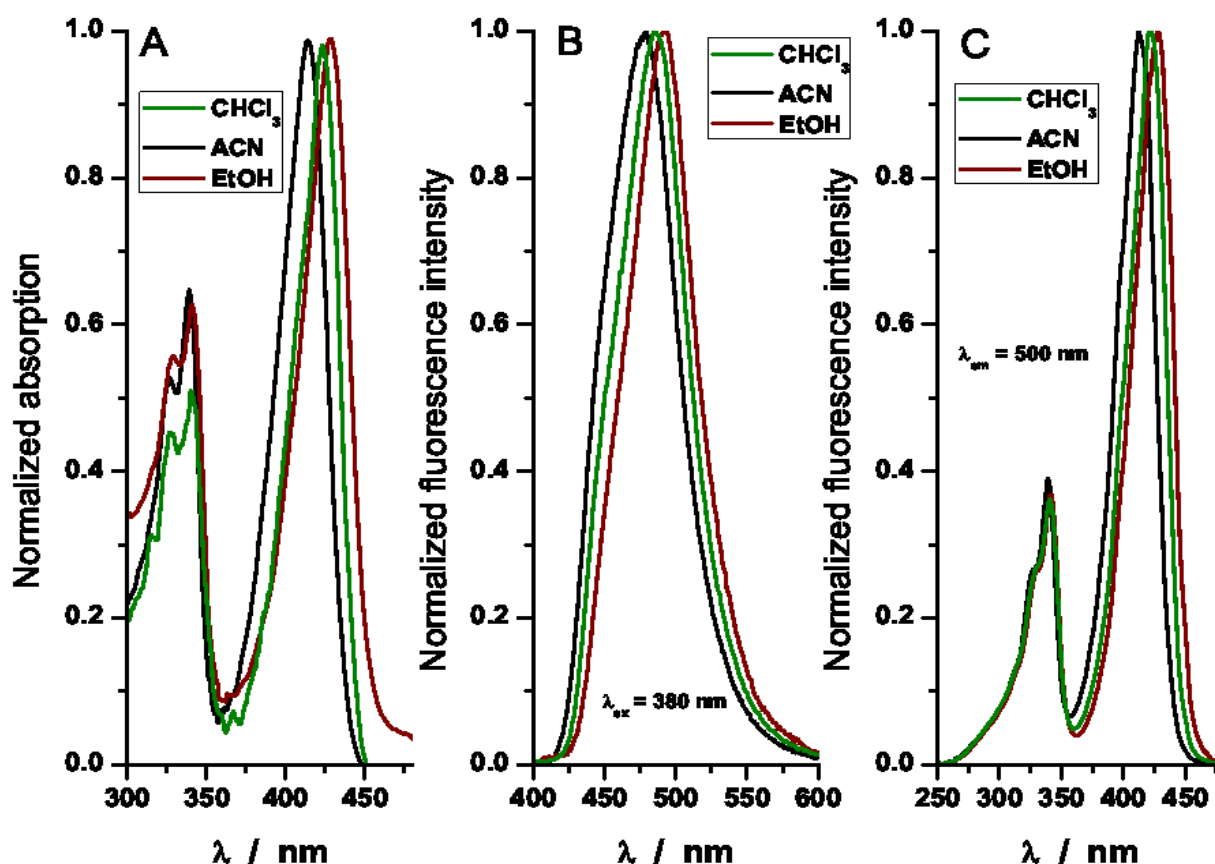


Figure 7.2. Spectral characteristics of BNP in different solvents

Normalized absorption spectra of BNP in different solvents (A). Corresponding normalized fluorescence emission spectra ($\lambda_{ex} = 380$ nm) (B). Corresponding normalized fluorescence excitation spectra ($\lambda_{em} = 500$ nm) (C).

A weaker and broader absorption band, attributed to S_0 - S_2 transition band, is independent of the solvent and was observed around 340 nm with a small shoulder at 329 nm.

For all the solvents, the excitation spectra match the absorption spectra. The molar extinction coefficient of BNP dissolved in ethanol is $\sim 36,000 \text{ M}^{-1} \text{ cm}^{-1}$ at 423 nm.

The fluorescence emission spectra of BNP in all studied solvents do not exhibit the typical features of BODIPY probes and display a broad band without vibrational structure. The position of the maximum varies between 475 nm (in acetone) and 496 nm (in acetic acid). The Stokes-shift is larger than for the common BODIPY probes (20-30 nm).

In water, the aggregation process takes place and the fluorescence emission becomes weaker and shifts to longer wavelengths (data not shown).

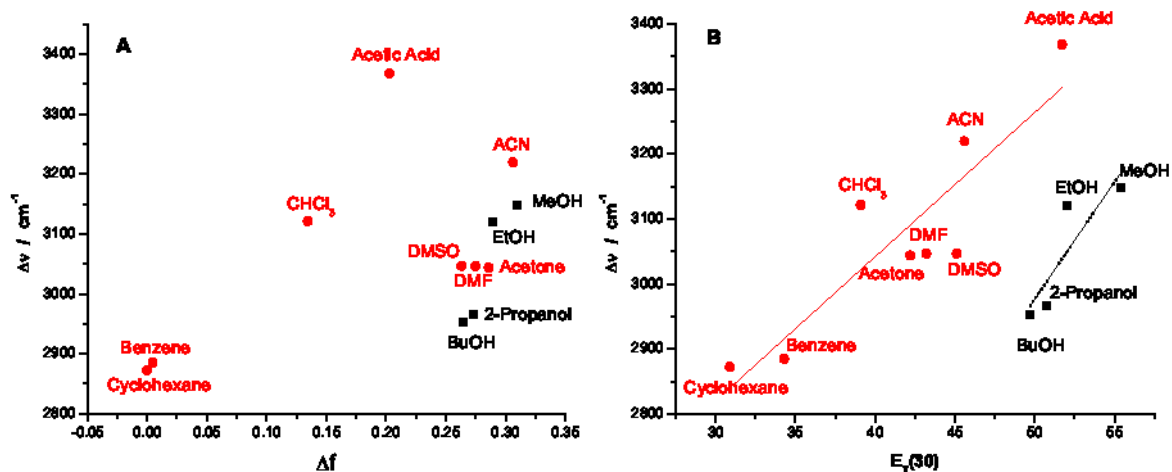


Figure 7.3. Plot of Stokes' shift versus different solvent polarity parameters.

Lippert solvent parameter $\Delta f = f(\epsilon) - f(n^2)$ (A) and $E_T(30)$ (B).

Lippert –Mataga equation is used to describe Stokes shift dependence of the probe on the solvent polarity parameter Δf :

$$\Delta f = \frac{\epsilon - 1}{2\epsilon + 1} - \frac{n^2 - 1}{2n^2 + 1},$$

where: ϵ – dielectric constant of the solvent and n – refractive index of the solvent.

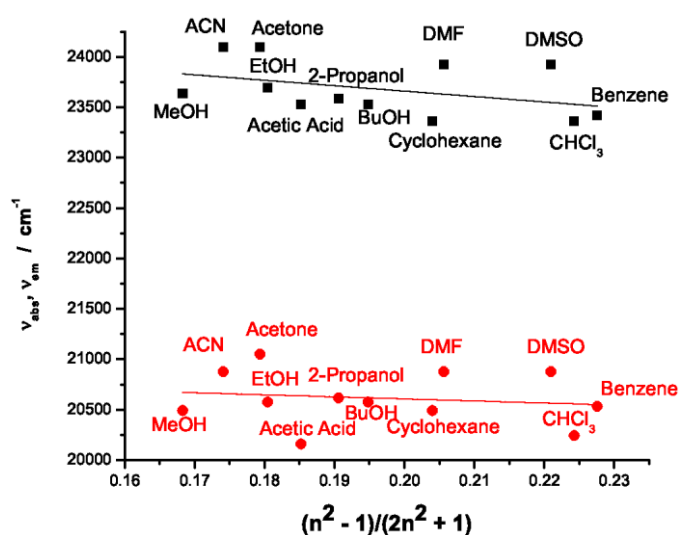


Figure 7.4. Plot of the absorption and emission maxima of BNP as a function of $f(n^2) = (n^2 - 1)/(2n^2 + 1)$

for all the studied solvents.

For the Lippert plot, the data points for alcohols fit on the same line, but alone. Contrary to the Lippert plot, for the $E_T(30)$ plot the alcohols fit clearly on a different line compared with the others solvents (Figure 7.3). This solvent polarity parameter takes into account the hydrogen bond donating and accepting character of the solvent. There is a poor linear fit for both the alcohols ($r = 0.6582$) and the other solvents ($r = 0.7675$) (Figure 7.4).

The fluorescence decay of the probe in all solvents studied is adequately described by a single exponential decaying curve. The fluorescence lifetimes values obtained are presented in Table 7.1. Part from DMSO and DMF, the lifetimes values are around 4 ns and not very sensitive to solvent polarity, while in water the probe it is only slightly fluorescent.

Table 7.1. Spectroscopic properties of the probe dissolved in different solvents.

Solvents	$\lambda_{\text{abs}}/\text{nm}$	$\lambda_{\text{em}}/\text{nm}$	$\lambda_{\text{ex}}/\text{nm}$	$\Delta\bar{\nu} / \text{cm}^{-1}$	$\text{fwhm}_{\text{abs}}/\text{cm}^{-1}$	τ / ns
EtOH	422	486	421	3,120	2,074	$4.16 \pm 0.05^{\text{a}}$
MeOH	423	488	422	3,149	2,127	4.43 ± 0.05
BuOH	425	486	425	2,953	2,054	4.01 ± 0.05
2-Propanol	424	485	422	2,966	2,101	4.02 ± 0.05
DMSO	418	479	419	3,047	2,088	1.59 ± 0.02
CHCl₃	428	494	428	3,122	2,097	3.99 ± 0.05
Acetone	415	475	413	3,044	2,118	3.38 ± 0.04
Acetic Acid	425	496	423	3,368	2,138	4.47 ± 0.05
ACN	415	479	413	3,220	2,146	3.78 ± 0.04
Cyclohexane	428	488	427	2,873	2,317	4.00 ± 0.05
Benzene	427	487	427	2,885	2,159	3.47 ± 0.04
DMF	418	479	418	3,047	2,125	2.62 ± 0.03
Toluene	429	486	429	2,734	2,247	3.31 ± 0.05
EtOAc	420	480	420	2,976	1,977	3.61 ± 0.04
Water	427	500	425	3,419	2,236	0.08 ± 0.03

^aThe uncertainties represent standard deviation of the lifetime calculated by the software.

Two-photon excitation was used for the microscopy measurements. Excitation fingerprinting of the probe in different solvents (MeOH, EtOH, DMSO and THF) was

performed between 700 nm and 960 nm obtaining a maximum, for all the solvents, at 840 nm (data not shown). This value is in a good agreement with the one obtained for the excitation spectra with 1-photon excitation (420 nm). The fluorescence lifetimes obtained under 1-photon and 2-photon excitation are compared in Table 7.2.

Table 7.2. Lifetimes obtained after 1-photon (342 nm) and 2-photon excitation (840 nm).

Solvent	τ/ ns (342 nm)	τ/ ns (840 nm)
THF	-	3.77 ± 0.04^c
DMSO	1.59 ± 0.02^b	1.71 ± 0.06
EtOH^a	4.16 ± 0.05	4.22 ± 0.05
MeOH	4.43 ± 0.05	4.39 ± 0.07

^a A lifetime of 4.20 ns was obtained by fluorescence up-conversion experiments at 420 nm and 840 nm excitation. See SI for more details.

^b The uncertainties represent the confidence interval of the lifetime calculated by the software.

^c The uncertainties represent the standard deviation.

7.2. Fluorescence properties of BNP in small unilamellar vesicles

SUVs with different compositions were studied: DPPC (16:0), DSPC (18:0), DOPC (18:1), an equal mixture of DOPC and DPPC and a mixture of DPPC with 30 % Chol. Recordings were performed at room temperature to obtain different lipid phases: DOPC in liquid disordered phase (L_d), DPPC and DSPC in gel phase (S_o), DOPC/DPPC in L_d/S_o phase coexistence and DPPC/Chol in liquid ordered phase (L_o). Fluorescence excitation and emission spectra of BNP in SUVs are presented in Figure 7.5. The SUVs prepared from DPPC and DSPC were used to determine if BNP properties are influenced by the length of saturated lipid chains (Figure 7.6). DSPC has two acyl chains of 18 carbons and it is expected to better accommodate the probe. While DPPC has only 16 carbons, the spectra do not show significant differences when recorded at room temperature.

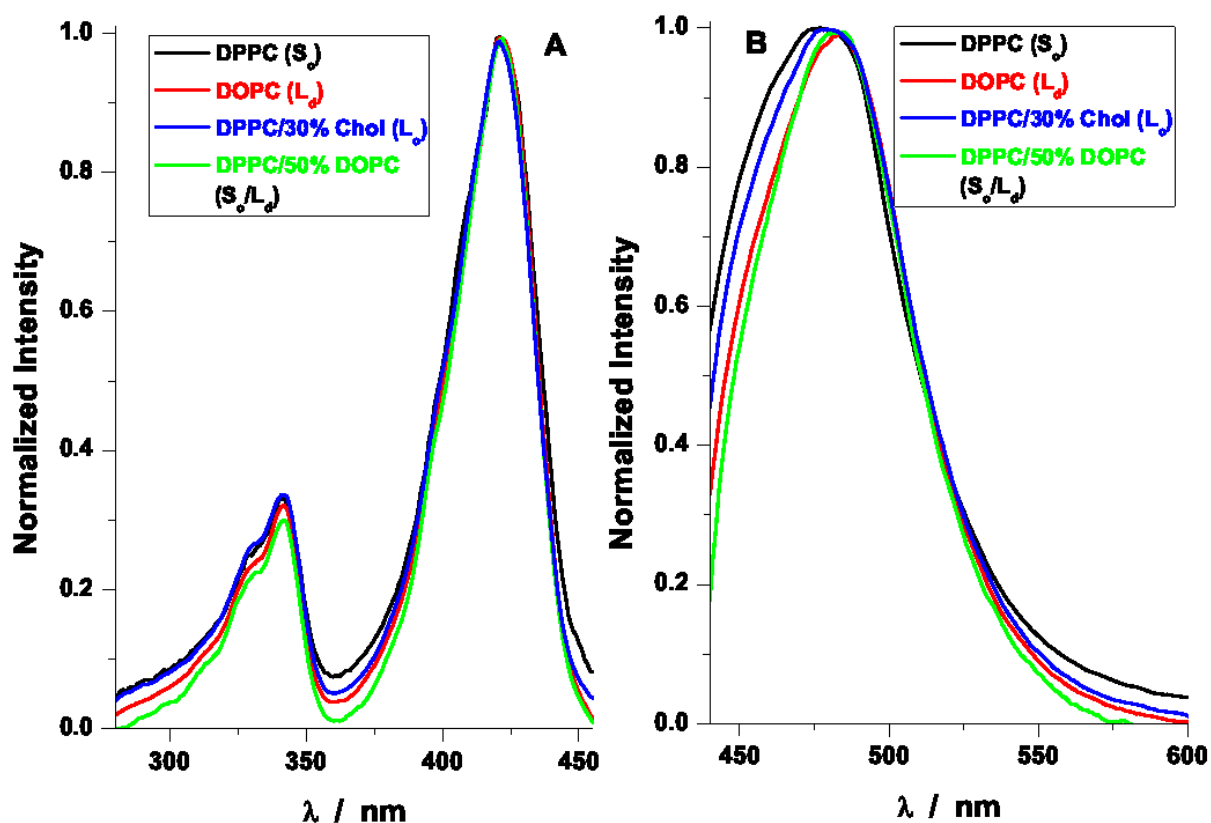


Figure 7.5. Fluorescence spectra of BNP in SUVs.

Excitation (A) and emission (B) spectra of Bodipy-NP in SUVs composed from DPPC (S_o phase), DOPC (L_d phase), an equal mixture of DOPC and DPPC (L_d/S_o phase coexistence) and a mixture of DPPC with 30 % Chol (L_d/L_o phase). The excitation spectra were recorded with the emission wavelength set at 500 nm. The emission spectra were recorded with the excitation wavelength set at 420 nm.

The excitation spectra of the probe recorded for all lipid systems are similar with almost no change of the excitation maximum wavelength (Table 7.3). The spectra are also similar with the ones recorded for the probe in pure solvents. The emission spectra are similar for all the lipid phases with a small red shift (8 nm) of the S_o phase compared to the L_d phase.

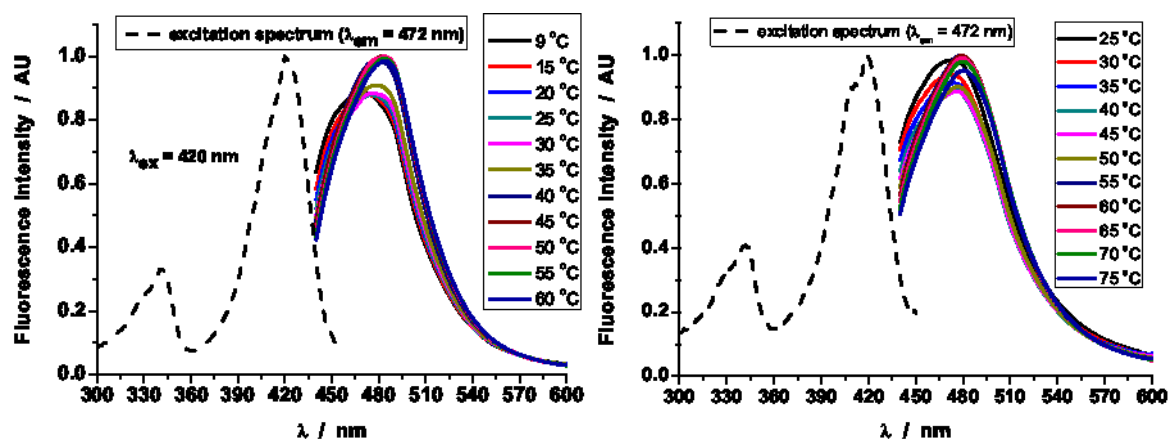


Figure 7.6. Excitation and emission spectra of BNP in DPPC SUVs (left) and DSPC SUVs (right)

The emission spectra of the probe when excited at 420 nm were recorded at different temperatures, from 9 °C to 60 °C for DPPC and 25 °C to 75 °C for DSPC. From the spectra (Figure 7.6) we can see a small shift of the maximum intensity from 473 nm in the gel phase to 482 nm in the fluid phase together with a small increase of the fluorescence intensity.

The fluorescence anisotropy of BNP in SUVs prepared from DPPC or DSPC was recorded at 472 nm, first with the excitation set first at 420 nm and after at 340 nm, at temperatures varying between 10 and 70 °C (Figure 7.7).

Table 7.3. Spectroscopic properties of BNP inserted in SUVs with different composition at room temperature

	DOPC	DPPC	DSPC	DOPC/ DPPC	DPPC/Chol
	L _d	S _o	S _o	S _o / L _d	L _o
λ_{ex} / nm	421	420	419	422	421
λ_{em} / nm	484	477	473	485	479
τ / ns	4.3 ± 0.1 ^a	4.3 ± 0.1	4.4 ± 0.2	4.3 ± 0.1	4.3 ± 0.1

^a The uncertainties represent the standard deviation of the lifetime calculated by the software.

For the first situation ($\lambda_{\text{ex}}=420$ nm and $\lambda_{\text{em}}=472$ nm) anisotropy values were decreasing with increasing temperature evidencing the increase of lipid membrane fluidity. Temperature dependence of anisotropy was fitted in Origin using a sigmoidal function. In this

case, from the inflection point we were able to estimate the transition temperature (T_m) of the lipids derived from these experiments. We obtained 39.1 ± 0.5 °C for DPPC and 51.9 ± 0.7 °C for DSPC. These values compare well with those reported in the literature for SUVs: 37.8 ± 1.0 °C for DPPC and 51.8 ± 1.1 °C for DSPC (Koynova and Caffrey 1998). Also, it appears that the length of the lipid chains does not influence the packing of the probe, similar anisotropy values being obtained.

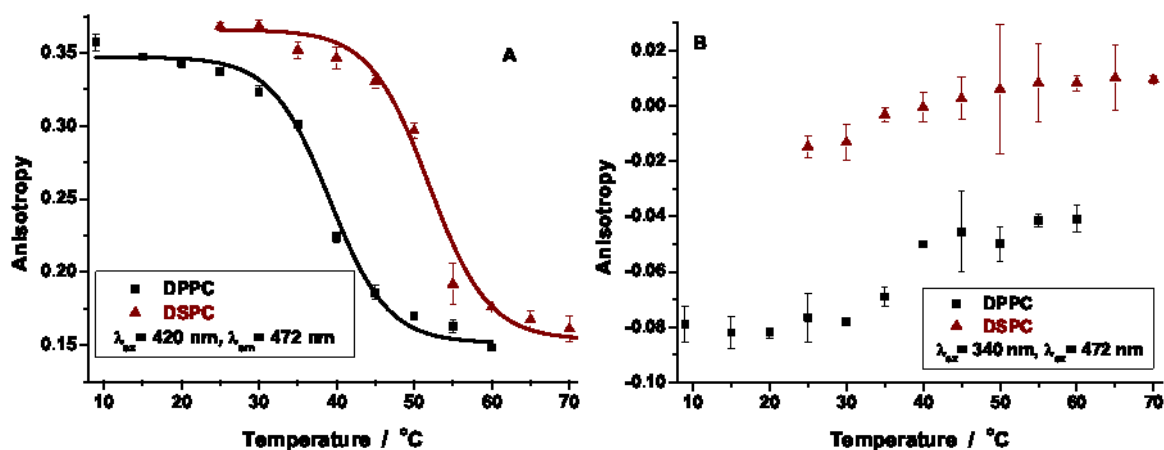


Figure 7.7. Anisotropy curves of BNP in LUVs.

Temperature dependence of the fluorescence anisotropy of BNP in DPPC and DSPC SUVs. $\lambda_{ex}=420$ nm and $\lambda_{em}=472$ nm (left) and $\lambda_{ex}=340$ nm and $\lambda_{em}=472$ nm (right). The error bars represent the standard deviation resulting from 4 repeats.

For the second condition ($\lambda_{ex}=340$ nm and $\lambda_{em}=472$ nm), the anisotropy had negative values and increased with increasing temperatures. If we consider that absorption and emission transition moments can have a different orientation relative to each other, theoretical values of anisotropy can go from +0.4 for parallel transition moments to -0.2 for perpendicular transition moments. Thus, these negative values correspond to a S_0 - S_2 transition, which for our probe cannot be used to determine T_m of the lipid.

Fluorescence lifetime measurements were performed for all types of SUVs prepared (Table 7.3) and the decays were fitted very well with only one decaying component. For DPPC and DSPC SUVs, the recordings were performed at different temperatures, but similar lifetime values are obtained independent of temperature (Table 7.4).

Table 7.4. Fluorescence lifetime of BNP in DPPC and DSPC SUVs.

Temperature / °C	τ / ns (DPPC)	τ / ns (DSPC)
20	4.3 ± 0.1	-
25	4.3 ± 0.1	4.4 ± 0.2
30	4.2 ± 0.1	4.3 ± 0.1
35	4.4 ± 0.1	4.3 ± 0.2
40	4.2 ± 0.1	4.3 ± 0.2
45	4.3 ± 0.1	4.4 ± 0.2
50	4.3 ± 0.1	4.2 ± 0.2
55	4.3 ± 0.1	4.2 ± 0.2
60	4.2 ± 0.1	4.2 ± 0.2
65	-	4.2 ± 0.2
70	-	4.3 ± 0.2
75	-	4.1 ± 0.3

Measurements were also performed on liposomes exhibiting phase separation to determine how the probe behaves. The decay was fitted well using only one component proving that similar lifetimes are recorded in both phases. These results show that lipid phase does not influence the fluorescence lifetime of BNP.

7.3. Discrimination of lipid phases in giant unilamellar vesicles by BNP

Measurements on GUVs were performed using CLSM (confocal laser scanning microscope) to determine the distribution of BNP into different lipid phases at room temperature: DPPC (S_o), DOPC (L_d), DOPC/DPPC (0.4:0.6 molar ratio) (L_d/S_o) and DOPC/SM/Chol (1:2:1 molar ratio) (L_o/L_d).

The GUVs were loaded simultaneously with the DiI-C18 probe to assign the type of lipid phase. DiI-C18 partitions preferentially in the S_o phase for DOPC/DPPC mixtures (Baumgart *et al.* 2007; Scherfeld *et al.* 2003) and in the L_d phase for DOPC/SM/Chol

mixtures for GUVs generated according to the same protocol (Kahya *et al.* 2003; Scherfeld *et al.* 2003).

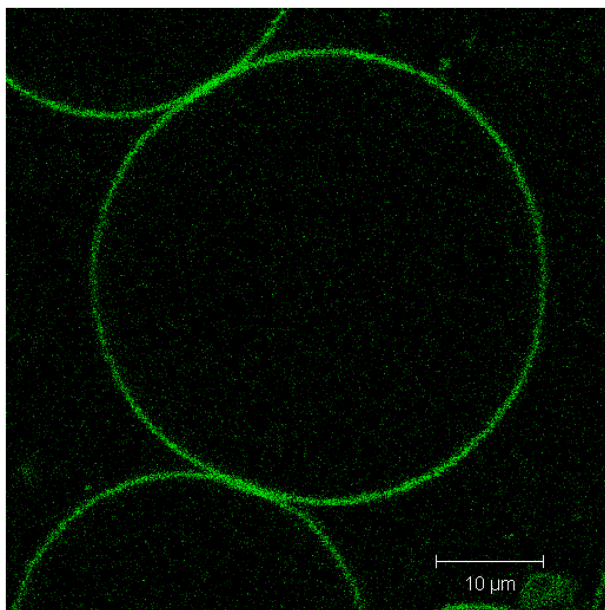


Figure 7.8. Fluorescence intensity image showing the uniform distribution of BNP for a GUV prepared from DOPC.

A uniform distribution for BNP is observed for the L_d and the S_o system (Figure 7.8). In the binary DOPC/DPPC mixture the probe tends to accumulate preferentially in the same phase as DiI-C18, i.e. the S_o phase (Figure 7.9A and B). For GUVs exhibiting L_o/L_d phase separation, the both dyes are partitioning into the L_d phase (Figure 7.9C and D).

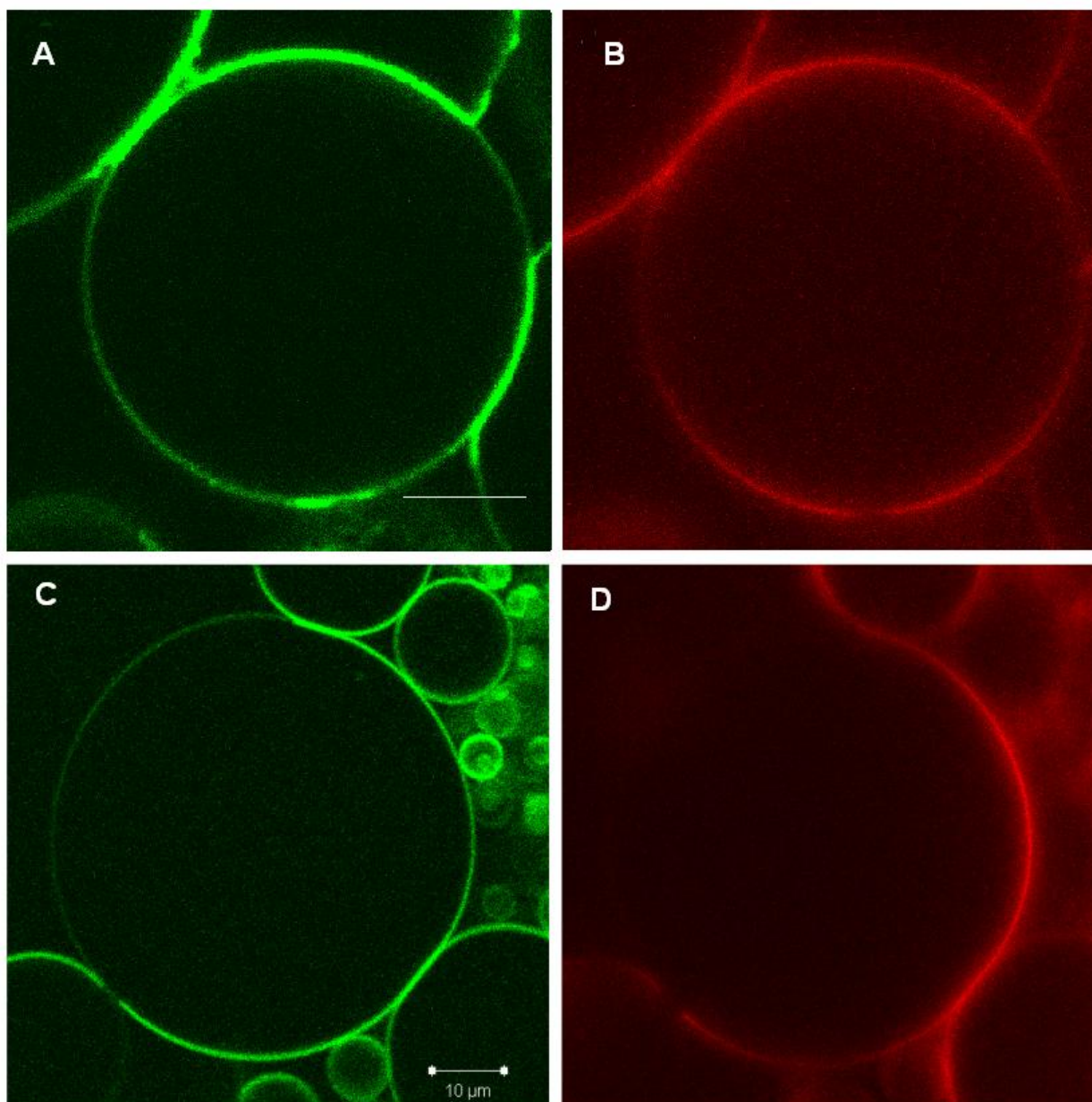


Figure 7.9. Fluorescence intensity images showing BNP and DiI-C18 partitioning in lipid phases of different types of GUVs.

L_d/S_o (DOPC/DPPC) phase mixture: both BNP (A) and DiI-C18 (B) are preferentially partitioning in the S_o phase. L_o/L_d (DOPC/SM/Chol) phase separation: both BNP (C) and DiI-C18 (D) are preferentially residing in the L_d phase. Plane of focus intersects with the GUVs. Both scale bars represent 10 μm .

Because we could image the top and bottom of the GUVs, a z-stack of the GUVs, with a step of 0.5 or 1 μm was collected to obtain a better visualization of the phase separation for the two mixed systems. One can observe the circular shape of the L_d phase for DOPC/SM/Chol mixture (Figure 7.10A) (Kahya *et al.* 2003; Wesolowska *et al.* 2009) and

stripes and patches representing the S_o phase of the DOPC/DPPC mixture (Figure 7.10.B) (Li and Cheng 2006; Wesolowska *et al.* 2009).

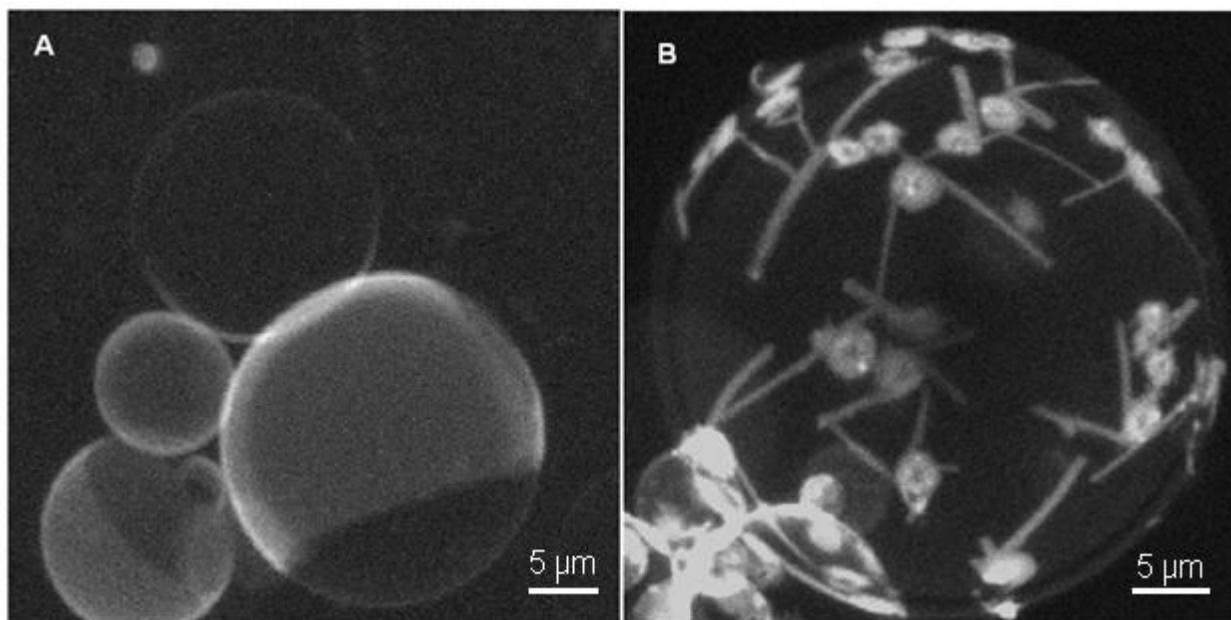


Figure 7.10. The intensity image of GUVs obtained by superimposing the images from a z-stack. (A) Shows the L_o/L_d phase separation (DOPC/SM/Chol) and (B) the L_d/S_o phase mixture (DOPC/DPPC). Measurements were performed at room temperature.

Fluorescence lifetime images were recorded for each type of GUV (Figure 7.11). An average lifetime was calculated for each homogeneous phase within each GUV and averaged over several GUVs (Table 7.5). Except for the values obtained for the solid phase of the DOPC/DPPC mixture no significant differences were observed for the various lipid phases.

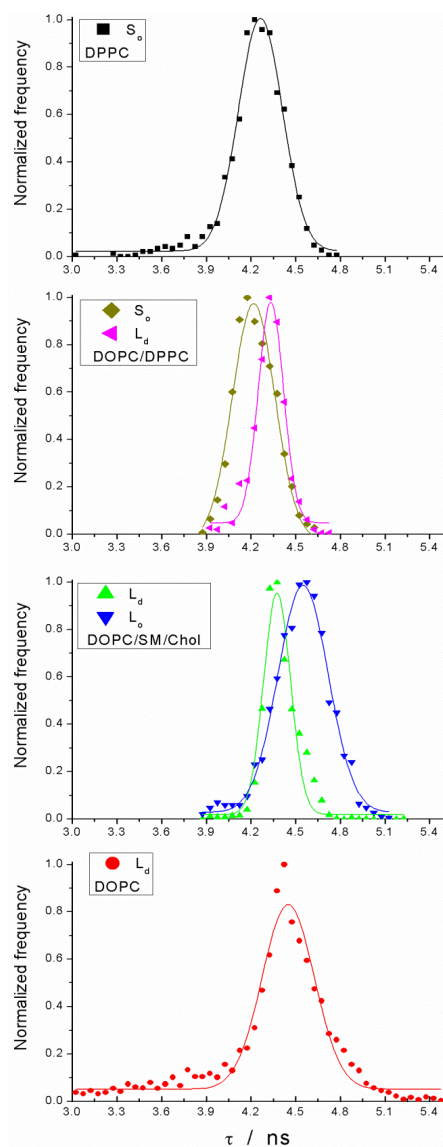


Figure 7.11. Distribution of the lifetime values obtained for different lipid phases.

Table 7.5. Average fluorescence lifetimes (in ns) of BNP obtained for the different lipid phases in the various types of GUVs.

L_d (DOPC)	L_o^* (DOPC/SM/Chol)	L_d^* (DOPC/SM/Chol)	$L_d^\#$ (DOPC/DPPC)	$S_o^\#$ (DOPC/DPPC)	S_o (DPPC)
4.32 ± 0.11^a	4.50 ± 0.22	4.41 ± 0.16	4.13 ± 0.16	3.98 ± 0.21	4.15 ± 0.16

* Average lifetimes of either the L_o or L_d phase from GUVs prepared from a mixture of DOPC/SM/Chol

Average lifetimes of either the L_d or S_o phase mixture from GUVs prepared from DOPC/DPPC

^a The uncertainties represent the standard deviation.

As the lifetime is essentially independent of the lipid phase we can consider that the fluorescence intensity reflects the number of dye molecules. Taking this into account we were able to determine a ratio of the dye molecules for the phase coexistence. Thus for the DOPC/SM/Chol mixture there is a ratio of one molecules of BNP in the L_o phase and 7-8 in the L_d phases, while for the DOPC/DPPC mixture the ratio was of 1/2-3 for L_d/S_o phases.

FRAP measurements were performed on GUVs prepared from either DOPC or DPPC and labeled with BNP. Measurements were performed on the top membrane of the GUVs.

In the gel phase we obtained an average diffusion coefficient (D) value of $0.13 \pm 0.02 \mu\text{m}^2/\text{s}$, while for the fluid phase, the increase of mobility leads to a higher D , of $4 \pm 2 \mu\text{m}^2/\text{s}$. In both cases the mobile fraction obtained are close: $110 \pm 1 \%$ (DPPC) and $97 \pm 4 \%$ (DOPC).

7.4. Measurements of BNP in biological cells

OLN-93 cells were loaded with BNP. The dye accumulates mostly in the plasma membrane, less into the cytoplasm, but is excluded from the nucleus (Figure 7.12). No segregation of BNP in the cell membrane was observed.

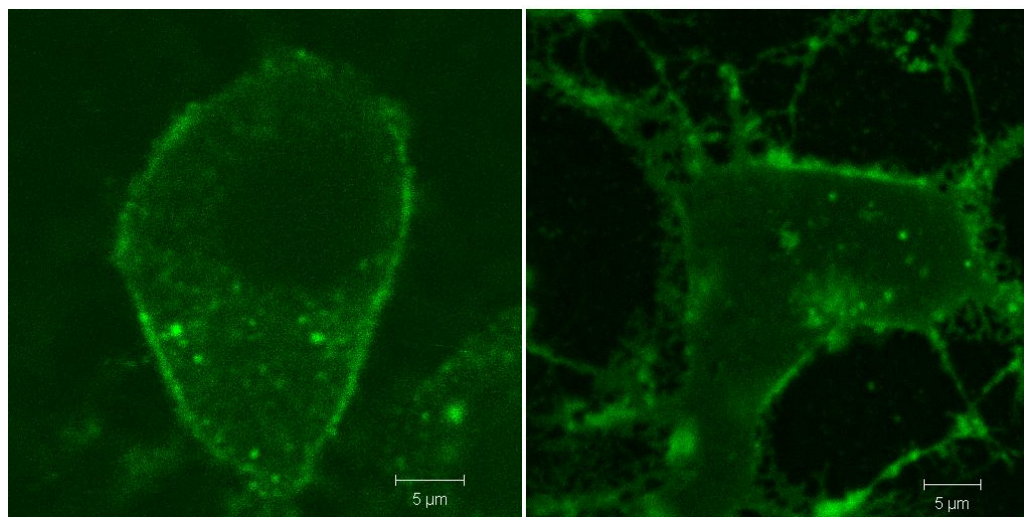


Figure 7.12. OLN-93 cells stained with BNP: cross-section (left) and bottom membrane (right). Measurements performed at room temperature.

In contrast to the neat solvents where the decays were fitted very well with a single exponential, the decays in the cells required two exponentials to get a good fit. Although two lifetimes are obtained, FLIM images do not show significant differences for the lifetime values recorded in plasma membrane or cytoplasm (Figure 7.13).

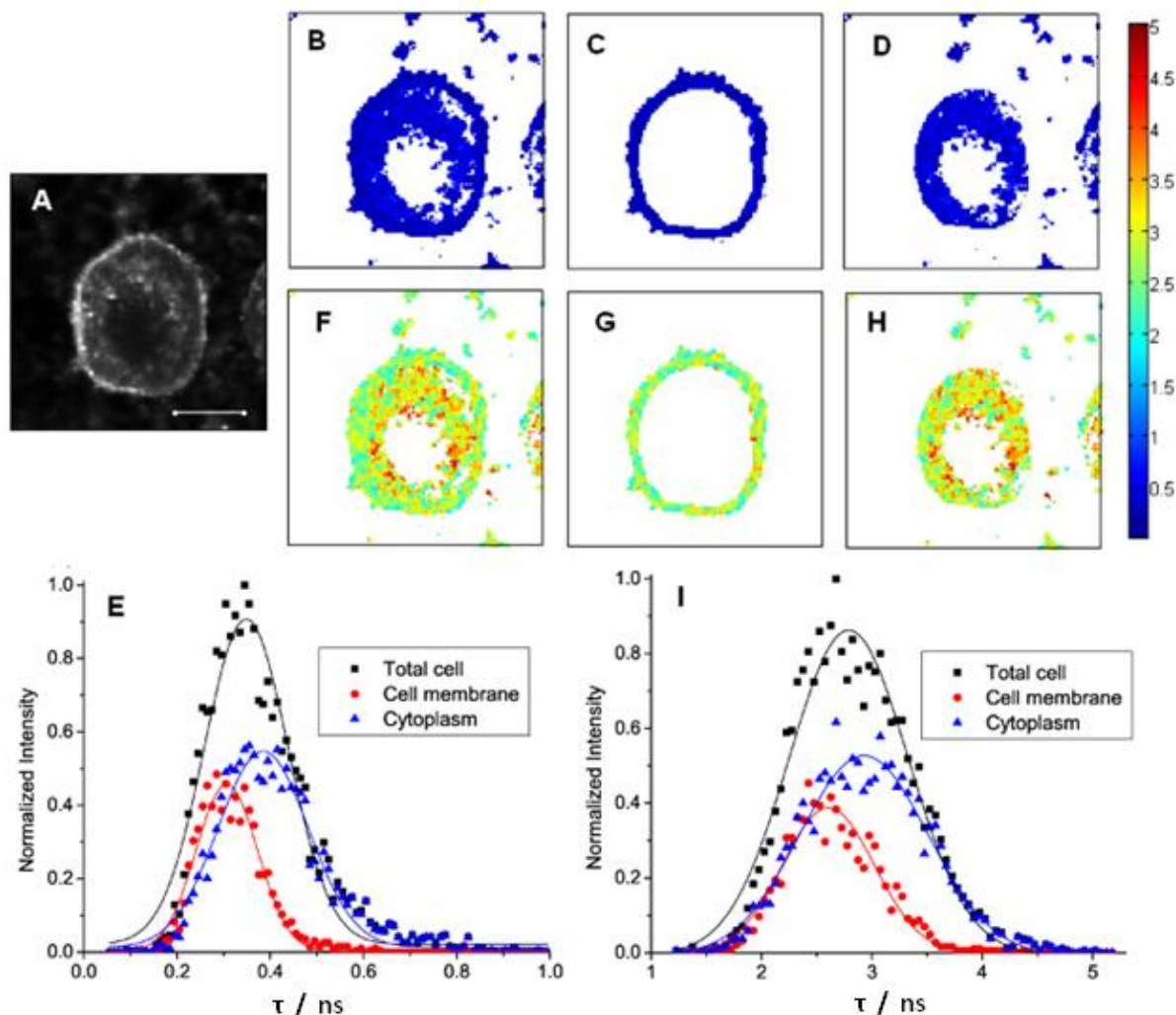


Figure 7.13. BNP fluorescence recorded on OLN-93 cells.

(A) The intensity image of OLN-93 cell. FLIM images of the entire OLN-93 cell (B and F), the plasma membrane (C and G) and the cytoplasm (D and H). Lifetime distribution of the shorter (E) and longer (I) lifetimes recorded in the cells.

FRAP measurements were performed on OLN-93 cells and the weighted average of D from 5 successful measurements is $0.1783 \pm 0.0190 \mu\text{m}^2/\text{s}$ (values are between 0.0814 and 0.4773), while the mobile fraction is $90.8 \pm 1.0 \%$.

7.5. Discussion

Fluorescent probes have proved to be a useful tool in characterizing and understanding the properties biological systems (Maier *et al.* 2002). As natural lipids are non-fluorescent fluorescent lipid probes were used for staining both the artificial and natural lipid membranes.

While biological membranes exhibit a more complex lipid structure, the lipid vesicles can be selected according to the considered research question and lipid probes can be used to monitor different lipid phases.

One of the best approaches to characterize these lipid systems is using fluorescent lipid probes which tend to behave similar with their analogous compounds (Maier *et al.* 2002).

Due to its properties, BODIPY is one of the dyes frequently used to synthesize new lipid probes. BODIPY lipid probes available until now are characterized by a yellow-red emission. Compared with the existent probes, the new probe synthesized represents the first blue BODIPY based lipid probe. Spectroscopic measurements were used to characterize BNP properties in both solvents and lipid systems (SUVs). The results showed that the photophysical properties of BNP are not influenced by solvent polarity or lipid order. Essentially the excitation maximum is around 420 nm and emission around 470 nm, with a fluorescence lifetime of ~ 4 ns.

Another characteristic of the BNP probe is given by the two 18 carbon lipid chain attached to each pyrrole group. The existent probes have the dye attached either to head group of the lipids or at different positions on the lipid chain (Boldyrev *et al.* 2007; Li *et al.* 2006). For the latter category two different patterns were observed: some of the probes are well positioned inside the bilayer while others, due to lipid chain bending end up close to the membrane surface (Boldyrev *et al.* 2007). Contrary to these probes BNP is well anchored into the lipid membrane with the help of the acyl chains. Since spectroscopic measurements could not give any information regarding BNP localization into the membrane, molecular simulations were performed. According to these results, after 40 ns, BNP position is equilibrated inside the membrane, with the BODIPY core located below the phosphor groups.

Beside its localization inside the membrane, an important factor of the probe is represented by the orientation of the dipole moment of the BODIPY core. Considering the

design we expect that the dipole moment of the dye to be parallel to the surface of the membrane. Thus, when the measurements are performed using a linearly polarized light we expected to observe the top and bottom membranes of both GUVs and cells. Although no photoselection effect could be observed for these regions we should expect to see a high photoselection effect along the path of the excitation light when recording a cross-section through the GUVs. Nonetheless, the photoselection effect observed in our images is not significant, meaning that the dipole moment cannot be parallel to the plane of the membrane. This assumption is confirmed by the molecular simulations which show that the BODIPY core upon insertion into the membrane is slightly tilted compared with the normal to the membrane.

Microscopic measurements performed on heterogeneous GUVs established that the probe partitions preferentially into lipid phases. BNP partition either into the L_d phase for the DOPC/SM/Chol mixture or in S_o phase for the DOPC/DPPC mixture. This behaviour is similar with the one of DiI-C18 probe (Baumgart *et al.* 2007).

DiI-C18, a dialkyl carbocyanine based lipid probe with 18 carbons lipid chains, is accepted that partitions into the L_d phase of the ternary mixtures containing sphingomyelin (Baumgart *et al.* 2007). A controversy appears in the case of binary mixtures of phospholipids. Depending on the method used to prepare the GUVs, the probe partitions either into the S_o phase (ITO plates) (Li and Cheng 2006) or into the L_d (platinum wires) (Juhász *et al.* 2012). Another parallel that can be made between BNP and DiI-C18 is regarding their localization inside the lipid membranes. Molecular dynamics simulation showed that the DiI-C18 probe resides below the interface water-lipid head groups, into the interior of the bilayer (Gullapalli *et al.* 2008), similarly with the BNP.

Considering BNP excitation/emission spectra and dipole orientation and the same characteristics of other fluorescent probes (i.e., some of the DiI and DiO probes), BNP can be used as a potential donor for a donor-acceptor FRET pair in lipid bilayers.

Although we can visualize different lipid phases in GUVs, when incorporated into de plasma membrane of the cells, we could not distinguish membrane domains. Neither FLIM measurements could give information regarding the lipid system. But, diffusion measurements were performed successfully both on GUVs and OLN-93 cells. Diffusion coefficients obtained for the gel and fluid phase of the GUVs are different by one order of magnitude: $0.13 \pm 0.02 \mu\text{m}^2/\text{s}$, and $4 \pm 2 \mu\text{m}^2/\text{s}$ respectively.

We can also try to compare lateral diffusion of BNP and DiI-C18 probes. Although FRAP measurements of DiI-C18 were performed only on oligodendrocytes, more FCS

studies were performed on both GUVs and cells. FRAP measurements performed on oligodendrocytes yield diffusion coefficient values from 0.4 to 2.8 $\mu\text{m}^2/\text{s}$ (Gielen *et al.* 2009) found within the same range as the one obtained for BNP. Similar diffusion coefficients were found also for FCS measurements, for GUVs found in the fluid phase (Bacia *et al.* 2004) or the ordered phase (Kahya *et al.* 2003). The close values obtained can be explained by similar mobilities for the two the probes in the lipid membrane of GUVs and cells.

Thus, based on the literature and our finding for the BNP we can say that the BNP can be used as a good lipid probe, but can also be seen as an alternative of the DiI-C18 probe for the blue region of the spectrum.

PARTIAL CONCLUSIONS

In this chapter we characterized the properties of a new based BODIPY lipid probe. The probe is not sensitive to solvent polarity, and the fluorescence lifetimes values are independent of the environment properties, but similarly with other membrane probes, BNP can be used for anisotropy measurements and to determine T_m of the lipids.

Because of its structure BNP allows visualization of lipid phase segregation. For binary lipid mixtures (DOPC/DPPC), the probe accumulates in the S_o phase, while in the ternary lipid mixtures (DOPC/SM/Chol) the probe accumulates in the L_d phase.

BNP can be used successfully for diffusion measurements both in model and natural lipid membranes. Due to its characteristics, BNP can be seen as an alternative for the DiI-C18 in the blue region of the spectrum. Also, in combinations with some of the DiI and DiO probes or adequate BODIPY probes can be used to perform FRET experiments.

CHAPTER 8

TGF- β EFFECT ON OLN-93 CELLS

INTRODUCTION

TGF- β modulates cell proliferation and induces apoptosis in cells through SMAD or DAXX pathways. In the SMAD pathway TGF- β cytokines binds to two different receptors (type I and II) that contain serine/threonine kinase domains. Type II receptor is activated first, leading to heteromeric assembly of type I and II receptors, then the phosphorylation of type I receptor phosphorylate and activate the Smad proteins (R-Smad, Co-Smad and I-Smad) signaling to nucleus (Ma *et al.* 2007; Miyazawa *et al.* 2002). In DAXX pathway apoptosis is triggered by TGF- β via the death domain-associated protein (Daxx) which binds itself to the type II receptor after TGF- β activates it (Salomoni *et al.* 2006). The control of the type II receptor at the cell surface is important to the cellular response to TGF- β : at low concentration of type II receptor an uncontrolled cell proliferation and pathological phenomena appears and high concentration lead to ligand-independent activation (Ehrlich *et al.* 2001).

TGF- β responsiveness is modulated by type I/II receptor partitioning between lipid raft-mediated and clathrin (non raft)-mediated endocytosis pathways (Chen *et al.* 2008). Lipid raft-mediated endocytosis results in a rapid degradation of TGF- β with a diminished TGF- β responsiveness whereas clathrin-mediated endocytosis leads to endosomal signaling and promotes TGF- β responsiveness. One can hypothesize that modulating the partition of receptors by disrupting the rafts by influencing the membrane Chol could lead to enhanced effects of TGF- β . Förster resonance energy transfer (FRET) microscopy can be used to test this hypothesis.

8.1. Preliminary studies of TGF- β effects on OLN-93 cells

In order to reveal and characterize the effects of Chol modulating factors (SV and T09), the analysis at the membrane level was combined with apoptosis measurements. The work was performed on differentiated OLN-93 cell.

TGF- β induced apoptosis was analyzed by means of two assays: MTS assay and Caspase 3 assays. This allows us to explore the relationship between the apoptosis index and the TGF- β concentration in presence/absence of SV or T09.

The OLN-93 cells were cultured in medium containing 0.5% FCS and treated with different concentration of SV: 0.1, 1, 2.5 and 5 μ M.

As already shown (see section 5), the morphology of cells changes with increasing SV concentration: the arborized cells observed in control conditions, loose the branches and become mostly bipolar cells under treatment with 1 μ M SV. For concentrations higher than 2.5 μ M the cells start to round up, a mark of increased toxicity, which is confirmed by the decrease in cells viability (Figure 8.1).

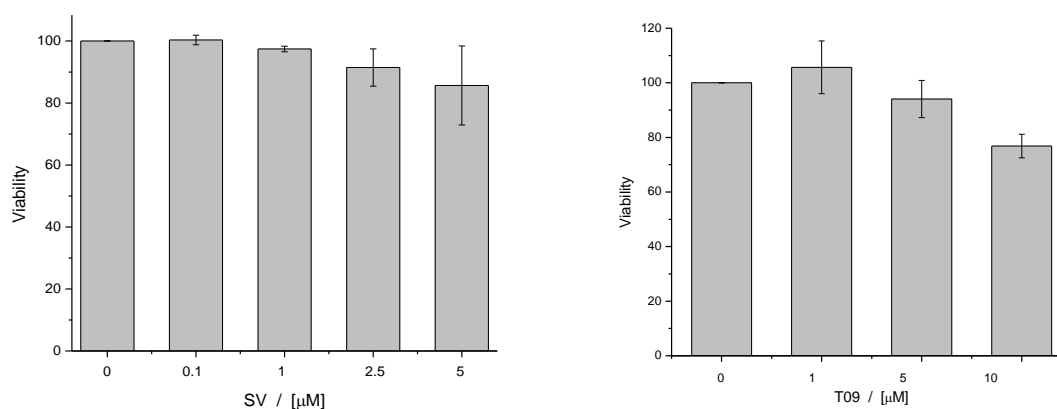


Figure 8.1. Effect of different concentration of SV or T09 on the OLN-93 viability.

The error bars are the standard deviations resulting from three repeated measurements for each condition.

A similar observation can be made for the cells treated with T09 (1, 5 and 10 μ M). The cells lose their branches with increasing concentration of T09, and for concentrations higher than 10 μ M the viability of the cells decreases.

Cells found in control conditions or treated with SV or T09 were subjected to different concentrations of TGF- β (1, 3, 6 and 10 nM). First was checked the effect of TGF- β treatment on the viability of the control cells. For the TGF- β concentration tested, the viability of the cells was not affected (Figure 8.2).

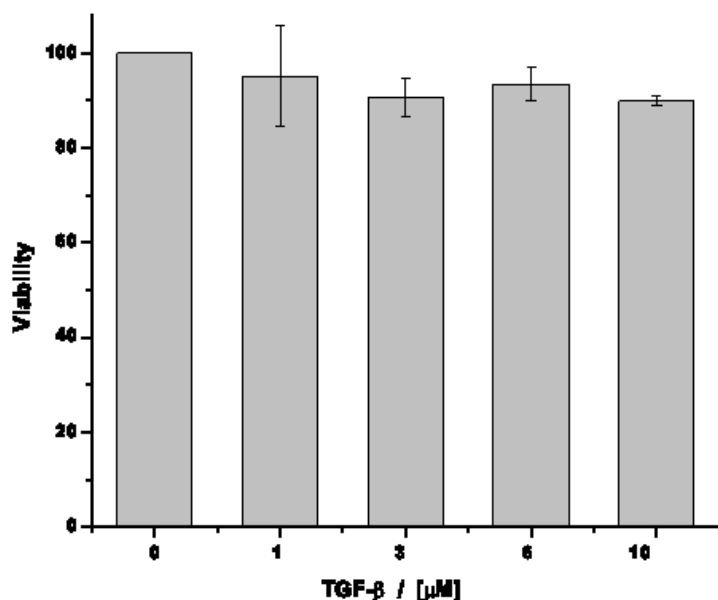


Figure 8.2. Effect of different concentration of TGF- β on the OLN-93 viability.

The error bars are the standard deviations resulting from three repeated measurements for each condition.

The same concentrations were applied to cells treated with SV to determine how the SV influences the effects induced by TGF- β . Only under SV treatment, the viability starts to decrease for concentrations higher than 2.5 μ M. When TGF- β is added, for 0.1 and 1 μ M SV the viability is not affected, but for 2.5 and 5 μ M the viability of the cells decreases even more (Figure 8.3).

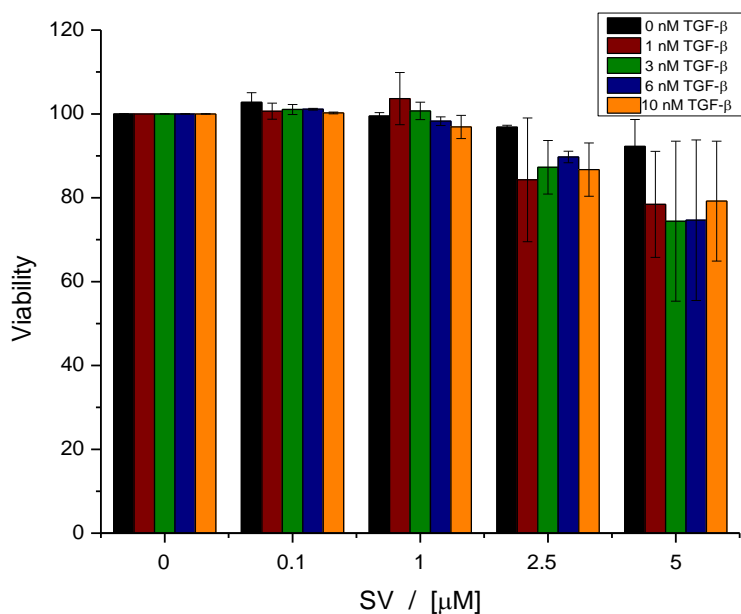


Figure 8.3. Effect of different concentration of SV and TGF- β on the OLN-93 viability.

The error bars are the standard deviations resulting from three repeated measurements for each condition.

A totally different effect was observed if the TGF- β was added to the cells treated with T09. No effect was observed for cells treated with 1 μM T09, but for the cells treated with 5 and 10 μM T09 which alone lead to a decrease in viability, in the presence of TGF- β the number of viable cells increases (Figure 8.4).

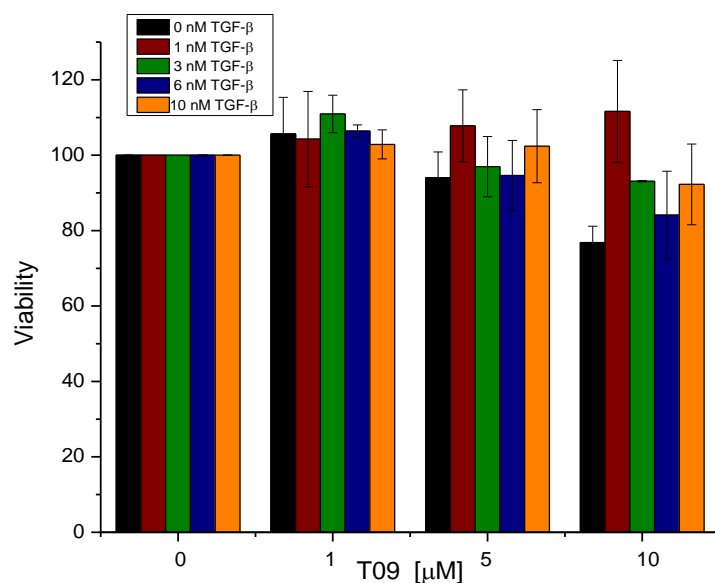


Figure 8.4. Effect of different concentration of T9 and TGF- β on the OLN-93 viability.

The error bars are the standard deviations resulting from three repeated measurements for each condition.

Because the viability test cannot differentiate between the living cells and the early apoptotic ones, an apoptosis test was performed to see if the treatment can induce apoptosis. A Caspase3/7 kit was used. As positive control, the cells were treated with Bleomycin (40 μ g/mL), for 1h. At the same time, the cells treatment with SV or T9 started.

In Figure 8.5 are presented the results obtained for SV and T9 treatments. For SV, the quantities of caspase increases with increasing concentration. This shows that SV treatment induces apoptosis to OLN-93 cells. Contrary to SV, T9 does not induce any apoptosis to cells.

Then, it was investigated the effects induced by TGF- β and the combination between SV and TGF- β .

For control cells treated only with TGF- β we can see an increase of caspase activity which suggests that TGF- β induces an apoptotic effect on OLN-93 cells.

When SV was added, the caspase activity increases further, proportional with the concentration of SV.

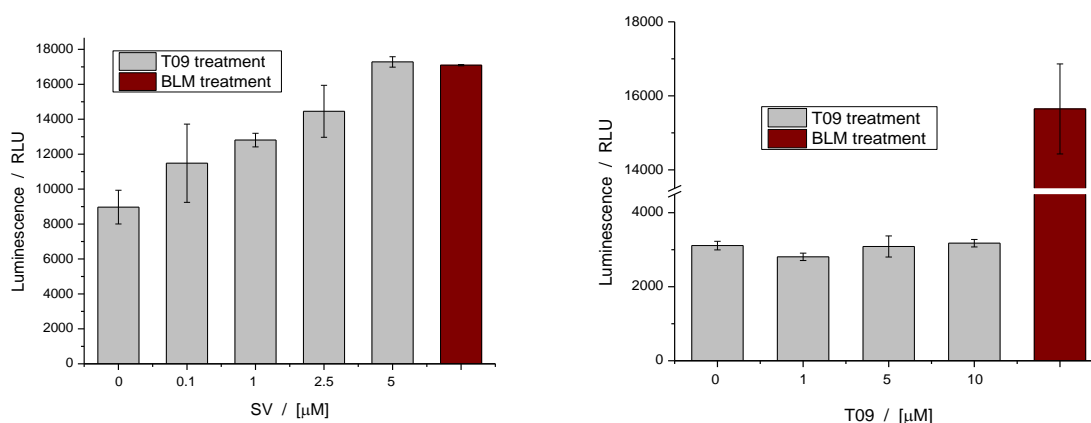


Figure 8.5. Apoptotic effects of different concentration of SV and TGF- β on the OLN-93.

The error bars are the standard deviations resulting from three repeated measurements for each condition

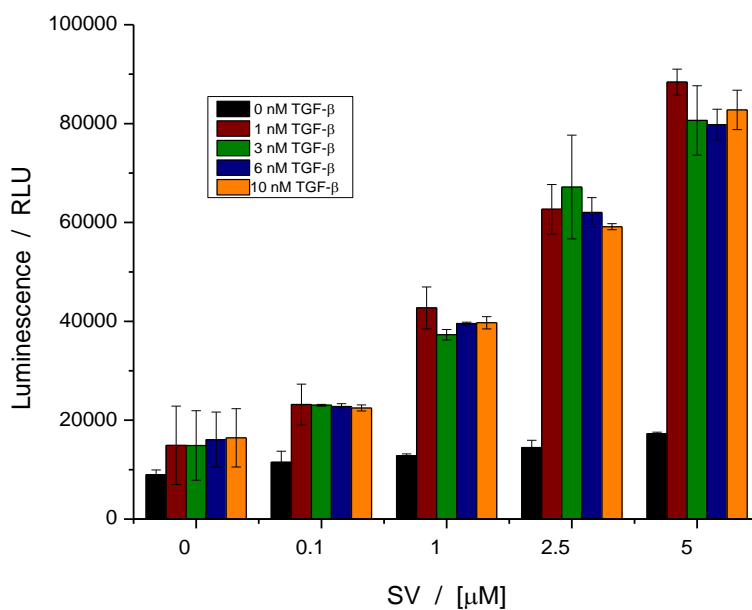


Figure 8.6. Apoptotic effects of different concentration of SV and TGF- β on the OLN-93.

The error bars are the standard deviations resulting from three repeated measurements for each condition.

In the case of TGF- β and T09 treatment no change was observed between the cells treated only with TGF- β or with the combination of the two factors.

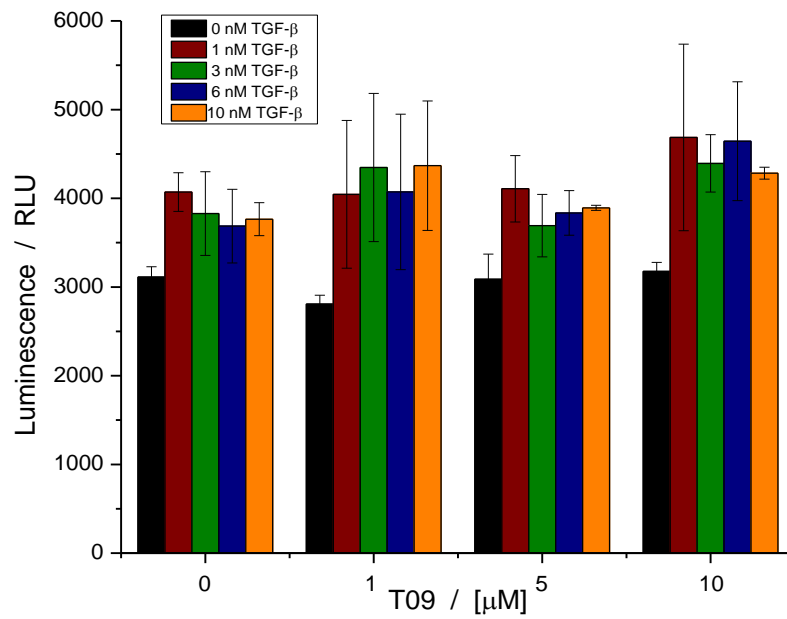


Figure 8.7. Apoptotic effects of different concentration of T09 and TGF- β on the OLN-93.

The error bars are the standard deviations resulting from three repeated measurements for each condition.

8.2. Discussion

Statins are responsible for inhibiting HMG-CoA reductase activity reducing Chol synthesis, thus modifying the organization of the membranes. Because of this, it has been shown to cause growth arrest and apoptosis to a large variety of tumoral and non-tumoral cells (Gullu *et al.* 2005; Hillyard *et al.* 2004; Xiang and Reeves 2009), activating the caspases 9,8, and 3, necessary for apoptosis (Cafforio *et al.* 2005; Chapman-Shimshoni *et al.* 2003; Koyuturk *et al.* 2004). Except this, many cellular processes are disturbed leading in the end to growth arrest or apoptosis. The molecular mechanisms activated by SV that lead to apoptosis are still unclear, but it is supposed that apoptosis is induced by activating the mitochondrial pathway of caspase 9 (Chapman-Shimshoni *et al.* 2003).

Gullu *et al.* investigated both *in vivo* and *in vitro* the effects of statins on lymphocytes from patients with Hashimoto's thyroiditis, proving that statins cause apoptosis in a dose-dependent manner and may improve the thyroid functions of the patients from the study (Gullu *et al.* 2005).

Xiang *et al.* studied the effect of SV (at clinically relevant concentrations) to the Purkinje cells and oligodendrocytes, and have showed that, in the early stage of myelination SV induces the death of almost all cells, from the lower concentration tested. In the late stage of myelination, significant damages were observed only at greater concentration, Purkinje cells being more vulnerable than oligodendrocytes. In the stage of fully myelination all neurons and almost all of the oligodendrocytes were dead at the higher SV concentrations (Xiang and Reeves 2009).

We showed that SV treatment can be toxic to OLN-93 cells for concentrations higher than 2.5 μ M and can lead to caspase activity even for lower concentrations. The effects are enhanced when TGF- β is used in the presence of SV treatment and is a process dose dependent.

Wente *et al.* studied the effect T0901317 (LXR agonist) and 9cRA (RXR agonist) on MIN6 cells and rat pancreatic islets. They showed that T09 all-alone has a weak effect on the cells, but with the RXR agonist it was observed an apoptotic effect (Wente *et al.* 2007).

We obtained similar results for the OLN-93 cells. T09 does not affect the viability of the cells and does not induce any apoptotic effects even if it is used alone or in the presence of TGF- β .

PARTIAL CONCLUSIONS AND PERSPECTIVES

Treatment of TGF- β in conjunction with SV induces an even higher apoptotic effect on the OLN-93 cells. Instead, if T09 is used, no effect is observed compared with the cells treated only with TGF- β .

The studies need to be continued to understand better the difference of TGF- β behavior when found in the presence of SV or T09.

Modulation of raft/non-raft partition of TGF- β receptors will be studied by FRET. FRET is based on the very close proximity (order of nm) of donor and acceptor molecules and will be used to monitor the distribution of TGF- β -R over rafts and non-rafts. GM1, a ganglioside also found in OLs (Arvanitis *et al.* 2005), will be used as a raft marker. The donor-acceptor pair will be formed by TGF- β -R (labeled by anti type I/II antibody carrying the donor) and GM1 (labeled with the pentameric subunit B of cholera toxin carrying the acceptor). The FRET analysis will be performed according to Kenworthy *et al.* (Kenworthy *et al.* 2000). A shift of the TGF- β -R towards a non-raft phase can be monitored by a decrease in FRET efficiency. This shift may promote TGF- β induced apoptosis.

GENERAL CONCLUSIONS

Due to its solvatochromic properties, Laurdan spectra conceal a lot more information regarding its environment and particularly about the lipid packing order of the lipid membrane, then it is used at the moment.

In this study Laurdan emission spectra in homogeneous solutions of solvents with various polarities were used to propose a new method to evaluate the complex spectrum of Laurdan inserted into the membrane of LUVs. Starting from an asymmetric LN function, which can accommodate better to the fluorophore peaks, was proposed and adapted a decomposition algorithm specific for Laurdan. **The studies proved that using this procedure one can obtain a much better characterization of the hydration level of the membrane where Laurdan is located. Also a new parameter, more sensitive than GP , was proposed to evaluate Laurdan emission spectra (ΔAr).**

GP values and fluorescence lifetimes measurements were performed on model membranes. Fluorescence lifetimes were recorded in two channels, allowing the characterization of Laurdan molecules emitting from two different states: molecules which are not affected by dipole relaxation (blue channel) and molecules affected by dipole relaxation (green channel). **The results show that the lifetime in the blue channel, although shorter than the one in the green channel, is more sensitive to changes in the membrane.**

Both GP and lifetimes can detect changes in the lipid packing order of the membrane and assess T_m . Contrary to GP , the lifetimes allow to distinguish between the phospholipids used.

Measurements performed on GUVs are consistent with the ones performed on LUVs and show that **GP and fluorescence lifetimes reflect membrane characteristics and that increasing GP values are correlated with increasing lifetimes.**

Unexpectedly, using linearly polarized light, **a photoselection effect was observed for the lifetimes and** not only for the GP values. This allows obtaining information regarding the **orientation of Laurdan molecules**, but also about the **microheterogeneity** of the membrane.

GP and fluorescence lifetimes measurements in the blue and green channel were performed on Laurdan in the plasma membrane of biological cells. *GP* values and fluorescence lifetimes can be used to generate **topographic maps** which can reveal the **complex situation in biological membranes** when information at the pixel scale is used.

Laurdan was used to detect the changes in membrane fluidity induced by Chol modulating factors (SV or T09). The measurements performed were able to sense the changes and also to **highlight** a different behavior for the two treatments used.

Because in the case of **SV treatment** Chol synthesis is blocked, the amount of Chol in the membrane is reduced. Both ***GP* values and fluorescence lifetimes were decreasing with increasing SV concentration**, independent of the temperature of the measurements.

On the other hand, for **T09 treatment**, both ***GP* values and fluorescence lifetimes are decreasing with increasing T09 concentration** for measurements performed at **37 °C**, but a **small increase of both *GP* and lifetimes** was observed for the cells recorded at **21 °C**.

Preliminary results on TGF- β effects, in the absence or presence of SV/T09 treatment, were reported in this Thesis. Treatment with **TGF- β together with SV** induces an even **higher apoptotic effect on the OLN-93 cells**. Instead, if **T09** is used **no apoptotic effect is observed** compared with the cells treated only with TGF- β .

The results presented here suggest that it is relevant to continue these studies in which modulation of raft/non-raft partition of TGF- β receptors will be correlated with changes in membrane fluidity and biological effects on OLN-93 cells.

A new BODIPY based lipid probe was characterized and tested on GUVs and OLN-93 cells. The studies showed that due to its structure, **BNP allows visualization of lipid phase segregation** and can be used for **diffusion measurements**. Because of its similarities to DiI-C18, BNP can be seen as **an alternative for the blue region of the spectrum** and is **adequate to perform FRET experiments** with lipid probes similar to DiI or DiO.

BIBLIOGRAPHY

- A. Gaw, C. J. Packard and J. Shepherd *Statins: The HMG-CoA Reductase Inhibitors in Perspective*, ed. 2, Informa Healthcare. (2003).
- Aggarwal, S., L. Yurlova and M. Simons *Central nervous system myelin: structure, synthesis and assembly*. Trends in cell biology **21**(10): 585-593. (2011).
- Aguilar, L. F., J. A. Pino, M. A. Soto-Arriaza, F. J. Cuevas, S. Sanchez and C. P. Sotomayor *Differential Dynamic and Structural Behavior of Lipid-Cholesterol Domains in Model Membranes*. Plos One **7**(6). (2012).
- Ameloot, M., H. Hendrickx, W. Herreman, H. Pottel, F. Vancauwelaert and W. Vandermeer *Effect of Orientational Order on the Decay of the Fluorescence Anisotropy in Membrane Suspensions - Experimental-Verification on Unilamellar Vesicles and Lipid Alpha-Lactalbumin Complexes*. Biophys. J. **46**(4): 525-539. (1984).
- Angelova, M. I. and D. S. Dimitrov *Liposome Electroformation*. Faraday Discuss. **81**: 303-+. (1986).
- Arbeloa, F. L., J. Banuelos, V. Martinez, T. Arbeloa and I. P. Arbeloa *Structural, photophysical and lasing properties of pyromethene dyes*. Int. Rev. Phys. Chem. **24**(2): 339-374. (2005).
- Arvanitis, D. N., W. X. Min, Y. P. Gong, Y. M. Heng and J. M. Boggs *Two types of detergent-insoluble, glycosphingolipid/cholesterol-rich membrane domains from isolated myelin*. J. Neurochem. **94**(6): 1696-1710. (2005).
- Bacia, K., D. Scherfeld, N. Kahya and P. Schuille *Fluorescence correlation spectroscopy relates rafts in model and native membranes*. Biophys. J. **87**(2): 1034-1043. (2004).
- Bagatolli, L. A. *To see or not to see: lateral organization of biological membranes and fluorescence microscopy*. Biochim. Biophys. Acta **1758**(10): 1541-1556. (2006).
- Bagatolli, L. A. and E. Gratton *Two-photon fluorescence microscopy observation of shape changes at the phase transition in phospholipid giant unilamellar vesicles*. Biophys. J. **77**(4): 2090-2101. (1999).
- Bagatolli, L. A. and E. Gratton *Two photon fluorescence microscopy of coexisting lipid domains in giant unilamellar vesicles of binary phospholipid mixtures*. Biophys. J. **78**(1): 290-305. (2000).
- Bagatolli, L. A., E. Gratton and G. D. Fidelio *Water dynamics in glycosphingolipid aggregates studied by LAURDAN fluorescence*. Biophys. J. **75**(1): 331-341. (1998).
- Bagatolli, L. A., B. Maggio, F. Aguilar, C. P. Sotomayor and G. D. Fidelio *Laurdan properties in glycosphingolipid-phospholipid mixtures: a comparative fluorescence and calorimetric study*. Biochim. Biophys. Acta **1325**(1): 80-90. (1997).
- Bagatolli, L. A., T. Parasassi, G. D. Fidelio and E. Gratton *A model for the interaction of 6-lauroyl-2-(N,N-dimethylamino)naphthalene with lipid environments: implications for spectral properties*. Photochem. Photobiol. **70**(4): 557-564. (1999).
- Bagatolli, L. A., S. A. Sanchez, T. Hazlett and E. Gratton *Giant vesicles, laurdan, and two-photon fluorescence microscopy: Evidence of lipid lateral separation in bilayers*. Methods Enzymol. **360**: 481-500. (2003).
- Banuelos, J., V. Martin, C. F. A. Gomez-Duran, I. J. A. Cordoba, E. Pena-Cabrera, I. Garcia-Moreno, A. Costela, M. E. Perez-Ojeda, T. Arbeloa and I. L. Arbeloa *New 8-Amino-BODIPY Derivatives: Surpassing Laser Dyes at Blue-Edge Wavelengths*. Chem-Eur J **17**(26): 7261-7270. (2011).
- Baranowski, M. *Biological Role of Liver X Receptors*. J Physiol Pharmacol **59**(4): 31-55. (2008).
- Barucha-Kraszewska, J., S. Kraszewski, P. Jurkiewicz, C. Ramseyer and M. Hof *Numerical studies of the membrane fluorescent dyes dynamics in ground and excited states*. Biochim. Biophys. Acta **1798**(9): 1724-1734. (2010).
- Barucha-Kraszewska, J., S. Kraszewski and C. Ramseyer *Will C-Laurdan Dethrone Laurdan in Fluorescent Solvent Relaxation Techniques for Lipid Membrane Studies?* Langmuir. (2013).

- Bauer, N. G., C. Richter-Landsberg and C. Ffrench-Constant *Role of the oligodendroglial cytoskeleton in differentiation and myelination*. *Glia* **57**(16): 1691-1705. (2009).
- Baumann, N. and D. Pham-Dinh *Biology of oligodendrocyte and myelin in the mammalian central nervous system*. *Physiological reviews* **81**(2): 871-927. (2001).
- Baumgart, T., G. Hunt, E. R. Farkas, W. W. Webb and G. W. Feigenson *Fluorescence probe partitioning between L-o/L-d phases in lipid membranes*. *Bba-Biomembranes* **1768**(9): 2182-2194. (2007).
- Becker, W. *Fluorescence lifetime imaging - techniques and applications*. *Journal of microscopy* **247**(2): 119-136. (2012).
- Berg, J., J. Tymoczko and L. Stryer *Lipids and Cell Membranes*. Biochemistry 5th edition. New York, W H Freeman.(2002).
- Bjorkhem, I. and S. Meaney *Brain cholesterol: long secret life behind a barrier*. *Arteriosclerosis, thrombosis, and vascular biology* **24**(5): 806-815. (2004).
- Boens, N., W. W. Qin, M. Baruah, W. M. De Borggraeve, A. Filarowski, N. Smisdom, M. Ameloot, L. Crovetto, E. M. Talavera and J. M. Alvarez-Pez *Rational Design, Synthesis, and Spectroscopic and Photophysical Properties of a Visible-Light-Excitable, Ratiometric, Fluorescent Near-Neutral pH Indicator Based on BODIPY*. *Chem-Eur J* **17**(39): 10924-10934. (2011).
- Boldyrev, I. A., X. Zhai, M. M. Momsen, H. L. Brockman, R. E. Brown and J. G. Molotkovsky *New BODIPY lipid probes for fluorescence studies of membranes*. *J. Lipid Res.* **48**(7): 1518-1532. (2007).
- Boldyrev, I. A., X. Zhai, M. M. Momsen, H. L. Brockman, R. E. Brown and J. G. Molotkovsky *New BODIPY lipid probes for fluorescence studies of membranes*. *J Lipid Res* **48**(7): 1518-1532. (2007).
- Bradl, M. and H. Lassmann *Oligodendrocytes: biology and pathology*. *Acta neuropathologica* **119**(1): 37-53. (2010).
- Brejchova, J., J. Sykora, K. Dlouha, L. Roubalova, P. Ostasov, M. Vosahlikova, M. Hof and P. Svoboda *Fluorescence spectroscopy studies of HEK293 cells expressing DOR-Gi1alpha fusion protein; the effect of cholesterol depletion*. *Biochim. Biophys. Acta* **1808**(12): 2819-2829. (2011).
- Brown, D. A. *Lipid rafts, detergent-resistant membranes, and raft targeting signals*. *Physiology (Bethesda)* **21**: 430-439. (2006).
- Brown, D. A. and E. London *Functions of lipid rafts in biological membranes*. *Annu. Rev. Cell Dev. Biol.* **14**: 111-136. (1998).
- Bruck, W. and C. Stadelmann *Inflammation and degeneration in multiple sclerosis*. *Neurological sciences : official journal of the Italian Neurological Society and of the Italian Society of Clinical Neurophysiology* **24 Suppl 5**: S265-267. (2003).
- Buckinx, R., I. Smolders, S. Sahebali, I. Smets, M. Vandeven, M. Ameloot and J. M. Rigo *Morphological changes do not reflect differentiation stage in OLN-(93) oligodendrocytes*. *Neuron Glia Biol* **2**: S48-S48. (2007).
- Burstein, E. A., S. M. Abornev and Y. K. Reshetnyak *Decomposition of protein tryptophan fluorescence spectra into log-normal components. I. Decomposition algorithms*. *Biophys. J.* **81**(3): 1699-1709. (2001).
- Burstein, E. A. and V. I. Emelyanenko *Log-normal description of fluorescence spectra of organic fluorophores*. *Photochem. Photobiol.* **64**(2): 316-320. (1996).
- Cafforio, P., F. Dammacco, A. Gernone and F. Silvestris *Statins activate the mitochondrial pathway of apoptosis in human lymphoblasts and myeloma cells*. *Carcinogenesis* **26**(5): 883-891. (2005).
- Calkin, A. C. and P. Tontonoz *Liver x receptor signaling pathways and atherosclerosis*. *Arteriosclerosis, thrombosis, and vascular biology* **30**(8): 1513-1518. (2010).
- Chapman-Shimshoni, D., M. Yuklea, J. Radnay, H. Shapiro and M. Lishner *Simvastatin induces apoptosis of B-CLL cells by activation of mitochondrial caspase 9*. *Experimental hematology* **31**(9): 779-783. (2003).
- Chen, C. L., S. S. Huang and J. S. Huang *Cholesterol modulates cellular TGF-beta responsiveness by altering TGF-beta binding to TGF-beta receptors*. *J Cell Physiol* **215**(1): 223-233. (2008).

- Chen, C. L., I. H. Liu, S. J. Fliesler, X. Han, S. S. Huang and J. S. Huang *Cholesterol suppresses cellular TGF-beta responsiveness: implications in atherogenesis*. *J. Cell Sci.* **120**(20): 3509-3521. (2007).
- Dean, M., A. Rzhetsky and R. Allikmets *The human ATP-binding cassette (ABC) transporter superfamily*. *Genome Res* **11**(7): 1156-1166. (2001).
- DeBruin, L. S., J. D. Haines, L. A. Wellhauser, G. Radeva, V. Schonmann, D. Bienzle and G. Harauz *Developmental partitioning of myelin basic protein into membrane microdomains*. *J Neurosci Res* **80**(2): 211-225. (2005).
- Debruin, L. S. and G. Harauz *White matter rafting--membrane microdomains in myelin*. *Neurochem Res* **32**(2): 213-228. (2007).
- Digman, M. A., V. R. Caiolfa, M. Zamai and E. Gratton *The phasor approach to fluorescence lifetime imaging analysis*. *Biophys. J.* **94**(2): L14-L16. (2008).
- Eddidin, M. *The state of lipid rafts: From model membranes to cells*. *Annu. Rev. Biophys. Biomol. Struct.* **32**: 257-283. (2003).
- Ehrlich, M., A. Shmueli and Y. I. Henis *A single internalization signal from the di-leucine family is critical for constitutive endocytosis of the type II TGF-beta receptor*. *J. Cell Sci.* **114**(9): 1777-1786. (2001).
- Elangovan, M., R. N. Day and A. Periasamy *Nanosecond fluorescence resonance energy transfer-fluorescence lifetime imaging microscopy to localize the protein interactions in a single living cell*. *J Microsc-Oxford* **205**: 3-14. (2002).
- Emel'ianenko, V. I., K. Reshetniak Ia, O. A. Andreev and E. A. Burshtein *[Analysis of log-normal components of fluorescence spectra of prodan and acrylodan bound to proteins]*. *Biofizika* **45**(2): 207-219. (2000).
- Endo, A. *A gift from nature: the birth of the statins*. *Nat Med* **14**(10): 1050-1052. (2008).
- Esquembre, R., M. L. Ferrer, M. C. Gutierrez, R. Mallavia and C. R. Mateo *Fluorescence study of the fluidity and cooperativity of the phase transitions of zwitterionic and anionic liposomes confined in sol-gel glasses*. *J. Phys. Chem. B* **111**(14): 3665-3673. (2007).
- Gasecka, A., T. J. Han, C. Favard, B. R. Cho and S. Brasselet *Quantitative Imaging of Molecular Order in Lipid Membranes Using Two-Photon Fluorescence Polarimetry*. *Biophys. J.* **97**(10): 2854-2862. (2009).
- Gaus, K., E. Gratton, E. P. Kable, A. S. Jones, I. Gelissen, L. Kritharides and W. Jessup *Visualizing lipid structure and raft domains in living cells with two-photon microscopy*. *Proc. Nat. Acad. Sci. USA* **100**(26): 15554-15559. (2003).
- Gaus, K., T. Zech and T. Harder *Visualizing membrane microdomains by Laurdan 2-photon microscopy*. *Mol. Membr. Biol.* **23**(1): 41-48. (2006).
- Gielen, E., W. Baron, M. Vandeven, P. Steels, D. Hoekstra and M. Ameloot *Rafts in oligodendrocytes: evidence and structure-function relationship*. *Glia* **54**(6): 499-512. (2006).
- Gielen, E., N. Smisdom, M. vandeVen, B. De Clercq, E. Gratton, M. Digman, J. M. Rigo, J. Hofkens, Y. Engelborghs and M. Ameloot *Measuring Diffusion of Lipid-like Probes in Artificial and Natural Membranes by Raster Image Correlation Spectroscopy (RICS): Use of a Commercial Laser-Scanning Microscope with Analog Detection*. *Langmuir* **25**(9): 5209-5218. (2009).
- Gullapalli, R. R., M. C. Demirel and P. J. Butler *Molecular dynamics simulations of DiI-C18(3) in a DPPC lipid bilayer*. *Physical chemistry chemical physics : PCCP* **10**(24): 3548-3560. (2008).
- Gullu, S., R. Emral, M. Bastemir, A. B. Parkes and J. H. Lazarus *In vivo and in vitro effects of statins on lymphocytes in patients with Hashimoto's thyroiditis*. *Eur J Endocrinol* **153**(1): 41-48. (2005).
- Hardin, J., G. P. Bertoni and L. J. Kleinsmith *Becker's World of the Cell, 8 ed*, Benjamin Cummings; . (2011).
- Hardin, J., G. P. Bertoni and L. J. Kleinsmith *Membranes: Their Structure, Function, and Chemistry. Becker's World of the Cell* Benjamin Cummings. (2011).
- Harris, F. M., K. B. Best and J. D. Bell *Use of laurdan fluorescence intensity and polarization to distinguish between changes in membrane fluidity and phospholipid order*. *Bba-Biomembranes* **1565**(1): 123-128. (2002).

- Hillyard, D. Z., A. J. Cameron, K. J. McDonald, J. Thomson, A. MacIntyre, P. G. Shiels, M. Panarelli and A. G. Jardine *Simvastatin inhibits lymphocyte function in normal subjects and patients with cardiovascular disease*. *Atherosclerosis* **175**(2): 305-313. (2004).
- Houck, K. A., K. M. Borchert, C. D. Hepler, J. S. Thomas, K. S. Bramlett, L. F. Michael and T. P. Burris *T0901317 is a dual LXR/FXR agonist*. *Mol Genet Metab* **83**(1-2): 184-187. (2004).
- Huang, S. S. and J. S. Huang *TGF-beta control of cell proliferation*. *J Cell Biochem* **96**(3): 447-462. (2005).
- Ionescu, D. and C. Ganea *A study of quercetin effects on phospholipid membranes containing cholesterol using Laurdan fluorescence*. *Eur Biophys J Biophys* **41**(3): 307-318. (2012).
- Ipsen, J. H., K. Jorgensen and O. G. Mouritsen *Density-Fluctuations in Saturated Phospholipid-Bilayers Increase as the Acyl-Chain Length Decreases*. *Biophys. J.* **58**(5): 1099-1107. (1990).
- Jackman, N., A. Ishii and R. Bansal *Oligodendrocyte development and myelin biogenesis: parsing out the roles of glycosphingolipids*. *Physiology (Bethesda)* **24**: 290-297. (2009).
- Jaureguiberry, M. S., M. A. Triccerri, S. A. Sanchez, H. A. Garda, G. S. Finarelli, M. C. Gonzalez and O. J. Rimoldi *Membrane organization and regulation of cellular cholesterol homeostasis*. *J. Membr. Biol.* **234**(3): 183-194. (2010).
- Jessen, K. R. *Glial cells*. *The international journal of biochemistry & cell biology* **36**(10): 1861-1867. (2004).
- Jorge Bañuelos, Fernando Lopez Arbeloa, Teresa Arbeloa, Virginia Martinez and I. L. Arbeloa *BODIPY Laser dyes applied in sensing and monitoring environmental properties*. Applied Science Innovations Pvt. Ltd. (2012).
- Juhasz, J., J. H. Davis and F. J. Sharom *Fluorescent probe partitioning in GUVs of binary phospholipid mixtures: implications for interpreting phase behavior*. *Biochimica et biophysica acta* **1818**(1): 19-26. (2012).
- Jurkiewicz, P., L. Cwiklik, P. Jungwirth and M. Hof *Lipid hydration and mobility: an interplay between fluorescence solvent relaxation experiments and molecular dynamics simulations*. *Biochimie* **94**(1): 26-32. (2012).
- Jurkiewicz, P., A. Olzyska, M. Langner and M. Hof *Headgroup hydration and mobility of DOTAP/DOPC bilayers: a fluorescence solvent relaxation study*. *Langmuir* **22**(21): 8741-8749. (2006).
- Kahya, N., D. Scherfeld, K. Bacia, B. Poolman and P. Schwille *Probing lipid mobility of raft-exhibiting model membranes by fluorescence correlation spectroscopy*. *J. Biol. Chem.* **278**(30): 28109-28115. (2003).
- Kaiser, H. J., D. Lingwood, I. Levental, J. L. Sampaio, L. Kalvodova, L. Rajendran and K. Simons *Order of lipid phases in model and plasma membranes*. *Proc. Nat. Acad. Sci. USA* **106**(39): 16645-16650. (2009).
- Kenworthy, A. K., N. Petranova and M. Edidin *High-resolution FRET microscopy of cholera toxin B-subunit and GPI-anchored proteins in cell plasma membranes*. *Molecular biology of the cell* **11**(5): 1645-1655. (2000).
- Kim, H. M., H. J. Choo, S. Y. Jung, Y. G. Ko, W. H. Park, S. J. Jeon, C. H. Kim, T. Joo and B. R. Cho *A two-photon fluorescent probe for lipid raft imaging: C-laurdan*. *Chembiochem : a European journal of chemical biology* **8**(5): 553-559. (2007).
- Klymchenko, A. S., G. Duportail, A. P. Demchenko and Y. Mely *Bimodal distribution and fluorescence response of environment-sensitive probes in lipid bilayers*. *Biophys. J.* **86**(5): 2929-2941. (2004).
- Koynova, R. and M. Caffrey *Phases and phase transitions of the phosphatidylcholines*. *Biochim. Biophys. Acta* **1376**(1): 91-145. (1998).
- Koyuturk, M., M. Ersoz and N. Altioek *Simvastatin induces proliferation inhibition and apoptosis in C6 glioma cells via c-jun N-terminal kinase*. *Neuroscience letters* **370**(2-3): 212-217. (2004).
- Kramer, E. M., A. Schardt and K. A. Nave *Membrane traffic in myelinating oligodendrocytes*. *Microsc Res Tech* **52**(6): 656-671. (2001).
- Krasnowska, E. K., E. Gratton and T. Parasassi *Prodan as a membrane surface fluorescence probe: Partitioning between water and phospholipid phases*. *Biophys. J.* **74**(4): 1984-1993. (1998).
- Kubiak, J., J. Brewer, S. Hansen and L. A. Bagatolli *Lipid lateral organization on giant unilamellar vesicles containing lipopolysaccharides*. *Biophys. J.* **100**(4): 978-986. (2011).

- Lakowicz, J. R. *Principles of Fluorescence Spectroscopy*. Berlin, Germany, Springer, New York (USA). (2006).
- Landry, Y. D., M. Denis, S. Nandi, S. Bell, A. M. Vaughan and X. H. Zha *ATP-binding cassette transporter A1 expression disrupts raft membrane microdomains through its ATPase-related functions*. *J. Biol. Chem.* **281**(47): 36091-36101. (2006).
- Lanzillo, R., G. Orefice, M. Quarantelli, C. Rinaldi, A. Prinster, G. Ventrella, D. Spitaleri, G. Lus, G. Vacca, B. Carotenuto, E. Salvatore, A. Brunetti, G. Tedeschi and V. B. Morra *Atorvastatin Combined To Interferon to Verify the Efficacy (ACTIVE) in relapsing-remitting active multiple sclerosis patients: a longitudinal controlled trial of combination therapy*. *Mult Scler J* **16**(4): 450-454. (2010).
- Lasic, D. D. *Novel applications of liposomes*. *Trends Biotechnol* **16**(7): 307-321. (1998).
- Laurencikienė, J. and M. Ryden *Liver X receptors and fat cell metabolism*. *Int J Obesity* **36**(12): 1494-1502. (2012).
- Leventis, R. and J. R. Silvius *Use of cyclodextrins to monitor transbilayer movement and differential lipid affinities of cholesterol*. *Biophys. J.* **81**(4): 2257-2267. (2001).
- Li, L. and J. X. Cheng *Coexisting stripe- and patch-shaped domains in giant unilamellar vesicles*. *Biochemistry-US* **45**(39): 11819-11826. (2006).
- Li, Z., E. Mintzer and R. Bittman *First synthesis of free cholesterol-BODIPY conjugates*. *The Journal of organic chemistry* **71**(4): 1718-1721. (2006).
- Lingwood, D. and K. Simons *Lipid Rafts As a Membrane-Organizing Principle*. *Science* **327**(5961): 46-50. (2010).
- Liu, Y., Y. Y. Wu, J. C. Lee, H. P. Xue, L. H. Pevny, Z. Kaprielian and M. S. Rao *Oligodendrocyte and astrocyte development in rodents: An in situ and immunohistological analysis during embryonic development*. *Glia* **40**(1): 25-43. (2002).
- London, E. *Insights into lipid raft structure and formation from experiments in model membranes*. *Curr Opin Struc Biol* **12**(4): 480-486. (2002).
- Ma, X. Y., Q. Wang, Y. X. Jiang, Z. Y. Xiao, X. H. Fang and Y. G. Chen *Lateral diffusion of TGF-beta type I receptor studied by single-molecule imaging*. *Biochem. Biophys. Res. Commun.* **356**(1): 67-71. (2007).
- Maier, O., V. Oberle and D. Hoekstra *Fluorescent lipid probes: some properties and applications (a review)*. *Chem. Phys. Lipids* **116**(1-2): 3-18. (2002).
- Marini, A., A. Munoz-Losa, A. Biancardi and B. Mennucci *What is Solvatochromism?* *J. Phys. Chem. B* **114**(51): 17128-17135. (2010).
- McMullen, T. P. W., R. N. A. H. Lewis and R. N. McElhaney *Cholesterol-phospholipid interactions, the liquid-ordered phase and lipid rafts in model and biological membranes*. *Curr. Opin. Colloid Interface Sci.* **8**(6): 459-468. (2004).
- Meir, K. S. and E. Leitersdorf *Atherosclerosis in the apolipoprotein-E-deficient mouse: a decade of progress*. *Arteriosclerosis, thrombosis, and vascular biology* **24**(6): 1006-1014. (2004).
- Merrill, J. E. and N. J. Scolding *Mechanisms of damage to myelin and oligodendrocytes and their relevance to disease*. *Neuropath Appl Neuro* **25**(6): 435-458. (1999).
- Metso, A. J., A. Jutila, J. P. Mattila, J. M. Holopainen and P. K. J. Kinnunen *Nature of the main transition of dipalmitoylphosphocholine bilayers inferred from fluorescence spectroscopy*. *J. Phys. Chem. B* **107**(5): 1251-1257. (2003).
- Miller, D. H. and S. M. Leary *Primary-progressive multiple sclerosis*. *Lancet neurology* **6**(10): 903-912. (2007).
- Mirshafiey, A. and M. Mohsenzadegan *TGF-beta as a promising option in the treatment of multiple sclerosis*. *Neuropharmacology* **56**(6-7): 929-936. (2009).
- Mitro, N., L. Vargas, R. Romeo, A. Koder and E. Saez *T0901317 is a potent PXR ligand: Implications for the biology ascribed to LXR*. *FEBS Lett.* **581**(9): 1721-1726. (2007).
- Miyazawa, K., M. Shinozaki, T. Hara, T. Furuya and K. Miyazono *Two major Smad pathways in TGF-beta superfamily signalling*. *Genes to cells : devoted to molecular & cellular mechanisms* **7**(12): 1191-1204. (2002).
- Mukherjee, S. and A. Chattopadhyay *Monitoring the organization and dynamics of bovine hippocampal membranes utilizing Laurdan generalized polarization*. *Biochim. Biophys. Acta* **1714**(1): 43-55. (2005).

- Munro, S. *Lipid rafts: Elusive or illusive?* Cell **115**(4): 377-388. (2003).
- Nelissen, K., M. Mulder, I. Smets, S. Timmermans, K. Smeets, M. Ameloot and J. J. A. Hendriks *Liver X receptors regulate cholesterol homeostasis in oligodendrocytes.* J. Neurosci. Res. **90**(1): 60-71. (2012).
- Nelissen, K., K. Smeets, M. Mulder, J. J. A. Hendriks and M. Ameloot *Selection of reference genes for gene expression studies in rat oligodendrocytes using quantitative real time PCR.* J Neurosci Meth **187**(1): 78-83. (2010).
- Nelson, D. L. and M. M. Cox *Lehninger's Principles of Biochemistry, 4th Edition*, WH Freeman & Co. (2005).
- Niu, S. L., G. Ulrich, P. Retailleau, J. Harrowfield and R. Ziessel *New insights into the solubilization of Bodipy dyes.* Tetrahedron Lett. **50**(27): 3840-3844. (2009).
- Noseworthy, J. H., C. Lucchinetti, M. Rodriguez and B. G. Weinshenker *Multiple sclerosis.* The New England journal of medicine **343**(13): 938-952. (2000).
- O'Brien, J. S. and E. L. Sampson *Lipid composition of the normal human brain: gray matter, white matter, and myelin.* J Lipid Res **6**(4): 537-544. (1965).
- O'Connor, P. *Key issues in the diagnosis and treatment of multiple sclerosis. An overview.* Neurology **59**(6 Suppl 3): S1-33. (2002).
- Ohki, K. *Formation of micro-domains as functional regions in biomembranes: specific interactions inferred by differential scanning calorimetry and microscopic imaging of membrane fluidity.* J. Phys.: Condens. Matter **17**(31): S2957-S2963. (2005).
- Orlowski, S., C. Comera, F. Terce and X. Collet *Lipid rafts: dream or reality for cholesterol transporters?* Eur Biophys J Biophys **36**(8): 869-885. (2007).
- Orth, M. and S. Bellosta *Cholesterol: its regulation and role in central nervous system disorders.* Cholesterol **2012**: 292598. (2012).
- Owen, D. M. and K. Gaus *Optimized time-gated generalized polarization imaging of Laurdan and di-4-ANEPPDHQ for membrane order image contrast enhancement.* Microsc. Res. Tech. **73**(6): 618-622. (2010).
- Owen, D. M., C. Rentero, A. Magenau, A. Abu-Siniyeh and K. Gaus *Quantitative imaging of membrane lipid order in cells and organisms.* Nat. prot. **7**(1): 24-35. (2012).
- Parasassi, T., G. De Stasio, A. Dubaldo and E. Gratton *Phase Fluctuation in Phospholipid-Membranes Revealed by Laurdan Fluorescence.* Biophys. J. **57**(6): 1179-1186. (1990).
- Parasassi, T., G. De Stasio, G. Ravagnan, R. M. Rusch and E. Gratton *Quantitation of lipid phases in phospholipid vesicles by the generalized polarization of Laurdan fluorescence.* Biophys. J. **60**(1): 179-189. (1991).
- Parasassi, T., M. Di Stefano, M. Loiero, G. Ravagnan and E. Gratton *Influence of cholesterol on phospholipid bilayers phase domains as detected by Laurdan fluorescence.* Biophys. J. **66**(1): 120-132. (1994).
- Parasassi, T., M. Distefano, M. Loiero, G. Ravagnan and E. Gratton *Cholesterol Modifies Water Concentration and Dynamics in Phospholipid-Bilayers - a Fluorescence Study Using Laurdan Probe.* Biophys. J. **66**(3): 763-768. (1994).
- Parasassi, T., A. M. Giusti, M. Raimondi and E. Gratton *Abrupt Modifications of Phospholipid-Bilayer Properties at Critical Cholesterol Concentrations.* Biophys. J. **68**(5): 1895-1902. (1995).
- Parasassi, T., E. Gratton, W. M. Yu, P. Wilson and M. Levi *Two-photon fluorescence microscopy of laurdan generalized polarization domains in model and natural membranes.* Biophys. J. **72**(6): 2413-2429. (1997).
- Parasassi, T., E. K. Krasnowska, L. Bagatolli and E. Gratton *LAURDAN and PRODAN as polarity-sensitive fluorescent membrane probes.* J. Fluoresc. **8**(4): 365-373. (1998).
- Parisio, G., A. Marini, A. Biancardi, A. Ferrarini and B. Mennucci *Polarity-sensitive fluorescent probes in lipid bilayers: bridging spectroscopic behavior and microenvironment properties.* J. Phys. Chem. B **115**(33): 9980-9989. (2011).
- Paul, F., S. Waiczies, J. Wuerfel, J. Bellmann-Strobl, J. Dorr, H. Waiczies, M. Haertle, K. D. Wernecke, H. D. Volk, O. Aktas and F. Zipp *Oral high-dose atorvastatin treatment in relapsing-remitting multiple sclerosis.* Plos One **3**(4): e1928. (2008).

- Periasamy, N. and R. Winter *The effects of temperature, pressure and peptide incorporation on ternary model raft mixtures--a Laurdan fluorescence spectroscopy study*. *Biochim. Biophys. Acta* **1764**(3): 398-404. (2006).
- Pike, L. J. *Lipid rafts: bringing order to chaos*. *J. Lipid Res.* **44**(4): 655-667. (2003).
- Polito, A. and R. Reynolds *NG2-expressing cells as oligodendrocyte progenitors in the normal and demyelinated adult central nervous system*. *Journal of anatomy* **207**(6): 707-716. (2005).
- Quarles, R. H., W. B. Macklin and P. Morell *Myelin Formation, Structure and Biochemistry*. Basic Neurochemistry: Molecular, Cellular and Medical Aspects. G. S. Scott Brady, R. Wayne Albers, Donald Price, Elsevier, Inc.(2006).
- RichterLandsberg, C. and M. Heinrich *OLN-93: A new permanent oligodendroglia cell line derived from primary rat brain glial cultures*. *J. Neurosci. Res.* **45**(2): 161-173. (1996).
- Rudick, R. A., A. Pace, M. R. Rani, R. Hyde, M. Panzara, S. Appachi, J. Shrock, S. L. Maurer, P. A. Calabresi, C. Confavreux, S. L. Galetta, F. D. Lublin, E. W. Radue and R. M. Ransohoff *Effect of statins on clinical and molecular responses to intramuscular interferon beta-1a*. *Neurology* **72**(23): 1989-1993. (2009).
- Salomoni, P., I. Guernah and P. P. Pandolfi *The PML-nuclear body associated protein Daxx regulates the cellular response to CD40*. *Cell death and differentiation* **13**(4): 672-675. (2006).
- Salvatore, E., V. B. Morra and G. Orefice *Combining Beta Interferon and Atorvastatin May Increase Disease Activity in Multiple Sclerosis*. *Neurology* **73**(13): 1078-1078. (2009).
- Sanchez, S. A., G. Gunther, M. A. Tricerri and E. Gratton *Methyl-beta-cyclodextrins preferentially remove cholesterol from the liquid disordered phase in giant unilamellar vesicles*. *J. Membr. Biol.* **241**(1): 1-10. (2011).
- Sanchez, S. A., M. A. Tricerri and E. Gratton *Laurdan generalized polarization fluctuations measures membrane packing micro-heterogeneity in vivo*. *Proc. Nat. Acad. Sci. USA* **109**(19): 7314-7319. (2012).
- Sanchez, S. A., M. A. Tricerri, G. Gunther and E. Gratton *Laurdan Generalized Polarization: from cuvette to microscope*. Modern research and educational topics in microscopy: applications in physical/chemical sciences. A. Méndez-Vilas and J. Díaz, Formatex Research Center. **1**: 1007-1014.(2007).
- Scherfeld, D., N. Kahya and P. Schuille *Lipid dynamics and domain formation in model membranes composed of ternary mixtures of unsaturated and saturated phosphatidylcholines and cholesterol*. *Biophys. J.* **85**(6): 3758-3768. (2003).
- Schneckenburger, H. and M. Wagner *Time-resolved fluorescence in biomedical diagnostics*. Reviews in Fluorescence. C. D. Geddes and J. R. Lakowicz. New York, Springer: 153-168.(2005).
- Schneckenburger, H., M. Wagner, M. Kretschmar, W. S. Strauss and R. Sailer *Laser-assisted fluorescence microscopy for measuring cell membrane dynamics*. *Photochem. Photobiol Sci.* **3**(8): 817-822. (2004).
- Sena, A., R. Pedrosa and M. G. Morais *Therapeutic potential of lovastatin in multiple sclerosis*. *J Neurol* **250**(6): 754-755. (2003).
- Siano, D. and D. E. Metzler *Band Shapes of the Electronic Spectra of Complex Molecules* *J. Chem. Phys.* **51**(5): 1856-1862. (1969).
- Silvius, J. R. *Thermotropic phase transitions of pure lipids in model membranes and their modification by membrane proteins*. (1982).
- Simons, K. and E. Ikonen *Functional rafts in cell membranes*. *Nature* **387**(6633): 569-572. (1997).
- Simons, K. and W. L. Vaz *Model systems, lipid rafts, and cell membranes*. *Annu. Rev. Biophys. Biomol. Struct.* **33**: 269-295. (2004).
- Stancu, C. and A. Sima *Statins: mechanism of action and effects*. *J Cell Mol Med* **5**(4): 378-387. (2001).
- Stefl, M., N. G. James, J. A. Ross and D. M. Jameson *Applications of phasors to in vitro time-resolved fluorescence measurements*. *Anal Biochem* **410**(1): 62-69. (2011).
- Stehr, M., C. R. Estrada, J. Khoury, T. E. Danciu, M. P. Sullivan, C. A. Peters, K. R. Solomon, M. R. Freeman and R. M. Adam *Caveolae are negative regulators of transforming growth factor-beta1 signaling in ureteral smooth muscle cells*. *The Journal of urology* **172**(6 Pt 1): 2451-2455. (2004).

- Strelau, J. and R. Unsicker *GDNF family members and their receptors: Expression and functions in two oligodendroglial cell lines representing distinct stages of oligodendroglial development*. *Glia* **26**(4): 291-301. (1999).
- Tomin, V. I., M. Brozis and J. Heldt *The red-edge effects in Laurdan solutions*. *Z. Naturforsch.* **58a**: 109 – 117. (2003).
- Valeur, B. and M. N. Berberan-Santos *Molecular Fluorescence. Principles and applications*, Wiley-VCH, Weinheim (Germany). (2012).
- van Meer, G., D. R. Voelker and G. W. Feigenson *Membrane lipids: where they are and how they behave*. *Nat Rev Mol Cell Bio* **9**(2): 112-124. (2008).
- Vance, D. E. and J. E. Vance *Biochemistry of Lipids, Lipoproteins and Membranes 4th* Elsevier Science B.V. (2002).
- Vaughan, A. M. and J. F. Oram *ABCA1 redistributes membrane cholesterol independent of apolipoprotein interactions*. *J. Lipid Res.* **44**(7): 1373-1380. (2003).
- Vaughan, A. M., C. R. Tang and J. F. Oram *ABCA1 mutants reveal an interdependency between lipid export function, apoA-I binding activity, and Janus kinase 2 activation*. *J. Lipid Res.* **50**(2): 285-292. (2009).
- Vollmer, T., L. Key, V. Durkalski, W. Tyor, J. Corboy, S. Markovic-Plese, J. Preiningerova, M. Rizzo and L. Singh *Oral simvastatin treatment in relapsing-remitting multiple sclerosis*. *Lancet* **363**(9421): 1607-1608. (2004).
- Wente, W., M. B. Brenner, H. Zitzer, J. Gromada and A. M. Efanov *Activation of liver X receptors and retinoid X receptors induces growth arrest and apoptosis in insulin-secreting cells*. *Endocrinology* **148**(4): 1843-1849. (2007).
- Wesolowska, O., K. Michalak, J. Maniewska and A. B. Hendrich *Giant unilamellar vesicles - a perfect tool to visualize phase separation and lipid rafts in model systems*. *Acta Biochim Pol* **56**(1): 33-39. (2009).
- Wheeler, G. and K. M. Tyler *Widefield microscopy for live imaging of lipid domains and membrane dynamics*. *Biochim. Biophys. Acta* **1808**(3): 634-641. (2011).
- Whitney, K. D., M. A. Watson, J. L. Collins, W. G. Benson, T. M. Stone, M. J. Numerick, T. K. Tippin, J. G. Wilson, D. A. Winegar and S. A. Kliewer *Regulation of cholesterol Homeostasis by the liver X receptors in the central nervous system*. *Mol Endocrinol* **16**(6): 1378-1385. (2002).
- Williams, A. T. R., S. A. Winfield and J. N. Miller *Relative Fluorescence Quantum Yields Using a Computer-Controlled Luminescence Spectrometer*. *Analyst* **108**(1290): 1067-1071. (1983).
- Wong, W. W. L., J. Dimitroulakos, M. D. Minden and L. Z. Penn *HMG-CoA reductase inhibitors and the malignant cell: the statin family of drugs as triggers of tumor-specific apoptosis*. *Leukemia* **16**(4): 508-519. (2002).
- Xiang, Z. and S. A. Reeves *Simvastatin induces cell death in a mouse cerebellar slice culture (CSC) model of developmental myelination*. *Experimental neurology* **215**(1): 41-47. (2009).
- Yakupoglu, Y., A. Dinckan, A. Gurkan, M. Tuncer, O. Erdogan, H. Altunbas, U. Yakupoglu, R. Sari and A. Demirbas *Kidney-pancreas transplantation: Single-center experience at a University Hospital in Turkey*. *Transplantation proceedings* **37**(7): 3205-3208. (2005).
- Yu, W. M., P. T. C. So, T. French and E. Gratton *Fluorescence generalized polarization of cell membranes: A two-photon scanning microscopy approach*. *Biophys. J.* **70**(2): 626-636. (1996).
- Zhao, C. Y. and K. Dahlman-Wright *Liver X receptor in cholesterol metabolism*. *J. Endocrinol.* **204**(3): 233-240. (2010).

Publications

1. **Bacalum, M.**, B. Zorilă and M. Radu *Fluorescence spectra decomposition by asymmetric functions – Laurdan spectrum revisited*. Anal Biochem. 2013 Jun 5. pii: S0003-2697(13)00263-7. doi: 10.1016/j.ab.2013.05.031
2. **Bacalum, M.**, Bogdan Zorila, Mihai Radu and Aurel Popescu *Laurdan solvatochromism: influence of solvent polarity and hydrogen bonds*. Optoelectronics and Advanced Materials – Rapid Communications vol. 7, iss. 5-6/2013
3. **Bacalum, M.**, N. Smisdrom, A. Popescu and M. R. M. Ameloot *Exploring the correlation between Generalized Polarization and time-resolved fluorescence of Laurdan in lipid membranes (manuscript paper)*.
4. **Bacalum, M.**, L. Wang, V. Leen, P. Yuan, N. Smisdrom, E. Fron, W. Dehaen, N. Boens, S. Knippenberg, G. Fabre, P. Trouillas, D. Beljonne and M. Ameloot *A blue emitting BODIPY based lipid phase sensitive probe. (manuscript paper)*.

Oral presentations

1. Mihaela Bacalum, Nick Smisdrom, Ben de Clercq, Inge Smolders, Aurel Popescu, Marcel Ameloot, *Studiul fluiditatii membranare in celule HEK utilizand fluorescenta Laurdanului*, (in romanian)at RSBPA Bucharest Branch Conference, November 27, 2010, Biology Faculty, Bucharest University, Bucharest, Romania
2. Mihaela Bacalum, Nick Smisdrom, Aurel Popescu, Mihai Radu and Marcel Ameloot, *A Microfluorimetric Study of The Membrane Organization of Model and Natural Membranes Using Laurdan*, 12th National Conference on Biophysics "CNB 2013" - Biophysics for Health with International Participation, June 13-16, 2013, "Alexandru Ioan Cuza" University of Iași, Iași, Romania

Poster presentations

1. M. Bacalum, N. Smisdrom, B. De Clercq, I. Smolders, A. Popescu and M. Ameloot, *Using two-photon fluorescence lifetime imaging microscopy of Laurdan to investigate fluidity changes in plasma membranes of HEK cells*, International Autumn School

- Biophysics and Bioelectrochemistry for Medicine, Vulcan-Brasov, Romania, october 1-6, 2010
2. M. Bacalum, N. Smisdom, B. De Clercq, I. Smolders, A. Popescu and M. Ameloot, *Laurdan probing of the plasma membrane of OLN-93 oligodendroglial cells after simvastatin treatment using two-photon excitation microscopy and fluorescence lifetime imaging*, Advanced Light Microscopy Symposium, Gent, Belgium, 23-24 September 2010
 3. M. Bacalum, N. Smisdom, B. De Clercq, A. Popescu and M. Ameloot, *Simvastatin induced changes in plasma membranes of cells: a Laurdan based study using two-photon excitation fluorescence lifetime imaging microscopy*, Course: Stuying protein-protein interactions by advanced light microscopy and spectroscopy, Debrecen, Hungary, 16-23 August 2011
 4. M. Bacalum, N. Smisdom, A. Popescu and M. Ameloot, *Correlating generalized polarization and time-resolved fluorescence of Laurdan in the exploration of lipid membranes*, Dutch meeting on Molecular and Cellular Biophysics 2012

ACKNOWLEDGMENTS

After four year I'm finally here, at the end of this unique adventure!

This thesis is dedicated to my Mom and Dad and I think this is the best way to thank them for all they have done for me, and not only during these 4 years.

Hereinafter I want to thank all the persons who played a direct or indirect role, as they supported me and helped me finish this chapter of my life.

First I want to thank my promotor from University of Bucharest, prof. dr. Aurel Popescu, the first to introduce us to the interesting field of biophysics. I also want to thank him not only for the guidance and help he provided me during the 4 years of my PhD, but also for the ups and downs that he had to bear with during the final part of my PhD.

I also want to thank my "boss" from IFIN-HH, dr. Mihai Radu who was the first to introduce me to the real "research" when I started to prepare the experiments for my bachelor thesis in his lab. It is the same lab where I stayed and continue my formation as a biophysicist. I owe him a big "multumesc din inima" for letting me "play" with all the techniques that I wanted and because of this I still see the work in the lab as my "playground", in a serious way of course.

An equal consideration I have for my promotor from Hasselt University, prof. dr. Marcel Ameloot, for giving me the opportunity to learn and work with new techniques in his really nice lab. Although in your lab I was able to learn and work with new and exciting techniques, I don't know way, but the preparation of the GUVs sticks closer to my heart than all the others. I will always remember our discussions in which we tried our best to see what the through "colour" of Laurdan was. I also owe you a big thank you for the help you provided me for the things that were not related to my scientific work. Bedankt voor alles!

I want to thank to the member of the jury for accepting and for the trouble they got to be able to attend my defense.

To the guys from the basement (which theoretically is a semi-basement ☺) thank you for accepting this strange and crazy Romanian PhD student which came into your lab and "disturb" your "uniform" assembly. Nick, the Master, I owe you a big thanks for the help

you give me with the Matlab functions and also when I wanted to try new things (my topographic maps – I will never forget you made them possible). Ben thank you for the help you provided with the functions in Matlab. Kristof, the tallest person from the group, I will never forget you were the first to introduce me to the confocal and the lab. Rik thank you for helping me with the Matlab and also in “killing” the PC of the B&H. Kathleen thank you for all your help and encouragements and also for „1 Martie”. Dank u en ik zal nooit vergeten de icecreme en de wandeling in de natuur ☺.

Inge and Katherine thank you for the help with the OLN-93 cells and the SV and T09 treatments. Ellen thank you for helping me learn how to prepare GUVs. Also a big thank you to all the people from BIOMED who helped me during my time spent there (Jo, Ilse, Agnes, Ambily and many more).

A big “Va multumesc pentru tot!” goes to my somehow second family that I gain when I started working in DFVM (IFIN-HH).

Dr. Ileana Petcu, the mother of our group was able to always give me a word of encouragement when I needed the most and I’m very grateful for that. Di I want to thank you from the bottom of my heart for everything. Thank you for all the “crazy” and not so crazy things that we did and also for putting up with my temper during this time. Adi I want to thank you for your down to earth nature that helped me finding answers to some of my problems. Livia thank you for all the help you provided me with the simple and small matters that I would have overlooked. Nenea thank you for all the useful discussions in the field of chemistry, biochemistry, actually in all fields that I can think of. Bogdan, for the moment the only one with whom I can speak biophysics face to face, thank you for your help with the instrumentation and the smelly solvents. Cosmin and Mihaela, my room colleagues, thank you for bearing with my temper, my nagging and my way of making a winter day colder. Tanti Victorita, my second mother, thank you for just being this. I don’t have the words to tell you how much it helped me. Nenea Titi, as you are my second father here, thank you for the father like things that you did for me and also for making my mornings enjoyable. Papusa, this will be the first to use this, as I promised, thank you for your support and all the non-science related things, but necessary to science, that you thought me.

Also thank you to all the other colleagues from DFVM and IFIN-HH who supported and encouraged me during this time.

I want to thank my friends for still being my friends through all the good and bad moments that I passed during my PhD. Thank you for all your support and understanding. You were the best.

Finally, but not last, I want to thank to the most important people in my life, my family. Mom and Dad I don't have the words to thank you for all you have done for Eli and me.

Eli, my dear sister, thank you too for all the help, for your comforting words, your trust in me especially when I didn't had any, and your emails, especially when they were full with emoticons (☺ :D, >:D<, :P).